METAKAOLIN AS A CEMENT EXTENDER

NICHOLA JAYNE COLEMAN

Doctor of Philosophy

THE UNIVERSITY OF ASTON IN BIRMINGHAM

June 1996

SUMMARY

The University of Aston in Birmingham

METAKAOLIN AS A CEMENT EXTENDER

Nichola Jayne Coleman

Doctor of Philosophy June 1996

The effect of 10% and 20% replacement metakaolin on a number of aspects of hydration chemistry and service performance of ordinary Portland cement pastes has been investigated.

The analysis of expressed pore solutions has revealed that metakaolin-blended specimen pastes possess enhanced chloride binding capacities and reduced pore solution pH values when compared with their unblended counterparts. The implications of the observed changes in pore solution chemistry with respect to chloride induced reinforcement corrosion and the reduction in expansion associated with the alkali aggregate reaction are discussed.

Differential thermal analysis, mercury intrusion porosimetry, and nuclear magnetic resonance spectroscopy have been employed in the analysis of the solid phase. It is suggested that hydrated gehlenite (a product of pozzolanic reaction) is operative in the removal and solid state binding of chloride ions from the pore solution of metakaolin-blended pastes.

Diffusion coefficients obtained in a non-steady state chloride ion diffusion investigation have indicated that cement pastes containing 10% and 20% replacement metakaolin exhibit superior resistance to the penetration of chloride ions in comparison with those of plain OPC of the same water:cement ratio.

The chloride induced corrosion behaviour of cement paste samples, of water:cement ratio 0.4, containing 0%, 10%, and 20% replacement metakaolin, has been monitored using the linear polarization technique. No significant corrosion of embedded mild steel was observed over a 200 day period.

KEY WORDS: Pozzolan, Pore solution chemistry, Chloride ion diffusion, Solid state nuclear magnetic resonance spectroscopy, Chloride induced corrosion of embedded steel.

ACKNOWLEDGEMENTS

I am indebted to Professor C.L. Page for his supervision and advice throughout the execution of this research and during the writing of this thesis.

I am grateful to E.C.C.I. for initiating and financing the research project.

I acknowledge, with gratitude, the expert advice of my co-supervisor Professor W. R. McWhinnie.

Special thanks are due to Colin Thompson, Dr. George Sergi, and Dr. Mike Perry, for their support and encouragement throughout the course of this work.

Dr. D. A. L. Wilson's contribution to the statistical analysis of the diffusion data was vital and well appreciated.

I wish to convey my sincere appreciation of the help and friendship provided by Michael Smedley and Nicholas Tuliani prior to and during this project. Special thanks are also issued to Roger, Becki, Stuart, Su, Zahid, and Gerald.

Finally, I would like to express my gratitude to my family.

LIST OF CONTENTS

APPENDICES

LIST OF FIGURES

CHAPTER 6

LIST OF TABLES

CHAPTER 5

CHAPTER 1 INTRODUCTION

1.1 A BRIEF HISTORY OF CEMENT [1,2]

Cementitious materials have been in use since ancient times. Impure gypsum was used by the Egyptians; the Greeks and Romans used calcined limestone to which they later added aggregate to form the first concretes. These lime mortars were of comparatively poor quality. Roman cement fell into disuse. In 1824 Joseph Aspdin, a builder from Leeds, patented Portland cement, which was originally prepared by heating a mixture of clay and chalk. The cementitious calcium silicates, Ca_2SiO_4 and Ca_3SiO_5, were produced during the high temperature reactions. Currently various raw materials are used in its production: chalk, limestone or gypsum as a source of lime, together with sand, clay and iron oxide.

1.2 PROPERTIES OF ORDINARY PORTLAND CEMENT

The major constituents of ordinary Portland cement are as follows:

$3CaO.SiO_2$	(C_3S)
$2CaO.SiO_2$	(C_2S)
$3CaO.Al_2O_3$	(C_3A)
$4CaO.Al_2O_3.Fe_2O_3$	(C_4AF)
$CaSO_4.2H_2O$	gypsum

Several complex hydration reactions are initiated on addition of water to anhydrous cement. The products of such reactions finally constitute the hardened mass. Figure 1 (overleaf) is a schematic representation of the changes which occur during hydration, depicting the transformation of an aqueous dispersion of discrete particles to form an interconnected solid matrix [3].

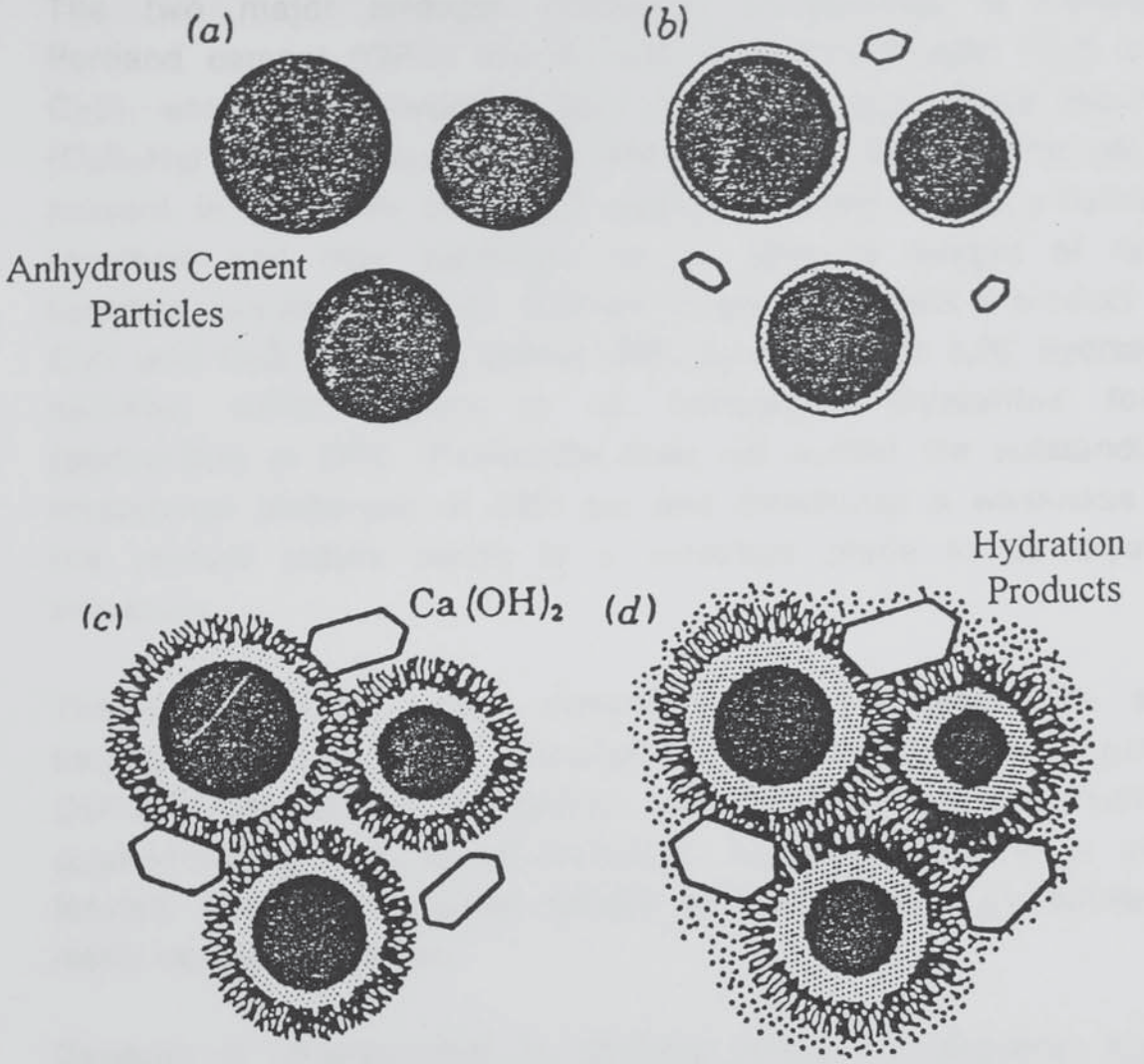

FIGURE 1.1
A SCHEMATIC REPRESENTATION OF THE SEQUENCE OF MICROSTRUCTURAL CHANGES WHICH OCCUR DURING THE HYDRATION OF CEMENT

The hydration of anhydrous cement particles results in a solid matrix containing interconnecting pores, the dimensions of which have been characterised. The ultra-fine 'gel pores' are of the order of nm in diameter whereas the coarser 'capillary pores' are in the μm range. Macroscopic voids, of the order of mm in size, may also exist which are a consequence of incomplete compaction. The significance of pore structure is discussed in Chapters 4, 5 and 6.

The two major strength rendering compounds in ordinary Portland cement (OPC) are di- and tricalcium silicate (C_2S and C_3S), which, when hydrated, give rise to calcium silicate hydrate ($C_3S_2H_3$) gel. $C_3S_2H_3$ is usually referred to as CSH gel. This gel is present in the form of a rigid network having a poorly-defined structure and may constitute up to 70% by weight of fully hydrated cement paste [4]. Calcium hydroxide is also a product of C_2S and C_3S hydration (about 20% by weight of fully hydrated cement) which occurs in an hexagonal crystalline form (portlandite) in OPC. Portlandite does not exhibit the outstanding mechanical properties of CSH gel and constitutes a weakness in the cement matrix owing to a cleavage plane in its crystal structure.

The other phases which constitute the remaining 10% are calcium aluminate trisulphate hydrate (ettringite, $C_3A.3CaSO_4.32H_2O$) and calcium aluminate monosulphate hydrate (approximately 7%). Some tricalcium aluminate hydrate is also formed. Unhydrated clinker residue and other minor constituents make up the remainder.

Gypsum is incorporated in cement clinker to prevent 'flash setting'. In the absence of gypsum, tricalcium aluminate hydrates rapidly precipitating an hydrated coating on the clinker particles which prevents the full hydration of the calcium silicate species. An alternative hydration route for tricalcium aluminate is established in the presence of gypsum involving the formation of ettringite.

Sodium and potassium sulphates present in the cement are engaged in the formation of ettringite causing the release of alkali metal ions into the pore solution. The high pore solution pH values found in hydrated cements are a consequence of the balancing of these alkali metal cations by hydroxyl ions. The pore solution concentration of sodium and potassium hydroxides increases as hydration proceeds [5,6]. The importance of pore solution alkalinity is considered in Chapters 3 and 6.

1.3 POZZOLANIC BEHAVIOUR

Again it was the Romans who pioneered the first pozzolanic cements. To improve the quality of their lime mortars they added volcanic ash; a source of reactive silica and alumina.

A pozzolanic material (according to ASTM specification C618-78) is "a siliceous or siliceous and aluminous material which in itself possesses little or no cementitious value but will, in a finely divided form and in the presence of moisture, chemically react with calcium hydroxide at ordinary temperatures to form components possessing cementitious properties". Pozzolans tend to be composed of amorphous silica (as crystalline silica is of low reactivity). The obvious benefit of the pozzolanic reaction is that it removes portlandite from the cement matrix yielding products with superior mechanical properties and improved resistance to chemical attack caused by reactions with calcium hydroxide. Removal of calcium hydroxide from the cement matrix may impair the ability of a cement structure to protect its steel reinforcement. This phenomenon will be discussed in Chapter 6.

Some pozzolanic cements require curing over comparatively long periods as their hydration rates may be slow compared with that of OPC (e.g. those blended with pulverised fuel ash).

The retarded hydration rate also leads to a low rate of heat evolution which is important in mass concrete construction. Enhanced durability, permeability and strength are generally found for pozzolanic cements along with a total reduction in cost.

1.4 METAKAOLIN

Metakaolin ($Al_2Si_2O_7$) is a largely amorphous dehydration product of the china clay kaolin ($Al_2(OH)_4Si_2O_5$). It is an ill-defined mixture of amorphous silica and alumina in which 100nm diameter domains retaining the symmetry of kaolin exist. Upon heating in air kaolin loses water in the temperature range 450°C

to 800°C. Metakaolin forms at around 600°C and is stable up to 950°C above which it recrystallises rendering a mullite or spinel phase and amorphous silica [7]. The pozzolanic properties of metakaolin are already well documented [7,8,9,10,11].

In 1985 Murat et al. conducted a study of synthetic binders (employed in developing countries as cost-effective building materials) obtained from a blend of water, calcium hydroxide and particular (locally available) pozzolans [7]. The most pure and amorphous metakaolin was found to yield the most effective pozzolanic cement in a 28 day compressive strength study of binders produced from Illite, Montmorillonite and various kaolinites calcined at 750°C in air.

In a previous paper Murat et al. established that the products of reaction between metakaolin, calcium hydroxide and water are essentially hydrated gehlenite (C_2ASH_8), calcium silicate hydrate gel (CSH) and tetracalcium aluminate hydrate (C_4AH_{13}) [10]. Reference is also made to investigations conducted using ordinary Portland cement although results were not discussed in that paper due to their irrelevance to the synthetic binder project.

Palomo and Glasser [12] used infrared spectroscopy (IR), X-ray diffraction and electron microscopy in the investigation of cementitious materials based on metakaolin 'geopolymers' (as patented by Davidovitz [13,14]) prepared from various combinations of sodium silicate, metakaolin, silica fume, sodium hydroxide and water. The metakaolin was prepared by heating kaolin at 750°C for 24 hours, 850°C for 2 hours and 950°C for 2 hours. The most reactive metakaolin product was found to be that obtained by calcination at 750°C.

Order of mixing of reactants and cure regime significantly affected the phase development of the product. The mixes were found to have a period of workability but set within hours yielding dimensionally stable solids of good compressive strength. Compressive strength measurements indicated that a

gel binding phase (obtained by curing at or near ambient temperature) was more desirable than a crystalline binding phase (obtained during elevated temperature cure). The gel binding phase of the geopolymer systems was found to be similar to the CSH gel of Portland cement (although the compositions investigated possessed a low calcium:silicon ratio and contained aluminium species). The highest quality formulations required strongly alkaline conditions and although some of the sodium present was bound into the gel much remained in the pores and in a loosely bound state which was readily leachable.

Bijen and Larbi [11] working with mortars of water:solids ratio 0.4 having 0, 10 and 20% metakaolin additions and a suitable dispersing agent found that, for fresh cement mortars, additions of metakaolin also improved the homogeneity of the mix by 'virtually' preventing settlement of cement and aggregate particles and migration of water to the surface. An increase in compressive strength of mortars containing metakaolin was attributed to an improved interfacial interaction between cement paste and the aggregate particles as well as the reduction of the portlandite content by pozzolanic reaction.

OPC samples cured in water at 20°C having 0, 10, 20, 30, 40 and 50% replacement metakaolin obtained by dehydration of an 88% kaolin clay at 800°C were studied in an investigation of the microstructure and porosity of metakaolin blended cements by Bredy et al. [15]. A compressive strength improvement was noted for samples containing 10% metakaolin and was attributed to the effectiveness of the pozzolanic reaction. Higher values of metakaolin substitution were found to result in a loss of strength since it was believed that insufficient portlandite was available for complete reaction. Differential thermal analysis of all samples at 28, 90 and 190 days also indicated that metakaolin causes a reduction in the portlandite content as a consequence of pozzolanic reaction and promotes the formation of hydrated gehlenite, C_2ASH_8, which is absent in unblended OPC.

Dunster et al. [16] investigated the pozzolanic reaction of metakaolin in OPC pastes and in calcium hydroxide binders by differential thermal analysis and trimethylsilylation [17,18]. The presence of metakaolin was seen to accelerate the hydration of the silicate phases in OPC and increase the proportion of higher molecular weight silicates at a given degree of hydration.

In service glass-fibre reinforced cement suffers strength loss and embrittlement due to chemical attack from the growth of reactive hydration products around the glass filaments. This deterioration of physical properties is primarily due to the deposition of calcium hydroxide (portlandite) in the vicinity of the glass fibres. Reaction between the glass and calcium hydroxide results in the creation of point stresses and reduction in fibre flexibility. The quality and durability of glass-fibre reinforced cement may be improved by using a cement system in which the production of calcium hydroxide is substantially reduced. Some well established pozzolanic materials, such as silica fume and pulverised fuel ash, are sufficiently reactive to adequately reduce the quantity of portlandite in the matrix. However their rates of pozzolanic reaction in the early stages of hydration are often to slow to prevent the deposition of portlandite around the glass filaments. Also, since silica fume and pulverised fuel ash are industrial by-products their composition, alkali content and reactivity vary according to their origin. During the late 1980s metakaolin was widely studied in this application since its calcination parameters, particle size distribution and composition could be subject to stringent control [9,19]. Improvement of durability, mechanical properties and appearance of the composites studied were attributed to the superior pozzolanic activity of metakaolin.

More recently Oriol and Pera [20] used Fourier Transform IR and differential thermal analysis to investigate the effect of microwave curing on lime consumption in metakaolin-blended OPC cements for use in fibre-reinforced composites. The pozzolanic activity of metakaolin was found to increase under microwave treatment to such an extent that all calcium

hydroxide was consumed in systems containing 15% metakaolin subjected to microwave treatment whereas 30 to 40% metakaolin was required to achieve this effect in samples cured at room temperature. The reduction in required metakaolin content and curing period associated with microwave heating are believed to be important in the development of fibre-reinforced cement composites. The commercial use of metakaolin as a pozzolan has, to date, largely been confined to glass-fibre reinforced cement [11,19].

1.5 THESIS PLAN

Research presented in this thesis has been undertaken to enable an assessment of the properties of metakaolin-blended OPC with respect to those of other, commonly used pozzolanically-blended OPCs (e.g. those produced from microsilica, pulverised fuel ash (PFA), ground granulated blast furnace slag (GGBFS), etc.). Microsilica, PFA and GGBFS are by-products of silicon-metal smelting processes, exhaust fumes from coal-fired power stations, and waste products from the manufacture of pig-iron, respectively. Each of these pozzolans is subject to quality control in order to maintain the concentrations of possible deleterious materials below acceptable levels. Metakaolin-blended cements are intended for a less general market than those mentioned above as they are more costly to produce and believed to be of a superior quality.

The thesis is comprised of seven chapters. The introduction (Chapter 1) precedes an experimental chapter in which sample preparations and laboratory techniques are described. Experimental results are contained in the four following Chapters (3-6) as listed:

CHAPTER 3

This chapter presents the results of a pore solution investigation of metakaolin-extended OPC pastes. The significance of the pore solution electrolyte phase is discussed in relation to the experimental findings.

CHAPTER 4

The results of a solid phase investigation by Differential Thermal Analysis (DTA), Nuclear Magnetic Resonance Spectroscopy (NMR), and Mercury Intrusion Porosimetry (MIP) are reported in this chapter.

CHAPTER 5

The diffusion and permeation of aggressive agents through the cement matrix is discussed (with respect to corrosion of steel reinforcements) along with results of an non-steady state chloride diffusion investigation.

CHAPTER 6

This chapter assesses the corrosion behaviour of steel embedded in metakaolin-blended pastes.

CHAPTER 7

The final chapter contains the general discussion and conclusions inferred from the whole investigation.

All experimental chapters open with an introduction of the topic in the form of a literature review. A description of the experimental procedure is then followed by the results and a discussion.

CHAPTER 2 EXPERIMENTAL TECHNIQUES

Materials, sample preparations and experimental techniques are described in this chapter.

2.1 MATERIALS

A single cement type, Aston OPC, was used for all investigations. Its Bogue and oxide compositions are shown in Tables 2.1 and 2.2 respectively.

COMPOUND	CONTENT %
C_3S	61.3
C_2S	12.9
C_3A	9.7
C_4AF	7.9

TABLE 2.1
BOGUE COMPOSITION OF ASTON OPC

A single superior quality metakaolin (Polestar 501) was employed for solid state, non-steady state chloride diffusion and corrosion studies. Pore solution investigations were conducted using both Polestar 501 (MK 501) and Polestar 505 (MK 505). The two metakaolin types differed in composition with respect to minor contaminants. Chemical analyses of both minerals are given in Table 2.2 (overleaf) and their particle size distribution data are located in Table 2.3.

COMPOUND	CEMENT	MK 501	MK 505
CaO	65.3	0.4	0.07
SiO_2	20.6	54.2	52.1
Al_2O_3	5.3	40.8	41.0
Fe_2O_3	2.6	0.6	4.3
SO_3	3.0	0.3	
MgO	1.2	0.2	0.2
K_2O	0.8	2.1	0.6
Na_2O	0.1	0.1	0.3
Cl	0.02	-	-
P_2O_5	-	0.1	
TiO_2	-	0.04	0.8
Mn_2O_3	-	0.04	
L.O.I	0.8	1.0	0.6

TABLE 2.2
CHEMICAL ANALYSES OF ASTON OPC, MK 501 AND MK 505
(WEIGHT %)

SIZE (μm)	MK 501	MK 505
>10	4	12
>5	13	33
<2	58	37
<1	35	21
<0.5	15	12

TABLE 2.3
PARTICLE SIZE DISTRIBUTION DATA FOR
MK 501 AND MK 505 (WEIGHT %)

All minerals and cement were stored in re-sealable, air-tight plastic bins until required.

2.2 SAMPLE PREPARATIONS

In order to produce a consistent fineness of powder all materials were sieved to 150μm. All cement paste samples were hydrated with distilled water. Each cement sample was weighed and thoroughly mixed with the required mass of metakaolin before the appropriate mass of distilled water was added. Pastes containing 'internal' sodium chloride were prepared by dissolving the salt in the distilled water prior to mixing.

On addition of the mix water the cement paste constituents were intimately mixed for five minutes using a metal palate knife. The fresh paste was then poured into cylindrical PVC containers, 49mm diameter by 75mm height. The pots containing the pastes were then vibrated for up to three minutes (until bubbles ceased to appear on the surface) to remove air from the mixture and improve compaction. On vibration a layer of 'foam' formed on the surface. This layer was removed and replaced with fresh cement paste prior to sealing and curing. Before securing the lids pieces of polyethylene sheeting were placed over the pastes to prevent air entrapment.

The specimens were then rotated at approximately 8 r.p.m. for 24 hours to minimise segregation before being placed in an high humidity environment at 22 ±2°C to cure.

2.2.1 PORE SOLUTION AND SOLID STATE INVESTIGATIONS

Pastes containing 0, 10, and 20% replacement metakaolin MK 501 with sodium chloride additions of 0, 0.1, 0.4, and 1.0% (by mass of cement) were prepared at a water:solids ratio of 0.5. Pastes containing 0, 10, and 20% metakaolin MK 505 having 0 and 1.0% sodium chloride additions were also prepared at the same water:solids ratio.

The pastes required for pore solution analysis were demoulded after the requisite curing time (1, 7, 36, and 100 days). Portions of the pastes were then broken away from the cylinder to be

analysed by MIP, DTA, and NMR (Sections 2.8, 2.7.2 and 2.7.3 respectively). The remainder was subjected to pore fluid extraction (as described in Section 2.3).

2.2.2 UNSTEADY STATE CHLORIDE ION DIFFUSION INVESTIGATION

Quintuplicate cement paste cylinders containing 0, 10, and 20% metakaolin MK 501 of water:solids ratios 0.4, 0.5, and 0.6 were prepared for the unsteady state chloride diffusion investigation.

After curing (as described in Section 2.2) for 28 days the pastes were demoulded and the top 10mm of each sample was removed using a Cambridge micro-slice 2 diamond saw. The cut surface of each cylinder was then lightly ground on 600 grade carbide paper.

Each sample cylinder was then coated with a 2-3mm layer of paraffin wax excepting the cut surface which was to be exposed to an aqueous saline environment.

The specimens were then immersed in 1M sodium chloride in 0.034M sodium hydroxide for between 60 and 80 days. The saline solution was replaced by a fresh batch of the same type after 30 days.

Following the requisite exposure period the waxed cylinders were retrieved and the wax removed (by scraping). The cylinders were then sectioned into 7mm thick discs taken along the axis of each cylinder from the cut face.

2.2.3 EMBEDDED STEEL CORROSION INVESTIGATION

Three series of paste specimens were prepared for a corrosion behaviour investigation; the mix proportions of which are detailed in Table 2.4 (overleaf).

The levels of chloride addition investigated (0.4 and 1.0% by total mass of solids) were selected because site investigations in the UK have shown that the risk of chloride induced corrosion

developing in OPC concrete structures is generally low for total chloride contents below 0.4% by weight of the cement and high for total chloride contents in excess of 1.0% by weight of the cement [21].

It was not possible to rotate the cement paste samples produced for this investigation due to the protruding electrodes. The selection of a low water:solids ratio of 0.4 was intended to minimise segregation.

The pastes were prepared as described in Section 2.2. Into the tops of the moulds were inserted a pair of mild steel rod electrodes. Prior to immersion the rods had been centre drilled to a depth of at least 1cm. They were then degreased by washing in Tepol and rinsed successively with deionised water and AR grade acetone. Their surfaces were then abraded with grade 600 carbide paper and again rinsed (in a sonic bath) with AR grade acetone.

SERIES	%MK 501	W:S RATIO	%CHLORIDE
A	0	0.4	0/0.4/1.0
B	10	0.4	0/0.4/1.0
C	20	0.4	0/0.4/1.0

TABLE 2.4
COMPOSITION OF PASTE SPECIMENS
FOR CORROSION INVESTIGATION

After the surface preparation procedure the electrodes were placed in a desiccator over silica gel for 48 hours to allow the development of a fresh oxide layer. The rods were then weighed and masked with a white cement-styrene butadiene rubber layer on to which was coated cold-curing epoxy resin. Wire connections were made by crimping a steel ring onto the end of each wire which was then screwed in place. The connections were protected by a white cement-SBR paste coating which was

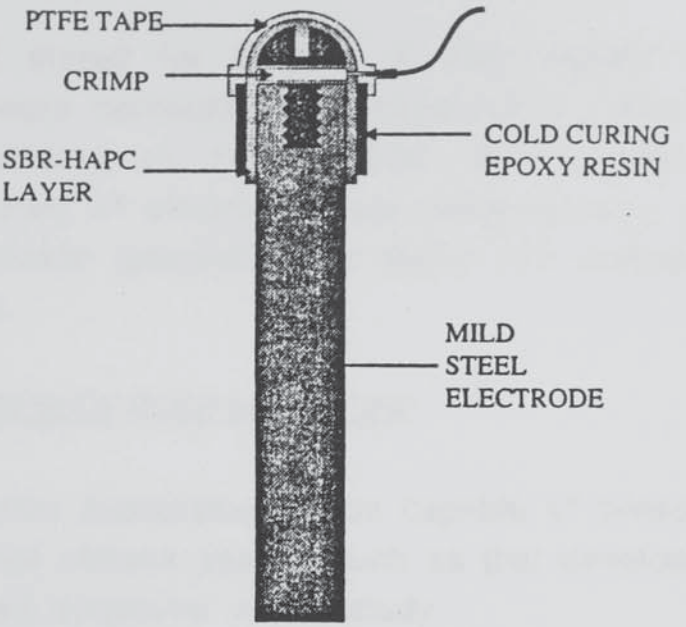

FIGURE 2.1
MASKED MILD-STEEL ELECTRODE

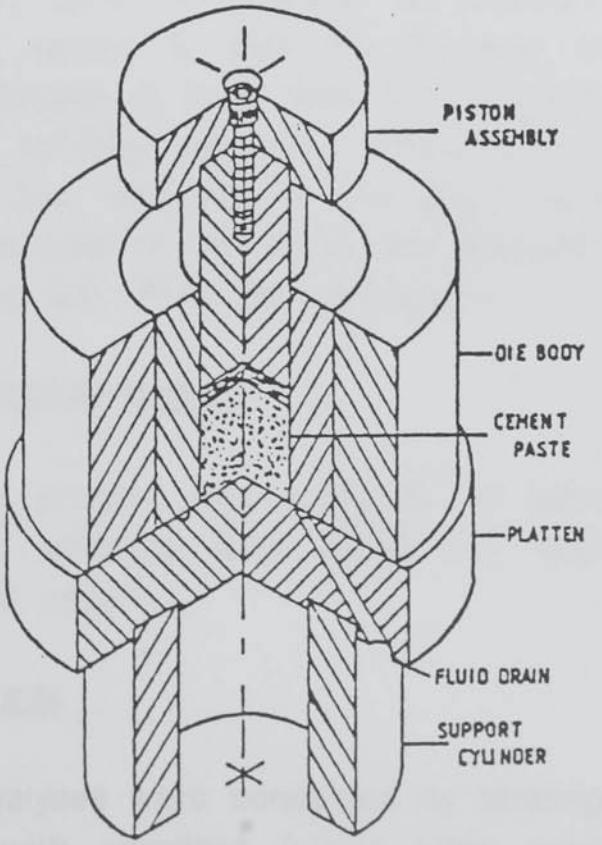

FIGURE 2.2
PORE SOLUTION EXPRESSION DEVICE

bound with PTFE tape. An electrode of this type is depicted in Figure 2.1.

After being stored for 7 days in their sealed containers the specimens were demoulded and exposed to saturated (i.e. 100% relative humidity) air at 22 $\pm$2°C. During the following 27 weeks, a series of electrochemical measurements was conducted on quadruplicate specimens for every mix composition detailed in Table 2.4.

2.3 EXPRESSION OF PORE SOLUTIONS

A pore solution expression device capable of pressing pore fluids from hardened cement pastes, such as that developed by Longuet et al. [5], was employed in this study.

The device consisted of a purpose built pressure vessel, piston assembly and platten with fluid drain as depicted in Figure 2.2. Cement paste samples were placed into the die and a PTFE frit inserted between piston and sample. As pressure was increased the PTFE disc spread to seal the diameter of the die body preventing the escape of liquid other than through the fluid drain. The expressed solution was then collected in a polypropylene sample tube. The portions of the pore press, after each expression, were cleaned with water and acetone and the mating surfaces sprayed with PTFE for lubrication.

2.4 PORE SOLUTION ANALYSES

Expressed pore solution was analysed for sodium, potassium, hydroxide, and chloride ions using the standard methods described in this section.

2.4.1 HYDROXYL ION

Hydroxyl ion analyses were conducted by titrating 100μl aliquots of pore fluid with standard 0.01M nitric acid from a 20μl

graduated burette using phenolphthalein indicator. pH values were calculated according to the following expression:

$$pH = 14 + \log_{10}[OH^-]$$

2.4.2 CHLORIDE ION

Chloride ion concentrations were determined by a spectrophotometric method. Chloride ions displace thiocyanate ions in solution, which, in the presence of iron (III) ions form a charge transfer complex (maximum absorption 460 nm) possessing an high extinction coefficient.

$$2Cl^- + Hg(SCN)_2 + 2Fe^{3+} \rightarrow HgCl_2 + 2Fe(SCN)^{2+}$$

The intensity of the colour is related to the chloride ion concentration.

2ml of iron (III) ammonium sulphate in 9M nitric acid and 2ml of saturated mercury (II) thiocyanate were added to 10ml aliquots of suitably diluted pore solution. The colours of the solutions were then allowed to develop for ten minutes before absorption readings were made using a Beckman model-24 spectrophotometer. Chloride ion concentrations were then estimated from the calibration curve shown in Figure 2.3 which was constructed from chloride standards.

2.4.3 SODIUM AND POTASSIUM IONS

Sodium and potassium ion concentrations were determined using a Jenway PFP 7 flame photometer.

Intensity measurements were made for suitably diluted solutions of pore liquid. The solutions were drawn into the flame photometer through a catheter and then sprayed over flame. When ionic species are burned in a flame, light of characteristic frequencies is emitted as excited electrons relax into lower energy states. A different filter for each ion type positioned

between the flame and detector enabled a certain frequency of that characteristic light to pass through for detection. The intensity measurements were then translated into concentration values using a coefficient determined by standards. A linear relationship between concentration and intensity reading exists for solutions of lower dilution than 7ppm.

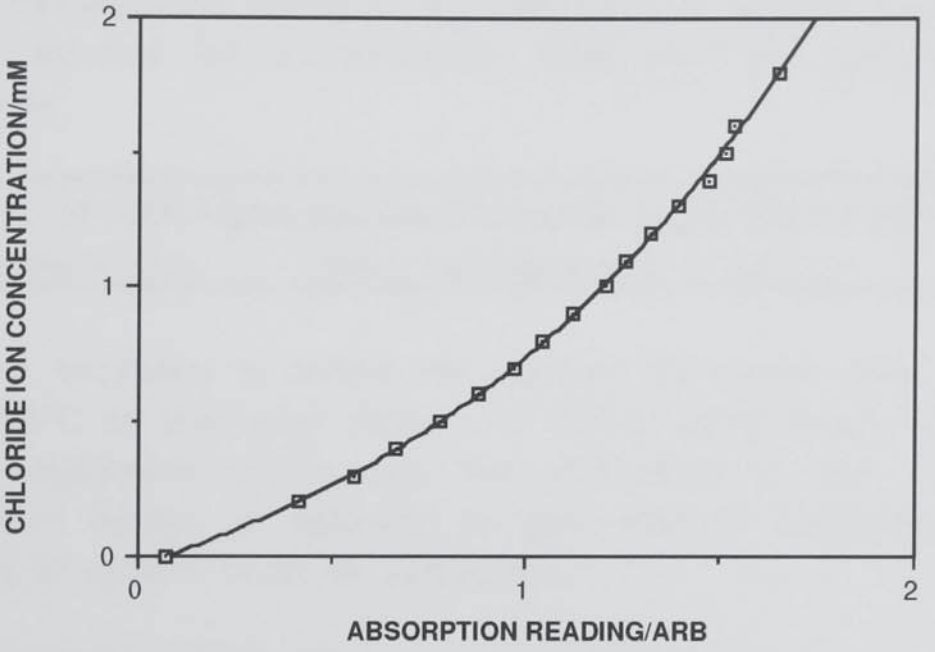

FIGURE 2.3
CHLORIDE ION CALIBRATION CURVE

2.5 TOTAL CHLORIDE CONCENTRATION DETERMINATION

For the construction of chloride diffusion profiles it was necessary to determine the total chloride concentration at intervals along the lengths of samples subjected to chloride penetration (see Chapter 5).

Cement paste discs were ground in a ball mill and graded through a 150μm sieve. The ground pastes were then oven dried at 105°C for 24 hours to remove the unbound water. 0.5 - 0.7 grammes of the powder, in each case, was accurately weighed and placed in a 200ml beaker. Approximately 10ml of deionised water was added

prior to 8ml of concentrated nitric acid (to dissolve the cement). A further 50ml of deionised water was added before the mixture was boiled and filtered through grade 1 filter paper into a volumetric flask (either 250 or 500ml). The filtrate was washed a number of times to minimise the proportion of chloride ions remaining in both the filtrate and filter paper. The solution was then made up to its standard volume and subjected to chloride ion concentration analysis (as described in Section 2.4.2). The total chloride ion concentration could then be calculated as follows:

$$\text{TOTAL CHLORIDE CONCENTRATION} = \frac{\text{TOTAL NUMBER OF MOLES OF CHLORIDE IN SOLUTION}}{\text{EQUIV. MASS OF SAMPLE AT 950°C (g)}} \text{ (mM)}$$

It was necessary to correct the mass of the sample after heating to 105°C to that after heating to 950°C using evaporable and non-evaporable water data (as described in the following Section) before an estimate of total chloride concentration in mM/g of cement could be calculated.

2.6 EVAPORABLE AND NON-EVAPORABLE WATER

In order to allow ionic species, such as chlorides, to be expressed as the total amount present as a fraction of the unhydrated cement paste it is necessary to determine the quantities of bound and unbound water present in the cement.

The distinction between evaporable (unbound) and non-evaporable (bound) water is arbitrary although the demarcation between evaporable and non-evaporable water is usually based on the loss of water upon drying at 105°C [22].

The method employed, in this study, to determine the quantities of bound and unbound water is as follows:

Approximately 4 grammes of cement paste were accurately weighed into a platinum crucible. The sample was then heated to constant weight at 105°C in an oven to remove the evaporable

water. The sample was then ignited at 950°C in a muffle furnace for 30 minutes. After cooling to room temperature, in the presence of silica gel to minimise rehydration, the sample was reweighed.

On ignition the cement sample undergoes a small loss in mass (ignition loss). This ignition loss was accounted for according to the British Standard method [23] whereby approximately 1 gramme of accurately weighed unhydrated cement was heated at 950°C for 30 minutes. The ignition loss was then converted into a percentage of the original mass.

The evaporable and non-evaporable water were then calculated as shown below:

$$\text{EVAPORABLE WATER (\%)} = \frac{M_O - M_{105}\,(100\text{-LOI+AD})}{M_{950}}$$

$$\text{NON-EVAPORABLE WATER (\%)} = \frac{M_{105}(100\text{-LOI+AD}) - M_{950}(100+\text{AD})}{M_{950}}$$

where

M_O is the mass of hydrated cement paste sample (grammes)

M_{105} is the sample mass at 105°C (grammes)

M_{950} is the sample mass at 950°C (grammes)

LOI is the loss-on-ignition (% grammes/gramme of cement)

AD is the admixture total (% grammes/gramme of cement)

As shown by the above relationships, consideration must also be made for the presence of admixtures such as sodium chloride and metakaolin.

Worked examples and results tables of evaporable and non-evaporable water and worked examples of total chloride determinations are located in Appendices 1, 2 and 3 respectively.

2.7 ANALYSIS OF THE SOLID PHASE

The two main techniques employed in this study for the investigation and identification of components of the solid phase are Differential Thermal Analysis and Nuclear Magnetic Resonance Spectroscopy.

2.7.1 PREPARATION OF SAMPLES FOR SOLID STATE ANALYSIS

For the analysis of the solid phase it was necessary to stop hydration at requisite periods by the removal of the pore solution. This may be achieved in many ways, for example, by freeze drying or heating in a vacuum oven (which causes a notable ageing in young (one and seven days) samples). Dehydration by solvent exchange was selected as the optimum method as it is an inexpensive and effective process which is believed to have negligible effect on the solid phase [24,25,26].

Samples were demoulded and broken into portions of approximately 5mm diameter. The portions were then immersed in approximately ten times their own volume of propan-2-ol and subjected to ultrasound. After ten minutes the supernatant liquor was decanted away and replaced with fresh propan-2-ol. The process was repeated five times. The sample portions were then dried in a vacuum desiccator after remaining in their final washings overnight. Dried samples were stored in a desiccator containing a self-indicating silica gel and 'Carbosorb', a self-indicating carbon dioxide absorbant.

2.7.2 DIFFERENTIAL THERMAL ANALYSIS

All thermoanalytical curves were obtained from a Stanton Redcroft 673-4 Differential Thermal Analyser.

Prior to analysis the cement paste samples were subject to solvent exchange drying (as described in the previous Section, 2.7.1). For each analysis a small quantity of sample was ground by mortar and pestle and sieved to 150μm. The sample was then transferred to a rhodium-platinum crucible which was seated over a thermocouple in the furnace of the DTA. A calcined alumina reference material (inert over the temperature range used) was also positioned over a second thermocouple inside the DTA furnace. Both materials were then heated at a rate of 20°C per minute to a maximum temperature of 950°C.

During heating the alumina reference and cement paste can be considered to be at the same temperature provided no thermal decomposition occurs in the cement sample. If a thermal change does occur (e.g. decomposition of CSH gel) thermal energy is absorbed or emitted by the sample. The majority of thermal reactions of OPC-based samples are endothermic dehydration reactions in which energy is required to decompose a certain phase. During such reactions the temperature of the sample falls to below that of the reference material and that temperature difference is detected and plotted on a chart recorder. This forms the basis of Differential Thermal Analysis.

2.7.3 NUCLEAR MAGNETIC RESONANCE SPECTROSCOPY

All NMR spectra were obtained from a Brucker A.C. Multinuclear Spectrometer. Magic Angle Spinning (MAS) silicon (^{29}Si) spectra were measured at 59.65MHz with rotor spin speeds of 4 and 4.2kHz. The silicon chemical shifts were expressed in ppm with reference to tetramethylsilane. Solid state aluminium (^{27}Al) spectra were measured at 78.20MHz with rotors spinning at 4.8 and 5.5kHz. The aluminium chemical shifts were expressed in ppm with reference to the aluminium hexaquo ion.

Acknowledgement of the nuclear magnetic resonance phenomenon began at the turn of the century when it was discovered that the hyperfine structure of electronic spectra could be attributed to the magnetic properties of the nucleus. NMR has been employed as a spectroscopic technique for about 40 years although its applications in the field of cement and concrete research didn't begin until the early 1980s (excepting proton NMR) with the advent of more sophisticated systems. A brief theory of the origin and mechanisms of NMR may be found in Akitt [27].

The requirement for a nucleus to be NMR active is the possession of a nuclear spin quantum number (QN) not equal to zero. Such species may be considered to possess the property of 'spin' and hence have associated magnetic moments. When subject to an applied magnetic field these give rise to a set of energy levels. A Boltzmann population distribution occurs with a small excess of nuclei in the lowest energy level. When energy in the radio frequency region is applied to the system transitions between these energy levels occur. For a given nucleus the energy level separation is dependent on its chemical environment. Hence a specific radio frequency will stimulate a particular transition. It is for this reason that species which differ chemically appear in different regions of the NMR spectrum.

Continuous wave NMR usually involves a fixed radio frequency and a scanning magnetic field. In FT NMR (as used in this study) all nuclei are stimulated by a broad band radio pulse and their (time dependent) relaxation is monitored. Background noise is averaged to zero and signal enhancement obtained by a repetition of this process. The relaxation information is then transformed into a frequency spectrum by use of the Fourier Transform.

Species having spin QN $^1/_2$ are in some ways preferred as higher values lead to line broadening and distortion of the signals due to the non spherical distribution of nuclear charge (quadrupole effects). Nuclei of importance in cement and concrete research are ^{1}H, ^{13}C, ^{27}Al, ^{29}Si.

2.8 PORE SIZE DISTRIBUTION INVESTIGATIONS

The pore size distributions of OPC pastes were compared with those of metakaolin-blended systems using a Micrometrics Instrument Corporation porosimiter model 9310.

Approximately 3 grammes of cement paste sample, which had previously been subject to solvent exchange drying, were broken into 5mm diameter portions and accurately weighed. The sample was then placed in a glass cell which was seated in the porosimeter and evacuated to remove gases and any residue liquid. A low pressure nitrogen gas intrusion run was then conducted and the information stored on computer. The glass vessel was then transferred to the high pressure port whereupon it was filled with mercury and subjected to increasing pressure. The quantity of mercury required to refill the vessel at a certain pressure is related to that volume which has penetrated a certain size of pores. As the pressure increased the pore size penetrated decreased. The high pressure intrusion data was also stored on computer.

The computer program then applied the Washburn equation (shown below) to calculate the pressure at which the mercury entered the pores of a given size [28],

$$\text{APPLIED PRESSURE} = -\frac{4\gamma \cos\theta}{d}$$

where

γ is the surface tension of the mercury (N/m)

θ is the contact angle between the mercury and the pore walls of the sample (degrees)

d is the pore diameter (μm)

Pore size distribution profiles do not accurately represent the exact pore size distribution for the following reasons:

Damage to the microstructure may occur during sample preparation.

Pores having narrow openings undergo intrusion at a pressure corresponding with that entrance diameter. This phenomenon is known as the ink-bottle effect and causes an over-estimation of the volume of small pores.

Damage may also be caused to the fine pore structure as a result of the high pressures required to intrude samples.

Due to the heterogeneous nature of cement paste there is no specific contact angle between that and a contacting liquid.

Some pores may prove too fine to intrude.

Despite obvious shortcomings this technique provides a useful and convenient means of comparing the microstructures of different cement types.

2.9 CORROSION MONITORING BY LINEAR POLARISATION

The linear polarization technique (also referred to as polarization resistance) is a well documented method of measuring corrosion intensities of embedded steel in cement and concrete [29,30]. An E.G. and G./P.A.R.C. model 350 microprocessor was employed in this study to carry out this technique.

Embedded steel reinforcements (and any other metal specimens) "in service" assume a potential, relative to a standard electrode, known as the corrosion potential, E_{CORR}. Anodic and cathodic regions exist on the surface of the material although no net current flows. Hence E_{CORR} may be defined as the potential at which the rates of oxidation and reduction are equal.

A sample may be polarised (i.e. forced to assume a potential other than E_{CORR}) in the positive (anodic) direction by an applied potential causing the anodic current to predominate at the expense of the cathodic current. As the specimen potential is driven further positive the cathodic component tends to zero. Polarisation in the negative (cathodic) direction causes the converse to occur.

The technique of linear polarization was performed by the application of a controlled potential scan over a small range, in this case ±10mV (at a scan rate of 10mV per minute) with respect to the corrosion potential E_{CORR}.

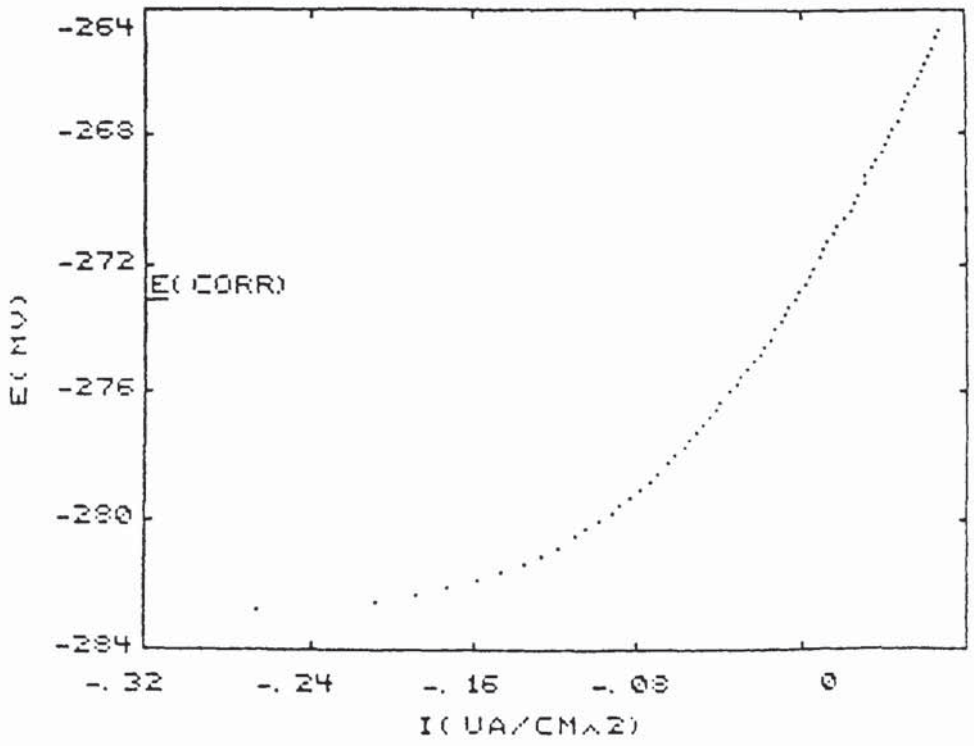

FIGURE 2.4
A TYPICAL LINEAR POLARISATION PLOT OBTAINED FROM THE P.A.R.C. MICROPROCESSOR

The gradient of the linear plot of applied potential difference against corresponding current at E_{CORR} represents the Polarization Resistance, Rp (Ohms Law), which was employed together with the Tafel Constants to determine the corrosion current, i_{CORR} (Figure 2.4).

At E_{CORR} the measured current i_{MEAS} is given by the following relationship:

$$i_{MEAS} = i_{CORR} - i_{RED} = 0 \quad \text{.....(vii)}$$

where i_{RED} is the cathodic current.

If the system is subject to an applied potential the rate of corrosive reaction can be expressed by the following activation energy relationships [31]:

$$i_R = i_{CORR}\, e^{-\eta/\beta`} \quad \text{.....(viiia)}$$

$$i_O = i_{CORR}\, e^{+\eta/\beta``} \quad \text{.....(viiib)}$$

where i_R and i_O are the cathodic and anodic currents respectively, $\beta`$ and $\beta``$ are constants and η is the difference between the applied potential and E_{CORR}. Taking logs and solving for η yields the following expressions:

$$\eta = -\beta_c \log (i_R / i_{CORR}) \quad \text{.....(ixa)}$$

$$\eta = +\beta_a \log (i_O / i_{CORR}) \quad \text{.....(ixb)}$$

where βc (= 2.3 $\beta`$) and βa (= 2.3 $\beta``$) are the Tafel constants.

The Tafel constants are characteristic of a particular system and may be obtained by a potential scan of a few hundred millivolts either side of E_{CORR}.

Tafel scans are, however, destructive hence in this study the generally accepted Tafel constant for mild steel embedded in cement paste of 120mV was adopted [29].

Stern and Geary [31] related the rate of change of the applied 'overvoltage' with respect to the 'applied' cathodic current and the relationships (ixa) and (ixb) yielding the following expression:

$$Rp = \Delta E/\Delta I = \beta_a\beta_c/\{2.3\ (i_{CORR})\ (\ \beta_a + \beta_c\ )\}.....(x)$$

The above relationship is referred to as the Stern-Geary equation and is used to calculate corrosion currents which are not obtainable by direct measurement.

Values of i_{CORR} for various corroding systems are representative of their corrosion rates and were used to assess the influence of metakaolin on the corrosion behaviour of embedded steel.

2.10 ENERGY DISPERSIVE X-RAY ANALYSIS

Energy dispersive X-ray analysis was conducted on small (2-3mm dia.) crystals which were seen to form in pore solution samples.

EDXA was obtained using a Cambridge S90B scanning electron microscope with a Link Systems (Oxford Analytical) energy dispersive X-ray analyser.

2.11 ATOMIC ABSORPTION SPECTROPHOTOMETRY

The concentration of chromium II ions in pore solution samples was determined by atomic absorption spectrophotometry using a Perkin Elmer 372 Atomic Absorption spectrophotometer. The pore solutions of 7 day OPC samples containing 1.0% chloride ions were pale blue. They were believed to contain the chromium II ion in low concentration. The presence of this ion was confirmed by atomic absorption spectrophotometry.

The basis of these and most other atomic absorption measurements is that the absorbance is directly proportional to the concentration of atoms in the cell (Beer's law). (The cell is that component of the spectrophotometer which is used to convert polyatomic samples into atoms and retains those atoms for a sufficiently long period such that the radiation may impinge on them.) For given conditions the concentration of atoms in the cell is proportional to the concentration of the element in the sample solution.

Chromium ion concentration values were determined by the use of standards. The absorbencies of four chromium standards were measured and the concentration of the sample solutions were estimated using the ratios of absorbence to concentration obtained by using the standards.

CHAPTER 3 THE PORE SOLUTION CHEMISTRY OF METAKAOLIN-BLENDED ORDINARY PORTLAND CEMENT PASTE SYSTEMS

3.1 INTRODUCTION

When modelling the behaviour of a cementitious system in an attempt to allow the prediction of environmental impact on its durability and hence, service life, the pore solution phase is an important area of assessment since the composition of the electrolyte influences the chemical reactions occurring in the cement matrix.

An example of this is the alkali aggregate reaction (AAR). AAR is the collective term for reactions between alkaline pore solution and certain reactive types or constituents of aggregates in mortars and concretes producing a gel which imbibes water and expands. Volume expansion of cementitious systems may cause cracking and failure in service. The specific roles of pore fluid components in alkali aggregate reactions remain a topic of investigation and debate although the importance of the degree of alkalinity of the pore solution is established [32]. Research into the effect of metakaolin in relation to AAR is not undertaken in this study although other workers have reported a reduction in the extent of AAR in metakaolin-blended systems [33]. This reduction is attributed to a decrease in pore solution hydroxide ion concentrations of metakaolin-blended systems as a consequence of pozzolanic reaction.

It is through the pore electrolyte phase that the ingress of deleterious species often occurs (although macro-fissures and mix contamination may also be responsible for the presence of contaminants). For example, diffusion of aqueous chloride species (Chapter 5) through the pore system in steel reinforced concretes may result in corrosive failure. The threshold chloride ion concentration required to initiate corrosion is largely dependent on the pore solution hydroxyl ion concentration [34]. Other physical factors are important and will be considered in Chapter 6.

BS 8110 : Part 1 : 1985 restricts the levels of 'internal' chlorides in concretes to the range 0.1% - 0.4% by weight of cement. The recommended concentration is dependent on the cement type. The 'chloride binding capacity' of a cement is its ability to bind free chloride ions in the cement matrix. Chloride ions are primarily bound in OPC in an insoluble form as calcium chloroaluminate hydrate $C_3A.CaCl_2.10H_2O$, Friedel's salt, a substance derived from tricalcium aluminate. Carbonation may lead to reinforcement corrosion by causing the release of a proportion of chloride ions, bound in this way, into the pore fluid as well as reducing the pore solution hydroxide ion concentration.

Page et al. [35] report that additions of silica fume to cement pastes reduce, not only the pore solution pH, but also the chloride binding capacity of the system. This latter phenomenon is attributed to the reduction in alkalinity of the pore fluid which causes the dissolution of Friedel's salt according to the following equilibrium:

$$3CaO.Al_2O_3.CaCl_2.10H_2O \rightleftharpoons 4Ca^{2+} + 2AlO_2^- + 4OH^- + 2Cl^- + 8H_2O$$

However Tritthart reports that decreases in pore solution pH result in increases in the extent to which chloride ions are bound in the solid phase [36].

Rasheeduzzafar et al. [37] found that 10 to 20% additions of replacement silica fume to OPC contaminated with 0.6 and 1.2% chloride ions more than doubled the free chloride ion concentration of the pore solution relative to that of the unblended specimens. Al-Amoudi et al. [38] compared the free chloride ion concentrations of expressed pore solution of unblended cement paste and paste containing 10% replacement silica fume. Similarly, a greater than two-fold increase in the free chloride ion concentration of the pore solution of the blended cement paste with respect to that of its unblended counterpart was noted. However, in contradiction with these observations Byfors et al. [39] report an increase in chloride

binding capacity of silica fume cement pastes with respect to that of OPC.

An increase in chloride binding capacity of blast furnace slag cement relative to that of unblended OPC was observed by Andrade and Page [40]. Similar findings have also been reported by Hussain [41] and Al-Amoudi et al. [38]. It is believed that the superior sorptive properties of the CSH gel of blast furnace slag cements is largely responsible for the enhanced exclusion of chloride ions from the pore solution phase. A number of workers have also reported increases in the chloride binding capacities of cements blended with pulverised fuel ash [41,42]. However, a moderate reduction in the chloride binding capacity of pastes containing 0.6% chloride ions blended with 20% pulverised fuel ash has also been reported [38].

Longuet et al. [5], in a study of OPC hydration, found that the hydroxyl, sodium and potassium ion concentrations increased to maximum values between 7 and 28 days. The calcium ion concentration at three and five hours was approximately 0.02M although diminished to 0.003M after two days and below the limit of detection after a few months. (The level of alkalinity arising from the presence of sodium and potassium is believed to depress the solubility of calcium such that the pore solution pH is effectively maintained by the alkali metal ions [44].) Of the samples studied it was found that the sulphate ion concentration was appreciable in the first few hours although became a trace constituent after one day. Periodic increases in sulphate levels between 0.01M and 0.02M occurred between seven days and six months.

The principal release of alkalis into the pore solution occurs by the dissolution of sodium and potassium sulphates from the anhydrous cement. Calcium and sulphate ions are released into the solution phase from gypsum. Some calcium hydroxide, liberated in the initial hydration reactions, also dissolves in the pore fluid. Reaction then occurs between the sulphate and calcium species and tricalcium aluminate which yields the

calcium sulphoaluminate product, ettringite. The removal of calcium and sulphate ions from the solution phase was therefore attributed to the precipitation of ettringite.

Glasser and Marr [44] analysed the expressed pore solution of 30, 90 and 180 day OPC and high alkali Portland cement samples blended with 15% additions of microsilicas, pulverised fuel ashes and blast furnace slag. All samples (of water:solids ratio 0.6) released the majority of their alkali into the pore fluids within 30 days. The role of slag (at this level of replacement) in the removal of alkali from the pore fluid solutions was reported to be 'neutral'.

The microsilicas appeared to cause a general reduction in pore solution alkali levels even after complete physical consumption. Two hypotheses are proposed to explain this phenomenon. It is believed that an increase in silica in the calcium silicate hydrate gel formed in microsilica blends results in superior sorptive properties leading to an enhanced 'uptake' of calcium, sodium and potassium ions. It is also suggested that an increase in silica in the CSH gel promotes the precipitation of alkali containing compounds.

Even though PFA-blended cements also possess CSH gel with an high proportion of silica, they were seen to be less effective in the removal of alkali from the pore solution phase due to the relatively large release of alkali from the PFA itself. It should be noted that the results of this investigation were obtained before a 'steady state' for the PFA systems was established.

Canham et al. [45] studied the effects of four PFAs (of different states of division and pozzolanicity) and three GBFSs (representing different methods of manufacture) on the alkalinity of the pore solution phase of cement pastes of water:solids ratio 0.45. Each replacement material differed in total alkali content. Pore solutions were expressed at 28, 84, 168 and 365 days.

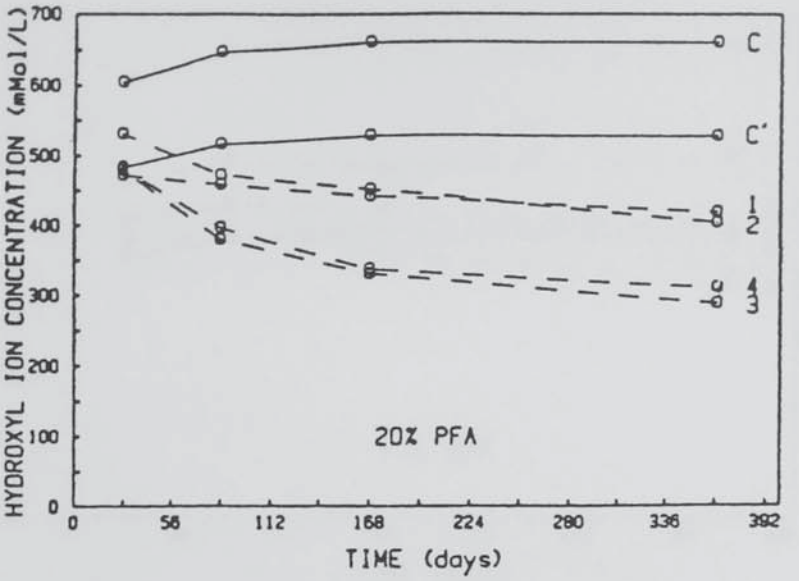

FIGURE 3.1

PORE SOLUTION HYDROXYL ION CONCENTRATIONS OF OPC (C), BLENDED PASTES CONTAINING 20% VARIOUS PFAs (1,2,3,4) AND 20% HYPOTHETICAL CEMENT OF ZERO ALKALI CONTENT (C'). AFTER CANHAM [45]

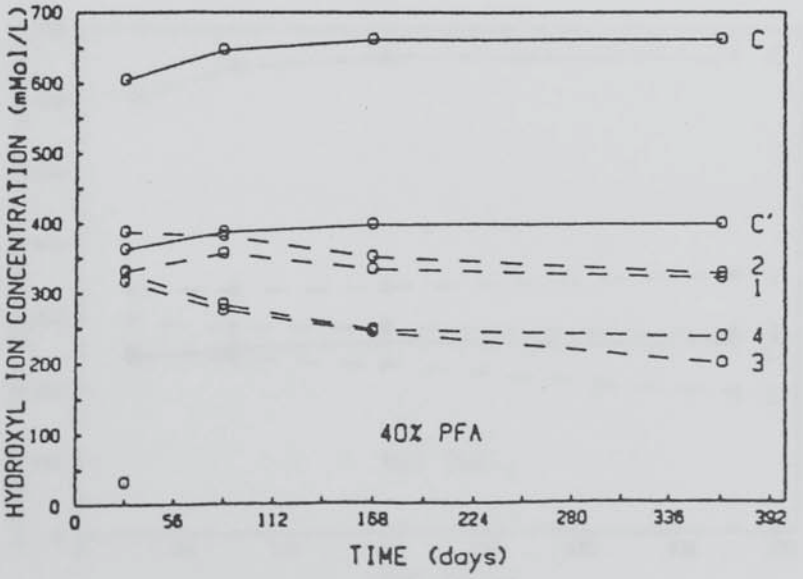

FIGURE 3.2

PORE SOLUTION HYDROXYL ION CONCENTRATIONS OF OPC (C), BLENDED PASTES CONTAINING 40% VARIOUS PFAs (1,2,3,4) AND 40% HYPOTHETICAL CEMENT OF ZERO ALKALI CONTENT (C'). AFTER CANHAM [45]

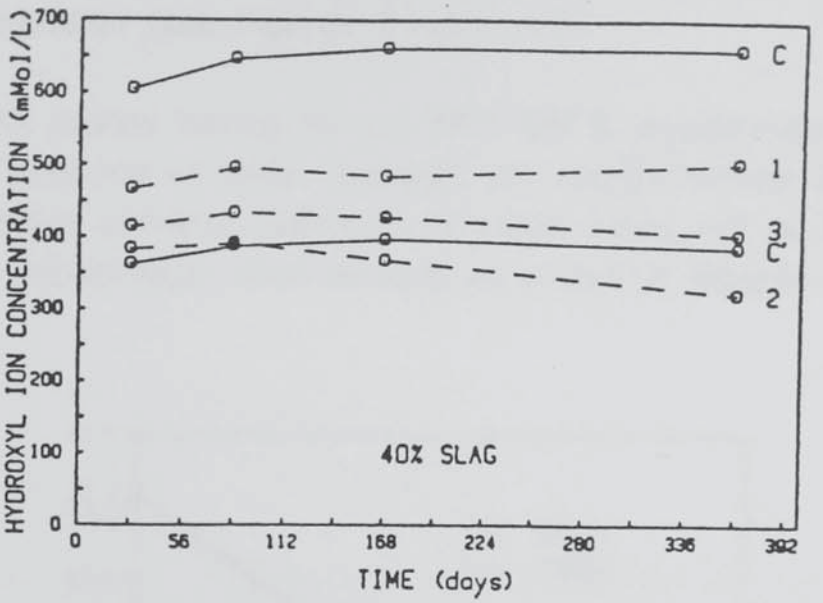

FIGURE 3.3

PORE SOLUTION HYDROXYL ION CONCENTRATIONS OF OPC (C), BLENDED PASTES CONTAINING 40% VARIOUS GBFSs (1,2,3) AND 40% HYPOTHETICAL CEMENT OF ZERO ALKALI CONTENT (C'). AFTER CANHAM [45]

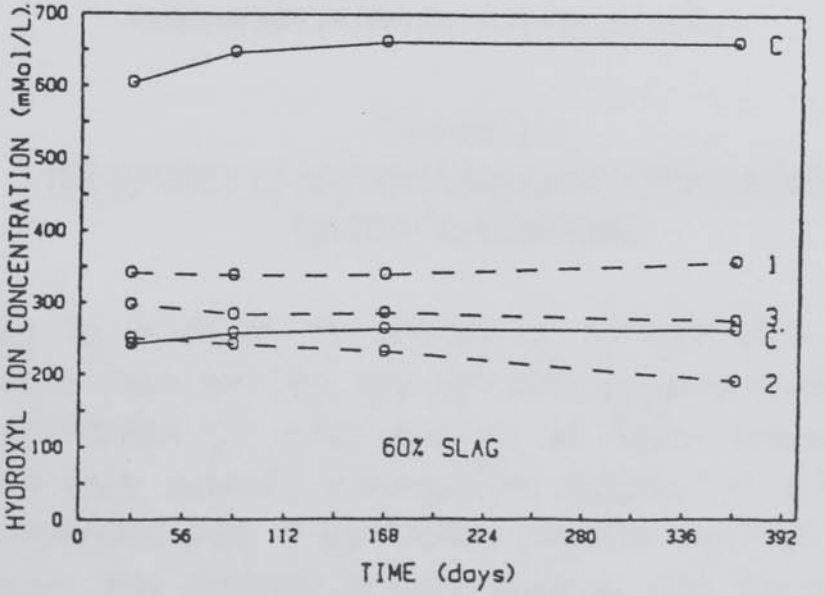

FIGURE 3.4

PORE SOLUTION HYDROXYL ION CONCENTRATIONS OF OPC (C), BLENDED PASTES CONTAINING 60% VARIOUS GBFSs (1,2,3) AND 60% HYPOTHETICAL CEMENT OF ZERO ALKALI CONTENT (C'). AFTER CANHAM [45]

The hydroxyl ion concentrations of cement paste samples having 20 and 40% replacement PFA were found to decrease with increasing time and level of replacement. State of division and total alkali content were found to influence the hydroxyl ion concentration (see Figures 3.1 and 3.2).

Cement pastes having 40 and 60% GBFS replacement gave rise to pore solutions of lower hydroxyl ion concentrations than those of unblended cements (although in some cases not as low as those of an hypothetical, inert diluent) as shown in Figures 3.3 and 3.4.

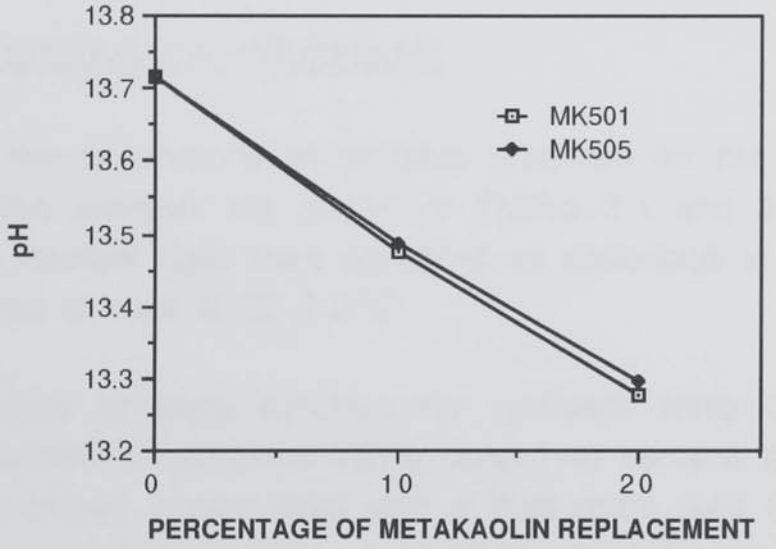

FIGURE 3.5
THE EFFECT OF METAKAOLIN ON PORE SOLUTION pH
(28 DAY SPECIMENS)

A study to establish the effects of 10 and 20% replacement metakaolin (both MK 501 and MK 505) on pore solution alkalinity was undertaken by other workers at Aston University shortly after the pore solution investigations reported in this thesis had been conducted [46]. It was noted that the effect of incorporating metakaolin into cements of high, medium and low alkalinity was to decrease the concentrations of pore solution hydroxide ions. The resultant pH drop was not believed to be sufficiently significant to cause concern about the depassivation of reinforcing steel. The pore solution pH values of 28 day samples

(prepared from medium alkali cement of water:solids ratio 0.5, cured at 22 ± 2°C) are represented in Figure 3.5.

An investigation into the effect of metakaolin additions on the pore fluid hydroxide ion concentration of OPC pastes has been conducted in this study employing both MK 501 and MK 505 metakaolin. The concentrations of sodium and potassium ions have also been monitored. Pore solutions extracted from samples containing various levels of internal chloride ions, introduced via the mix water, were subject to chloride ion concentration analysis to give a qualitative indication of the relative chloride binding capacities of metakaolin-blended and plain OPC pastes.

3.2 EXPERIMENTAL PROCEDURE

The mix proportions of samples prepared for the purpose of pore solution analysis are shown in Tables 3.1 and 3.2. Duplicates of each sample type were prepared as described in Section 2.2 and allowed to cure at 22 ± 2°C.

Samples of pore solution for analysis were obtained by the application of pressure (MPa range) to cement paste samples in an enclosed vessel fitted with a fluid drain (see Section 2.3). The magnitude and duration of pressure are believed to have a minor influence on the composition of the expressed pore solution although satisfactory agreement of results has been obtained by other workers employing this method of pore fluid extraction [45,46].

Conventional laboratory techniques of solution analysis were then conducted to determine the concentration of hydroxyl, chloride, sodium and potassium ions. The relevant methods of pore solution extraction and ion analysis are described in Sections 2.3 and 2.4 respectively. pH values were calculated from the hydroxide ion concentrations in accordance with the relationship in Section 2.4.1.

%MK	% CHLORIDE	W:S RATIO	AGE {DAYS}
0	0,0.1,0.4,1.0	0.5	1,7,36,100
10	0,0.1,0.4,1.0	0.5	1,7,36,100
20	0,0.1,0.4,1.0	0.5	1,7,36,100

TABLE 3.1
MIX PROPORTIONS OF OPC SAMPLES FOR PORE SOLUTION ANALYSIS BLENDED WITH MK 501 METAKAOLIN

%MK	% CHLORIDE	W:S RATIO	AGE {DAYS}
0	0,1.0	0.5	1,7,36,100
10	0,1.0	0.5	1,7,36,100
20	0,1.0	0.5	1,7,36,100

TABLE 3.2
MIX PROPORTIONS OF OPC SAMPLES FOR PORE SOLUTION ANALYSIS BLENDED WITH MK 505 METAKAOLIN

3.3 RESULTS

Figures 3.6 and 3.7 indicate the pore solution pH values for ordinary Portland cement paste, 10 and 20% metakaolin-blended pastes and ordinary Portland cement paste blended with 10 and 20% hypothetical cement of zero alkali content (C'). C' plots have been calculated as 90 and 80% of the total pore solution alkali concentration of the unblended OPC paste. They are intended to represent the effect of 10 and 20% additions of an hypothetical, inert diluent (which neither removes nor contributes to the alkali content of the pore solution).

Figures 3.8 to 3.11 depict the expressed pore solution chloride ion concentrations for paste samples containing 0.1, 0.4 and 1.0% internal chloride ions (by weight of total solids).

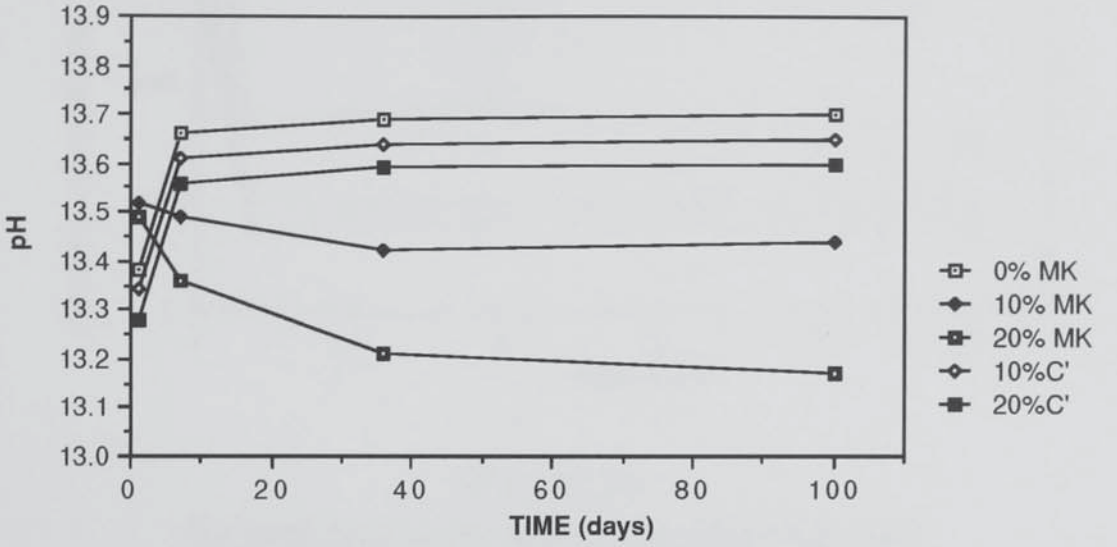

FIGURE 3.6
THE EFFECT OF ADDITIONS OF MK 501
ON PORE SOLUTION pH

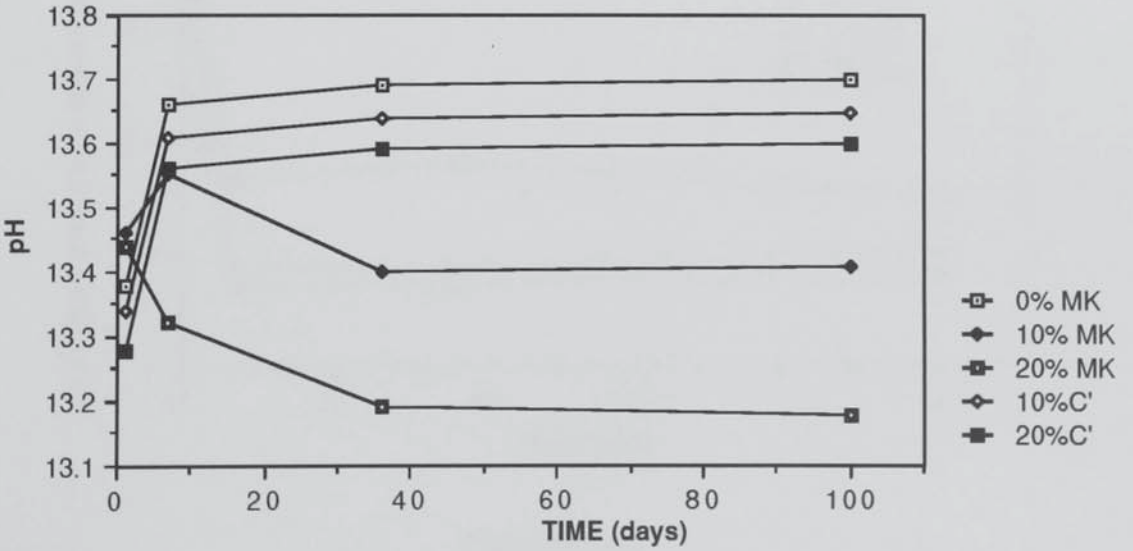

FIGURE 3.7
THE EFFECT OF ADDITIONS OF MK 505
ON PORE SOLUTION pH

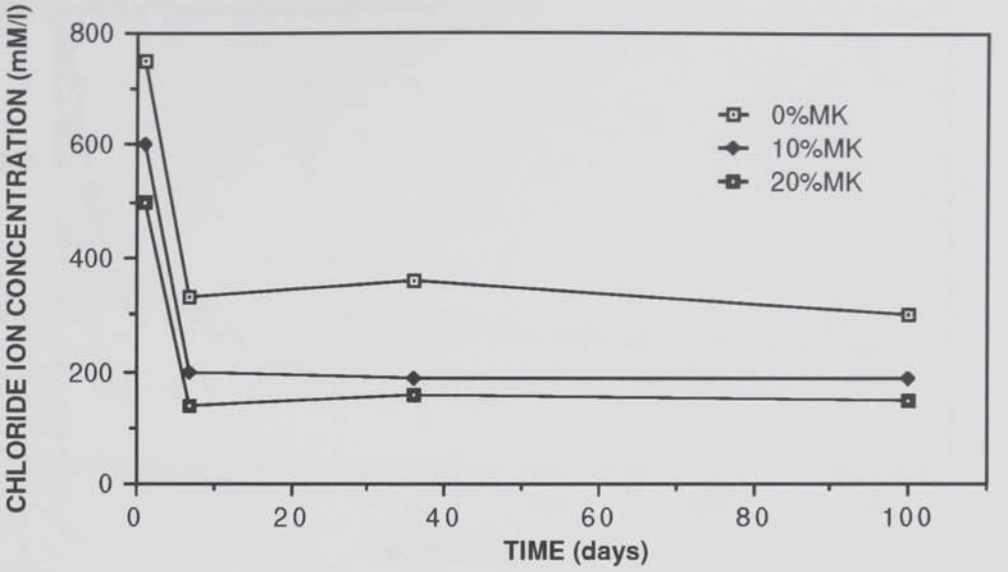

FIGURE 3.8

THE EFFECT OF MK 501 ADDITIONS ON PORE SOLUTION CHLORIDE CONCENTRATIONS FOR SAMPLES CONTAINING 1.0% INTERNAL CHLORIDE (BY WEIGHT OF TOTAL SOLIDS)

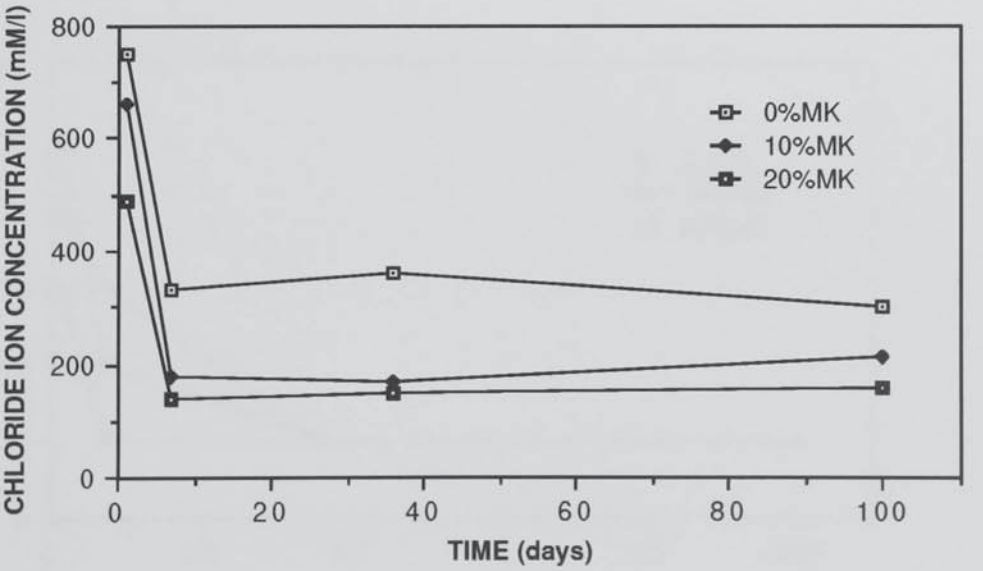

FIGURE 3.9

THE EFFECT OF MK 505 ADDITIONS ON PORE SOLUTION CHLORIDE CONCENTRATIONS FOR SAMPLES CONTAINING 1.0% INTERNAL CHLORIDE (BY WEIGHT OF TOTAL SOLIDS)

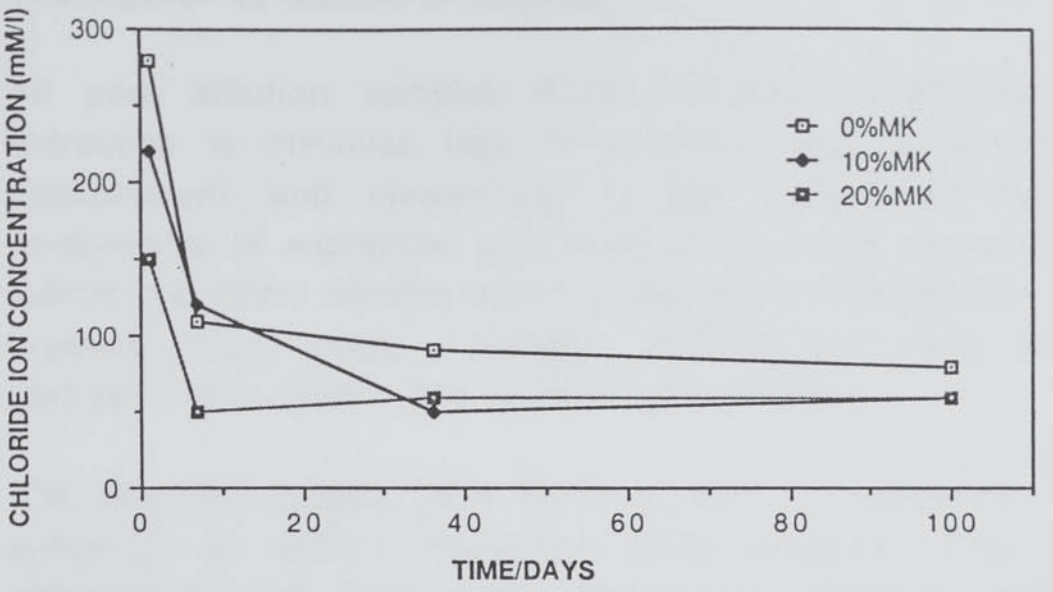

FIGURE 3.10

THE EFFECT OF MK 501 ADDITIONS ON PORE SOLUTION CHLORIDE CONCENTRATIONS FOR SAMPLES CONTAINING 0.4% INTERNAL CHLORIDE (BY WEIGHT OF TOTAL SOLIDS)

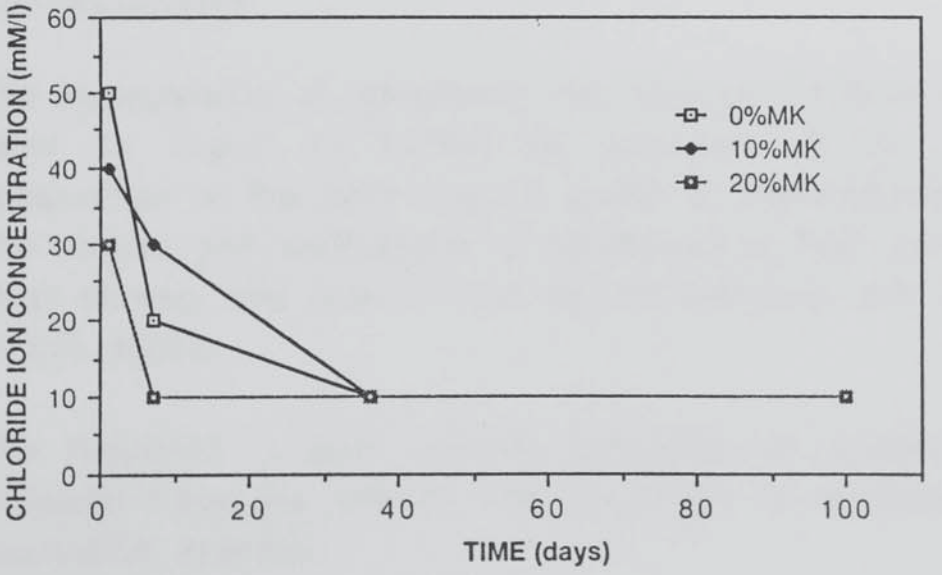

FIGURE 3.11

THE EFFECT OF MK 501 ADDITIONS ON PORE SOLUTION CHLORIDE CONCENTRATIONS FOR SAMPLES CONTAINING 0.1% INTERNAL CHLORIDE (BY WEIGHT OF TOTAL SOLIDS)

A complete suite of results obtained in the pore solution investigation is located in Appendix 4.

All pore solution samples were analysed immediately after extraction to minimise loss of alkalinity (due to atmospheric carbonation) and inaccuracy; it was discovered that the components of expressed pore fluid formed small (approximately 0.5mm diameter) crystals within a few hours of collection. Such crystals, from three unblended, chloride-free pore solution samples, were filtered and washed with ethanol.

The resulting crystals were found to vary in composition when subjected to energy dispersive X-ray analysis. Their major constituents were found to be calcium and potassium, with trace quantities of sulphur, silicon, aluminium and sodium.

The seven day unblended samples containing 1.0% chloride ions yielded pale blue coloured pore solutions which were believed to contain the chromate II ion in low concentration. The presence of this ion was confirmed by atomic absorption analysis.

3.4 DISCUSSION

The incorporation of metakaolin into ordinary Portland cement is seen to result in substantial changes in the chemical composition of the pore solution phase of the hydrated product. The origins and implications of reductions in both pore solution alkali content and free chloride ion concentration are considered in this section.

The reduction in pore solution hydroxide ion concentration in metakaolin-blended cement paste systems is attributed to the pozzolanic reaction.

Pozzolanically blended cements contain an higher proportion of CSH gel than do their unblended counterparts as a consequence of reaction between portlandite and the siliceous pozzolan. A relative increase in the proportion of silicon present in the CSH

gel (of blended systems) often results in a greater sorption (uptake) of alkali metal (sodium and potassium) ions from the pore solution [44,45] . The loss of alkali metal ions from the pore solution phase obviously results in a decrease in alkalinity (due to the loss of the counter ion which is associated with the hydroxide ion). It is to this mechanism that the reduction in pH of the pore electrolyte of metakaolin-blended cements may be attributed.

When blended with OPC (having medium alkali content), it has been found that, both MK 501 and MK 505 metakaolin varieties are capable of reducing pore solution pH to a greater extent than would be expected if they were to behave as a cement of zero alkalinity (see Figures 3.6 and 3.7). Hence, the observed reduction in hydroxide ion concentration for metakaolin-blended systems is known to be the consequence of pozzolanic reaction and is not a simple dilution effect owing to the effective increase in water:cement ratio for blended systems. The difference in behaviour of the two metakaolin types with respect to pore solution pH modification is minimal.

As mentioned in the introduction to this chapter, modification of the pore solution alkalinity is believed to be an important factor in controlling expansion associated with AAR. The reduction in pore solution pH exhibited by metakaolin-blended systems, reported here, compares favourably with that of the PFAs and is superior to that of the GBFSs in a study by Canham et al. although is not as great as that found for silica fume [35,37,45].

The second notable effect resulting from the presence of metakaolin in OPC specimens is the progressive increase in the extent to which chloride ions, introduced via the mix water, are excluded from the pore solution phase (see Figures 3.8 - 3.11).

Long term chloride ion concentrations of the pore solution phase of systems containing 0.1% 'internal' chloride ions (by weight of total solids) were found to be approximately 0.01 $moldm^{-3}$ irrespective of the metakaolin content (Figure 3.11).

Unblended samples containing 0.4 and 1.0% 'internal' chloride ions were found to have retained a notably higher proportion of chloride ions in the pore solution phase when compared with the metakaolin-blended samples of the same age (see Figures 3.8 - 3.10). This difference is particularly marked for samples which contain 1.0% 'internal' chloride ions. Thus it is demonstrated that metakaolin-blended systems possess an enhanced chloride binding capacity. The possible methods of binding of chloride ions in metakaolin-blended OPC pastes is discussed further in Section 4.6.

Additions of sodium chloride resulted in increases in the pore solution pH values (relative to those of the uncontaminated specimens) of the plain and metakaolin-blended pastes (see Appendix 4). These increases in alkalinity are attributed to the higher concentrations of sodium ions in the pore solution of the contaminated samples. In contrast, Rasheeduzzafar et al. [37] found that additions of sodium chloride to OPC pastes blended with silica fume tended to cause a relative reduction in the hydroxide ion concentration of the pore fluid.

The actual mechanisms by which chloride ions interact with steel in the formation of pits are not currently known although the ratio of free chloride to hydroxide ions present in the pore solution is established as an important parameter in the corrosion of embedded steel reinforcements [34]. This ratio is interrelated with other physical factors specific to each system considered (e.g. 'critical' pit depth, oxygen availability, concentrations of Fe^{2+}, $FeOH^{+}$, H^{+} etc.) and therefore may not be used as a rigorous corrosion index. However, low values of the $[Cl^{-}]/[OH^{-}]$ ratio are generally associated with passive steel since the concentration of chloride ion relative to that of hydroxide ion must be sufficiently large to cause pitting (in the absence of other major corrosion-promoting factors). A more detailed explanation of the corrosion behaviour of embedded steel reinforcements is located in Chapter 6.

Hausmann [43] proposed a critical $[Cl^-]/[OH^-]$ ratio of 0.6 based upon mild steel corrosion tests in concrete-simulated $Ca(OH)_2$ solution of pH 12.5. A critical ratio of this kind is not applicable to embedded steel in concrete owing to the influence of other factors (as described above).

Reference to Table A4.25 (located in Appendix 4) indicates that the values of the $[Cl^-]/[OH^-]$ ratio for 1 day samples exhibit the following trend: 0% MK > 10% MK > 20% MK. As the samples matured further (up to 100 days) the extent of the reduction in pH of the metakaolin-blended systems was such that this trend was generally reversed although all values were of the same order of magnitude. After 100 days the $[Cl^-]/[OH^-]$ ratios for plain OPC and 10% MK 501- and MK 505-blended pastes containing 1.0% chloride ions were 0.41, 0.43 and 0.38 respectively. The pore solutions of pastes of the same age and level of chloride addition blended with 20% MK 501 and MK 505 possessed $[Cl^-]/[OH^-]$ ratios of 0.56 and 0.52 respectively. The $[Cl^-]/[OH^-]$ ratios for plain, 10 and 20% replacement MK 501 pastes containing 0.4% chloride ions were 0.13, 0.19 and 0.27 respectively. The moderate increases in the values of $[Cl^-]/[OH^-]$ ratio for metakaolin-blended samples is not believed to be sufficiently significant to suggest that depassivation of reinforcing steel in metakaolin-blended samples is more likely to occur when compared with that of unblended OPC. This postulate and other affecting factors are discussed in Chapter 6.

Rasheeduzzafar et al. [37] report that 10% replacement silica fume results in a 4 to 5 fold increase in the $[Cl^-]/[OH^-]$ ratio. (This investigation was carried out on 180 day OPC pastes of water:solids ratio 0.6 cured at 20°C containing 0.6 and 1.2% chloride ions by mass of solids.) 77 and 39 fold increases in the $[Cl^-]/[OH^-]$ ratio (for 0.6 and 1.2% chloride additions respectively) were reported for pastes blended with 20% silica fume.

A 10 fold increase in the $[Cl^-]/[OH^-]$ ratio of the pore fluid of pastes blended with 10% silica fume was also reported by Al-

Amoudi et al. [38]. (The pore fluids in this investigation were expressed from 80 day old pastes of water:solids ratio 0.6 containing 0.6% chloride ions by total mass of solids.) In the same paper the $[Cl^-]/[OH^-]$ ratio of a 60% blast furnace slag cement (0.209) is reported to differ from that of the unblended paste (0.202) by less than 4%. The incorporation of 20% replacement pulverised fuel ash (class F) in cement paste was found to result in a greater than 2 fold increase in the ratio. Kayyali et al. [42] also found that 30% replacement (class F) PFA caused up to 2 fold increases in the $[Cl^-]/[OH^-]$ ratio of pore fluid expressed from mortars of varying ages and levels of sodium chloride contamination.

It is not possible to make a direct comparison between the effect of metakaolin and the other pozzolans reported in the literature on the $[Cl^-]/[OH^-]$ ratio owing to the differences in cement types (especially in C_3A and alkali content), curing times and regimes, proportions of replacement pozzolan and levels of chloride ion addition. Although, in general, it is suggested that additions of metakaolin to OPC are unlikely to result in the striking increases in $[Cl^-]/[OH^-]$ ratio that are associated with additions of silica fume. It also appears that metakaolin replacement is likely to cause similar increases in $[Cl^-]/[OH^-]$ ratio to those observed with replacement by (class F) PFA. However the presence of blast furnace slag investigated by Al-Amoudi et al. [38] is seen to have a moderately more favourable effect on chloride binding and $[Cl^-]/[OH^-]$ ratio than does metakaolin.

Obviously, due to the number of variables which influence pore solution chemistry, the comparisons made here between the effects of metakaolin and other pozzolans on $[Cl^-]/[OH^-]$ ratio may not apply in all circumstances.

It should be noted that all results presented in this investigation and those reported from the literature pertain to OPC pastes (or mortars) which have been contaminated with sodium chloride. Cation effects and the concomitant presence of chloride ions and

other aggressive agents (e.g. sulphates) are not considered here but are known to influence pore solution composition [38,40,42].

CHAPTER 4 A SOLID STATE INVESTIGATION OF METAKAOLIN-BLENDED ORDINARY PORTLAND CEMENT PASTE SYSTEMS

4.1 INTRODUCTION

The importance of solid state investigations into the cementitious matrix is without question since the durability of cementitious constructions is dependent on the chemical and mechanical properties of that matrix.

The diffusion and permeation of aggressive agents through the cement matrix are important areas of study since, in service, many cementitious systems are exposed to highly corrosive environments wherein they are subject to attack; for example, the penetration of chloride ions may result in the corrosion of embedded steel (see Chapter 6). The resistance of any system to failure of this nature requires the modification of the cementitious matrix such that the rate of diffusion of aggressive agents is reduced and the cement is able to 'tolerate' chlorides once contamination has occurred (if all other physical parameters are to remain the same).

Improved chloride binding capacity is one of a number of matrix factors including water:cement ratio, curing time and conditions, porosity, pore size distribution, pore geometry and the interconnectivity of the pores which affect the resistance to attack from chloride ions (and other aggressive agents).

It has already been noted that metakaolin-blended OPC pastes exhibit properties of improved chloride binding when compared with their unblended counterparts (Section 3.4). Some property of the blended matrix is seen to enhance the existing process whereby chloride ions are removed from the pore electrolyte phase and immobilised. It may prove possible to identify and usefully exploit this 'property' in the production of superior quality steel reinforced structures, in which, the likelihood of corrosive failure is reduced. This is just one illustration of the importance of solid state investigations.

Porosity and pore size distribution of the cementitious matrix are fundamentally important to the behaviour of many structures in service since it is through these channels, via the pore solution electrolyte, that substances, potentially deleterious to the structures, may enter. Fully hydrated cement paste comprises a distribution of pores of varying dimensions (both size and geometry) which influence the diffusion and permeation of species into the matrix from the immediate environment. It is obviously favourable to limit the rate of ingress of aggressive agents (such as sulphates and chlorides) in all cementitious constructions although particular control over porosity and pore size distribution is required in the design of marine and highway structures where chloride ions and aggressive de-icing salts are in significant concentration.

'Gel pores' and 'capillary pores' possess diameters of the orders of nm and μm respectively. Incomplete compaction may also result in the presence of macroscopic voids a few millimetres in diameter. It is the capillary pores which provide the major diffusion 'routes' along which deleterious substances penetrate the cementitious matrix during exposure to corrosive and otherwise harmful environments. Net porosity and proportion of capillary pores in 'fully' hydrated cement pastes decrease as the water:cement ratio is reduced [47]. Low water:cement ratios have a favourable effect on both strength and porosity.

Porosity (and again strength) and pore size distribution may be further modified by the addition of pozzolanic extenders. Diminished permeability of metakaolin-blended cement paste systems has already been documented by Bijen and Larbi [11] who discovered that the rates of water absorption of mortar samples containing 10 and 20% metakaolin were substantially reduced compared with those of similarly hydrated plain OPC mortar samples.

In the same paper Bijen and Larbi [11] report the enhanced compressive strength development of 10 and 20% metakaolin-

blended OPC mortars compared with that of unblended OPC (of water:cement ratio 0.4).

Bredy et al. [15] also found the pore structure of blended systems containing 10 and 20% metakaolin (by weight of cement) to be "more discontinuous and finer than that of plain cement pastes" in a mercury porosimetry study. (A brief synopsis of mercury intrusion porosimetry, MIP, is given in Section 2.8.) It is noted that MIP provides a satisfactory means for assessing the "larger pore system", i.e. the capillary pores which have "significant influence on durability" despite the limitations of the technique. However, the authors have compared samples of differing water:cement ratios, as indicated by the following:

OPC	100%	90%	80%
W/S	0.25	0.28	0.34

The authors attribute this reduction in porosity to the 'filler effect' of the relatively fine particles of metakaolin occupying the interstital volumes between cement particles. Irrespective of the increase in water:cement ratio with increase in metakaolin substitution (which would, if anything, cause an increase in the total porosity) a reduction in total porosity is observed.

The mercury intrusion porosimetry technique has been utilised in this study to compare the pore size distributions of 7 and 100 day (10 and 20%) metakaolin-blended OPC pastes with those of unblended samples. Results of this investigation are reported in Section 4.3.

Along with knowledge of porosity and pore size distribution it is often useful to be aware of the major hydration products of cementitious systems for the purposes of comparison and development. Two techniques, Differential Thermal Analysis (DTA) and Nuclear Magnetic Resonance Spectroscopy (NMR) have been employed here in the analysis of the solid state. Outlines of

both techniques are given in Sections 2.7.2 and 2.7.3 respectively.

The products of reaction between various proportions of calcium hydroxide, water, and metakaolin were investigated by Murat [10] using DTA. The results of the DTA investigation were supported by evidence obtained from the X-ray diffraction technique.

A similar, preliminary, X-ray diffraction investigation into the products of metakaolin-blended cement hydration was conducted as part of the research contained in this thesis although it has not been reported for the following reasons. It was found that signals from the highly crystalline portlandite dominated the diffractograms. Another problem with this application of X-ray diffraction is the 'overlapping' of a number of the reflections of the calcium aluminate hydrate species, gehlenite, and calcium silicate hydrate gel. An example of this is given below:

COMPOUND	d SPACING
C_4AH_{13}	2.81Å
C_2ASH_8	2.87Å
CSH_I	12.5Å
C_2ASH_8	12.58Å

TABLE 4.1

THE SIMILARITIES OF d SPACINGS OF SOME CEMENT CONSTITUENTS

Murat [10] observed the formation of CSH gel, hydrated gehlenite, and minor quantities of tetracalcium aluminate as shown by the endothermic peaks (at 120°C, 180-200°C, and 260°C respectively) in Figure 4.1.

Although not discussed in the paper, the sharp endothermic peaks positioned in the 500°C region signify the decomposition of (the

residual) calcium hydroxide [48] which are seen to diminish in intensity as the hydration reaction proceeds.

No mention is given of the endothermic peaks at 800°C nor the exothermic peaks in the 900°C region. However in the following paper of the series [49] Murat compared the hydration products of three different calcium hydroxide-activated metakaolin samples and observed that the magnitude of the exothermic peak at 930°C increased in accordance with increases in CSH gel content (as shown in Figure 4.2). The samples studied differed only in the quality (i.e. purity) of metakaolin used.

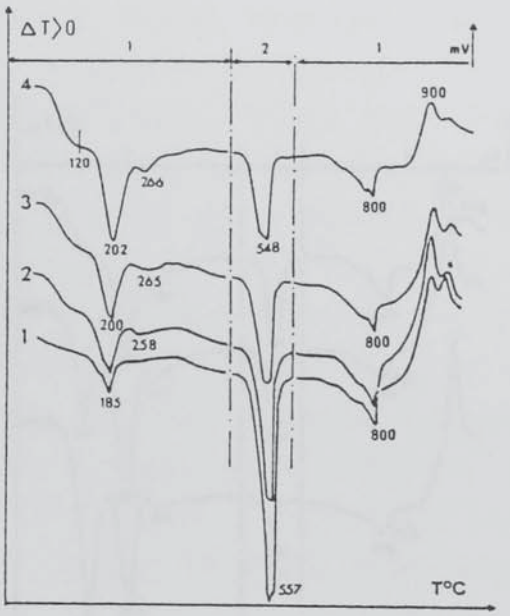

FIGURE 4.1
DTA CURVES OF HYDRATION PRODUCT OF MK-CH MIXTURE
AT 3 (CURVE 1), 7 (CURVE 2), 15 (CURVE 3)
AND 28 (CURVE 4) DAYS (AFTER MURAT [10])
(SENSITIVITY REDUCED BY A FACTOR OF TWO IN THE CENTRE REGION)

In the third paper of the series [50] the peaks occurring in the 900°C region are assigned to CSH_I gel (as classified by Taylor

[51]) and the peaks in the 800°C region were attributed to small quantities of calcite (calcium carbonate).

In research undertaken in this thesis differential thermal analysis has been carried out on 1, 7, 36 and 100 day (0, 10 and 20%) metakaolin-blended OPC pastes in an attempt to assess the hydration products of pozzolanic reaction. A similar suite of specimens containing 1.0% 'internal' chloride ions by weight of total solids were also subject to the same analysis.

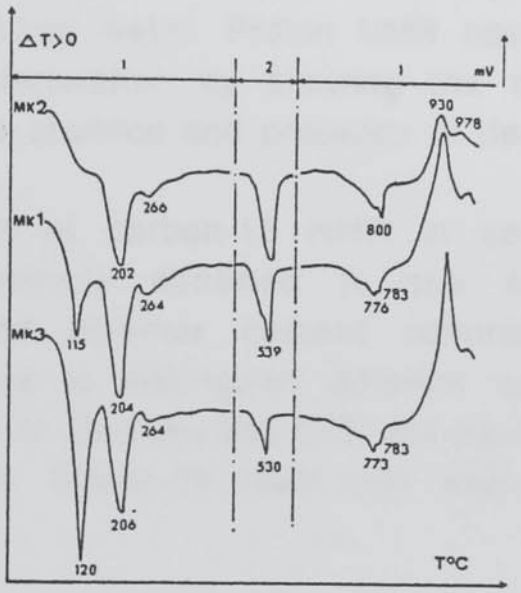

FIGURE 4.2
DTA CURVES OF HYDRATION PRODUCT OF MK-CH MIXTURE FOR THREE DIFFERENT METAKAOLIN TYPES MK1, MK2, MK3. (AFTER MURAT [10])
(SENSITIVITY REDUCED BY A FACTOR OF TWO IN THE CENTRE REGION)

Nuclear magnetic resonance spectroscopy has been utilised for approximately forty years although was not employed as an analytical tool in cement and concrete research until the 1980s (with the exception of proton NMR) [52]. The development of Fourier Transform NMR allows the collection of spectra (possessing high signal to noise ratios) of many 'NMR-active' nuclei of low natural abundance without enrichment. Silicon-29 (^{29}Si) is one such isotope with a natural abundance of approximately 4.7% (and a nuclear spin quantum number of $^1/_2$). This is to the advantage of cement chemistry since two of the major phases in anhydrous cement, C_3S and C_2S, contain this element. Other important nuclei in this field are the proton, carbon-13, and aluminium-27.

Cementitious hydration studies have been conducted using a complicated method called 'spin-grouping' proton NMR [53,54]. This allows the differentiation between water in gel pores and physically adsorbed water. Proton NMR has also been used to study frost deterioration by allowing the measurement of ice formation in the absence and presence of de-icing salts [52].

The application of carbon-13 NMR in cement and concrete research is mainly confined to the studies of organic plasticizers and polymer cement concrete. More recently, however, studies to distinguish different carbonate sites from the carbonation of $Ca(OH)_2$ and CSH gel have been performed by carbon-13 NMR. Silicon-29 NMR may also be utilised for this purpose [52].

Aluminium and silicon NMR have been selected for this study as they are capable of yielding information on the products of cement hydration with experimental ease and without the need for complicated data analysis.

Aluminium has only one naturally occurring isotope possessing an atomic mass of 27 and a nuclear spin quantum number of $^5/_2$. This means that the nucleus possesses an asymmetrical charge distribution. It is a 'quadrupolar' nucleus. For quadrupolar nuclei

the integrals of signals (which are recorded on the spectrum) from species in different chemical environments are not in direct relation to the concentration of those species present. Despite this apparent limitation aluminium NMR can provide information on coordination chemistry. Aluminium often assumes a tetrahedral or octahedral geometry in oxides with occasional five coordinated species. The chemical shift regions of the signals obtained for the various coordinated aluminium species are presented in Table 4.2 [52].

COORDINATION NUMBER	CHEMICAL SHIFT (ppm) w.r.t. $[Al(H_2O)_6]^{3+}$
6	-10 to +20
5	+30 to +40
4	+50 to +80

TABLE 4.2

THE RELATIONSHIP BETWEEN NMR CHEMICAL SHIFT AND COORDINATION NUMBER FOR ALUMINIUM-27

The standard zero chemical shift is obtained from the aluminium hexaquo ion.

Müller et al. [55] observed distinct ranges of aluminium-27 chemical shifts for AlO_4 units in polycrystalline samples depending on the type of neighbouring tetrahedra, TO_4, (T = Al, S and P) and octahedra. Distortion of the AlO_4 tetrahedron and the nature of the second coordination sphere were also considered as possible influences on the chemical shift.

Hjorth et al. [56] studied the hydration of tricalcium aluminate in white portland cement observing the transformation from four- to six-coordinate aluminium as hydration progressed. In a previous study Müller et al. [57] had noted a similar conversion of the coordination state of the aluminium species in an

investigation of the hydration of monocalcium aluminate (the main component of high alumina cement).

Rocha et al. [58] utilised aluminium-27 NMR to study rehydration of metakaolin to kaolin. Signals corresponding to 6-, 5-, and 4-coordinated aluminium were noted for the metakaolin spectrum. The spectrum was obtained using a rotor speed of 4-5 kHz. At this frequency some spinning side bands (peaks which occur as harmonic resonances) interfere with the main spectrum.

As previously stated, silicon-29 possesses a nuclear spin QN of $^1/_2$ and produces spectra with sharp peaks, the intensity ratios of which, are in linear relation to the concentrations of the silicon species from which they arose providing that saturation of the signal does not occur. The origin, consequences, and prevention of signal saturation are discussed at the beginning of Section 4.8.

Lippmaa et al. [59] studied the solid state ^{29}Si NMR spectra of several silicates and found that an isolated silicate tetrahedron (Q^0) gives a different resonance from a system in which two silicate tetrahedra share the same oxygen vertex (Q^1). Silicate species sharing two (Q^2), three (Q^3) and four (Q^4) oxygen vertices were all found to resonate at distinctly different regions of the spectrum, as shown in Table 4.3.

SILICATE	CHEMICAL SHIFT (ppm) w.r.t. T.M.S.
Q^0	-66.0 to -73.5
Q^1	-77.9 to -82.6
Q^2	-86.3 to -87.5
Q^3	-90.4 to -99.3
Q^4	-107.4 to -109.9

TABLE 4.3

THE RELATIONSHIP BETWEEN NMR CHEMICAL SHIFT AND SILICATE-TYPE FOR SILICON-29

The chemical shift is expressed with reference to the signal of tetramethylsilane which is taken to be zero.

Both di- and tricalcium silicate species of anhydrous cement are Q^0. During hydration most of the isolated silicates combine. The degree of hydration of a cement may thus be estimated by comparing the integrals of the Q^0 silicate signals before hydration has occurred and at any given time thereafter [52]. Pozzolanic activity may be determined by a similar method using the signals corresponding to the silicon species of the pozzolan [60].

The technique of cross-polarization may be employed to determine those silicon species having vicinial protons (i.e. those bonded to water, hydroxyl species etc.). The protons are aligned with the applied magnetic field giving order synonymous with that of thermodynamic cooling. Resonating silicon nuclei may then 'relax' (back to their ground state after having absorbed energy in the radio frequency region) by imparting their energy to the protons. Relaxed silicon species may again be brought to resonance. In this way resonance persists, since, should the system become saturated (the maximum possible number of species at resonance) no more absorption would be achieved and consequently the signal would collapse. It is for this reason that signals from species having no vicinial protons do not appear on cross-polarization spectra.

Cross polarization ^{29}Si NMR was used by Rodger et al. [61] to investigate the hydration of C_3S in the presence of accelerating and retarding admixtures. The technique has also been used to study the initial hydration processes of various ß-C_2S samples [62].

All solid state silicon-29 spectra in this study were obtained from the Magic Angle Spinning (MAS) technique. The magnetic fields arising from individual nuclei in solution are averaged to zero (usually) due to the continual translations and rotations of its constituents. In a solid no such averaging is observed and the

magnetic field produced by a nucleus at second nucleus (H_b) at a given distance is related to the angle between the applied magnetic field and the line joining the two nuclei:

$$H_b \alpha (3\cos^2\theta - 1)$$

When θ is 54.74° (the magic angle) H_b is zero and the magnetic interactions between the nuclei are 'cancelled out'. In practice samples are mounted at 54.74° to the main field and spun around this axis giving each internuclear vector a value of zero, thus reducing line broadening. Quadrupole interactions (e.g. those of aluminium-27) are reduced by spinning at an angle although a different angle (usually 30° or 70°) is required for their maximum reduction.

The results of a solid state NMR investigation are reported in Section 4.7. As mentioned above, silicon-29 and aluminium-27 species were selected for study as they are capable of providing information on the products of cement hydration with experimental ease. Silicon-29 and aluminium-27 NMR spectra have been collected for 1, 7, 36, and 100 day samples of water:solids ratio 0.5 containing 0 and 20% metakaolin.

The objectives of this study were to consider the possible identification, by NMR, of changes in the chemical environment of the aluminium species during hydration and to assess the degree of catenation ('polymerisation') of the silicon species in both the OPC and metakaolin as hydration proceeds. Both are important areas of study since aluminium containing species are believed to be associated with the removal of chloride ions from the pore solution and the CSH gel (which is comprised of silicate species) is responsible for the mechanical properties of the system.

4.2 EXPERIMENTAL PROCEDURE

The mix proportions of samples prepared for the purpose of solid state investigation are shown in Table 4.4 below. All samples were produced at a water:solids ratio of 0.5. MK 501 metakaolin was used for all blended systems. Each sample type was prepared according to the method described in Section 2.2 and allowed to cure at 22 $\pm$ 2°C.

%MK	%CHLORIDE	AGE(DAYS)
0	0,1.0	1,7,36,100
10	0,1.0	1,7,36,100
20	0,1.0	1,7,36,100

TABLE 4.4
MIX PROPORTIONS OF OPC SAMPLES FOR SOLID STATE ANALYSIS

To enable the analysis of the solid phase, hydration was stopped by the removal of pore solution by a process known as solvent exchange drying. An outline of this method is located in Section 2.7.1.

4.3 RESULTS OF POROSITY STUDY

Mercury intrusion porosimetry was conducted on 7 and 100 day samples containing 0%, 10%, and 20% metakaolin. The results are presented in graphical form in Figures 4.3 and 4.4.

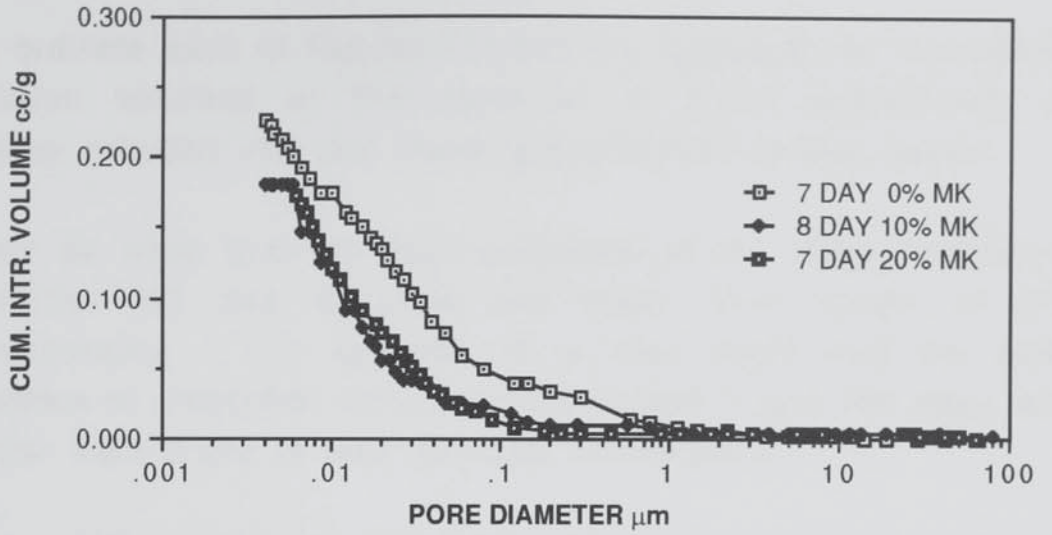

FIGURE 4.3
PORE SIZE DISTRIBUTIONS FOR 7 DAY W:S 0.5 SAMPLES
CONTAINING 0%, 10%, AND 20% METAKAOLIN

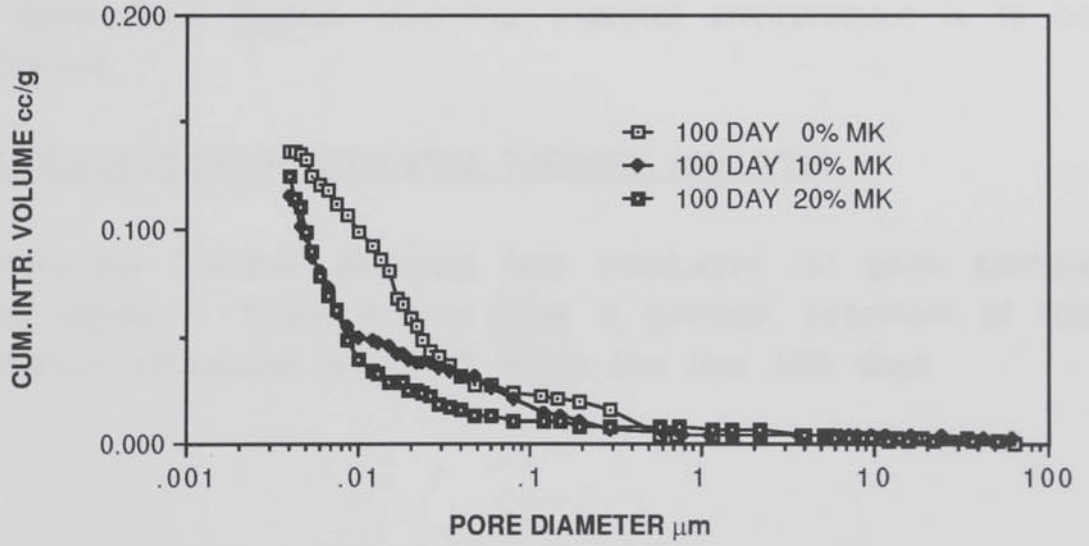

FIGURE 4.4
PORE SIZE DISTRIBUTIONS FOR 100 DAY W:S 0.5 SAMPLES
CONTAINING 0%, 10%, AND 20% METAKAOLIN

4.4 DISCUSSION OF POROSITY RESULTS

The ordinate axes in Figures 4.3 and 4.4 represent the cumulative intrusion volumes of the samples (in cubic centimetres of mercury intruded into unit mass (grammes) of cement paste).

It can be seen that the total porosities of the more thoroughly hydrated 100 day samples are lower than those of the corresponding 7 day samples. It is also noted that the total porosities of unblended OPC samples, of both 7 and 100 days, are greater than those of their blended counterparts.

The porosity profiles for the 8 day 10% metakaolin and the 7 day 20% metakaolin samples are very similar however by 100 days the 10% metakaolin sample possesses a relatively increased proportion of capillary pores in the 0.1 - 0.01 μm diameter region.

Such reduced porosity as is observed for the metakaolin-blended systems is obviously favoured if the restriction of the ingress of deleterious agents from the external environment is to be achieved.

4.5 RESULTS OF DIFFERENTIAL THERMAL ANALYSIS

Differential Thermal Analysis was conducted on each sample type listed in Table 4.4 to give a general overview of the hydration processes occurring within the first 100 days.

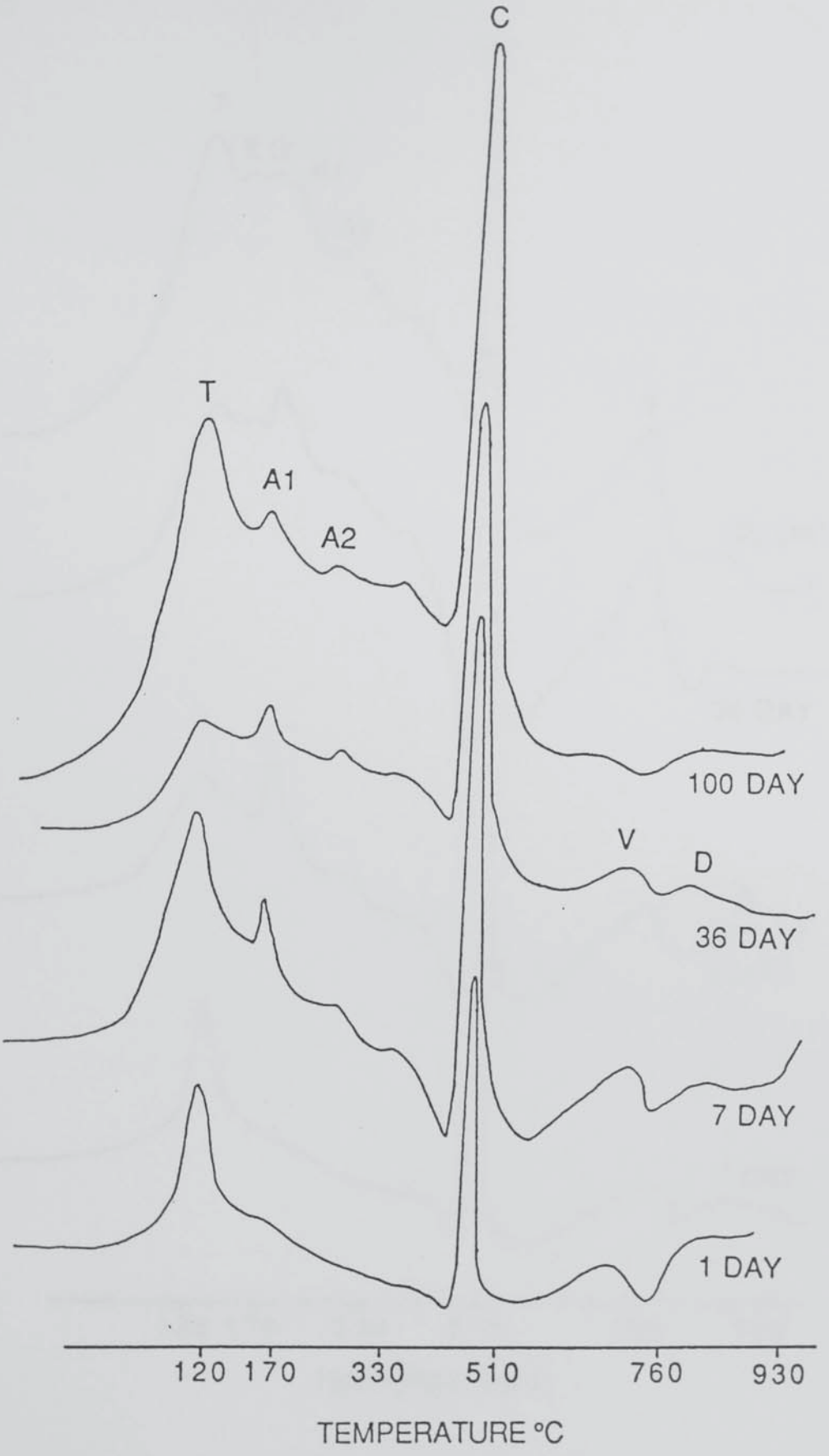

FIGURE 4.5
DTA TRACES OF THE HYDRATION PRODUCTS OF PLAIN OPC OF WATER:CEMENT RATIO 0.5

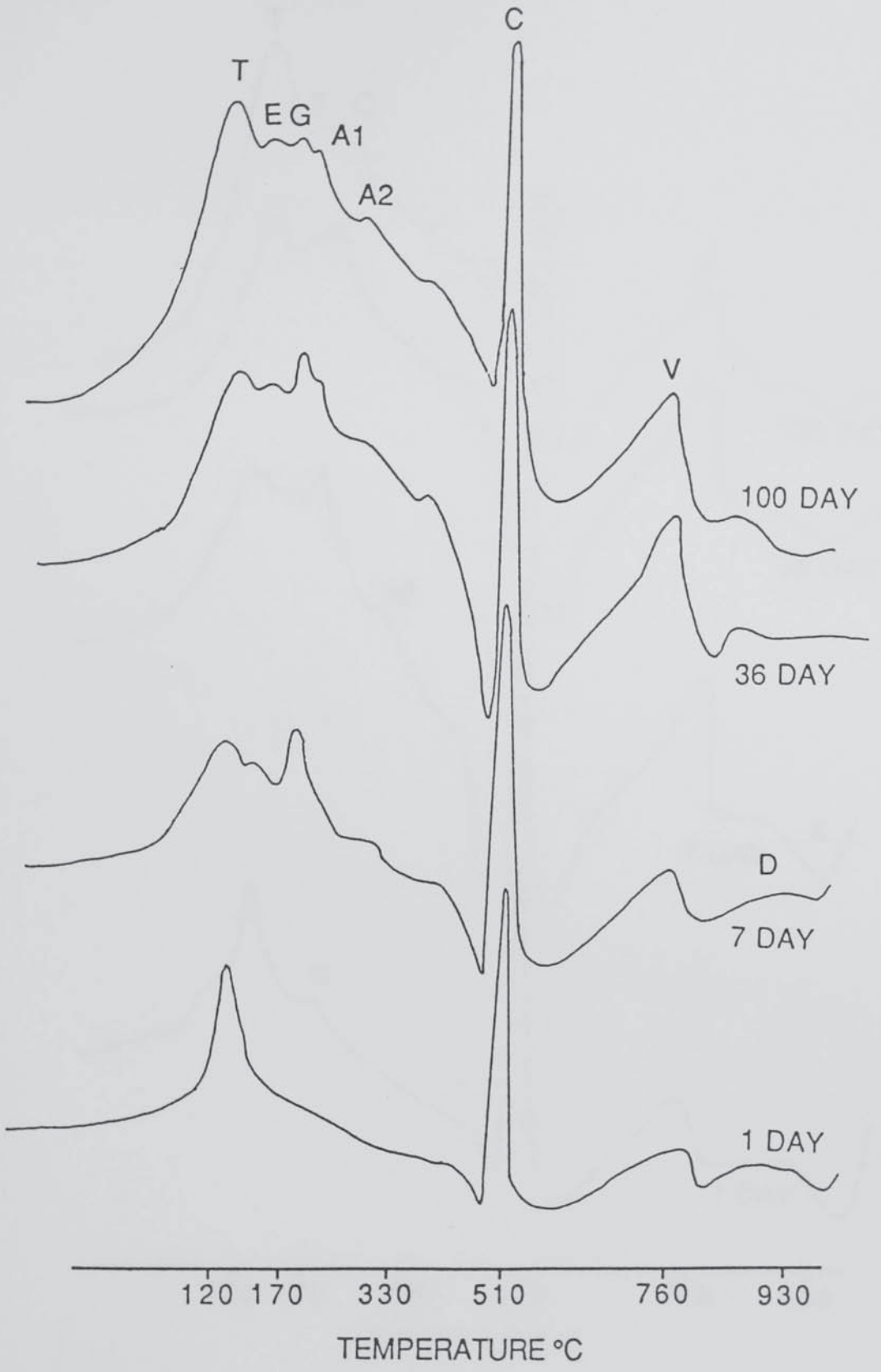

FIGURE 4.6
DTA TRACES OF THE HYDRATION PRODUCTS OF A BLEND OF 90% OPC AND 10% METAKAOLIN OF WATER:CEMENT RATIO 0.5

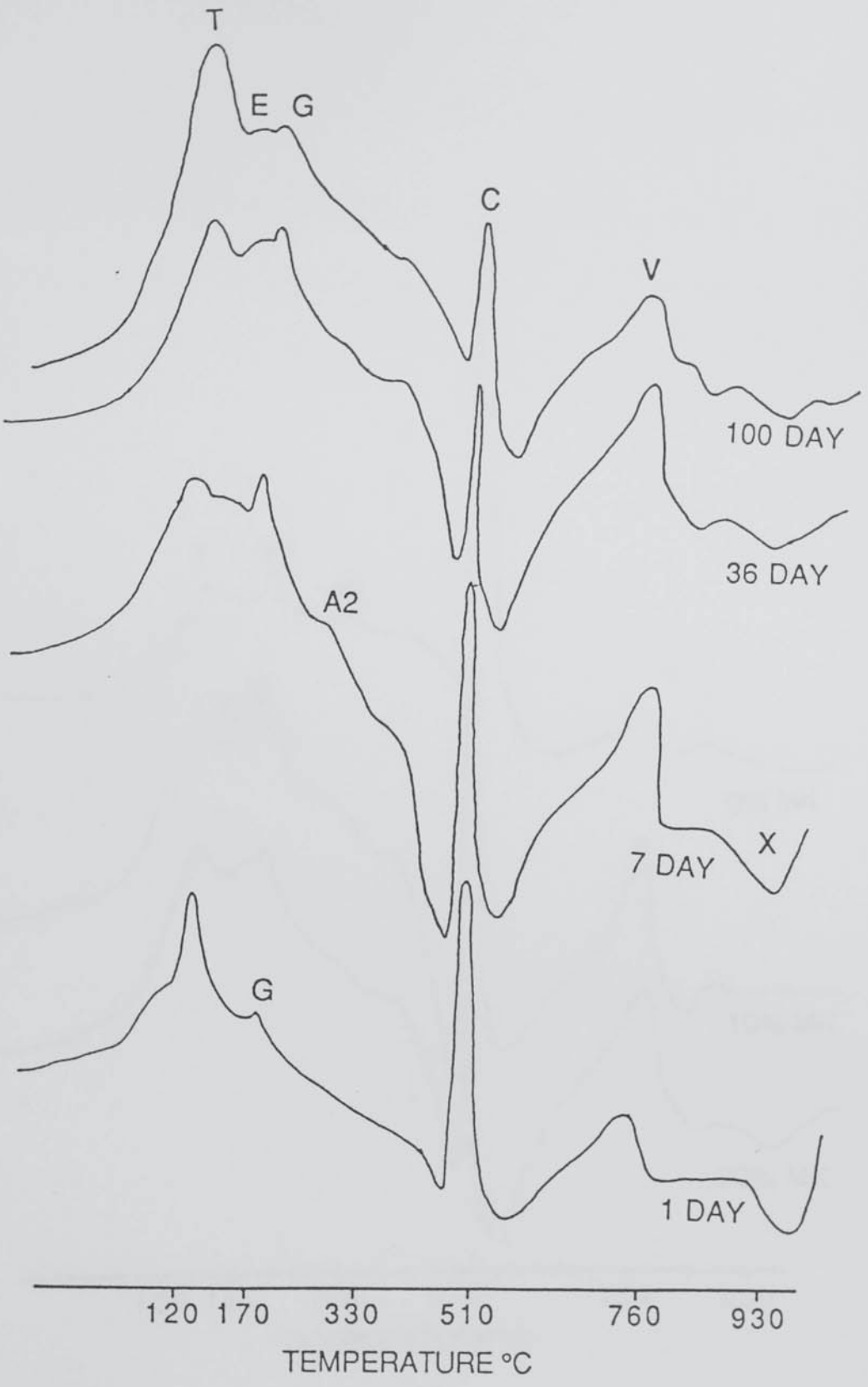

FIGURE 4.7
DTA TRACES OF THE HYDRATION PRODUCTS OF A BLEND OF 80% OPC AND 20% METAKAOLIN OF WATER:CEMENT RATIO 0.5

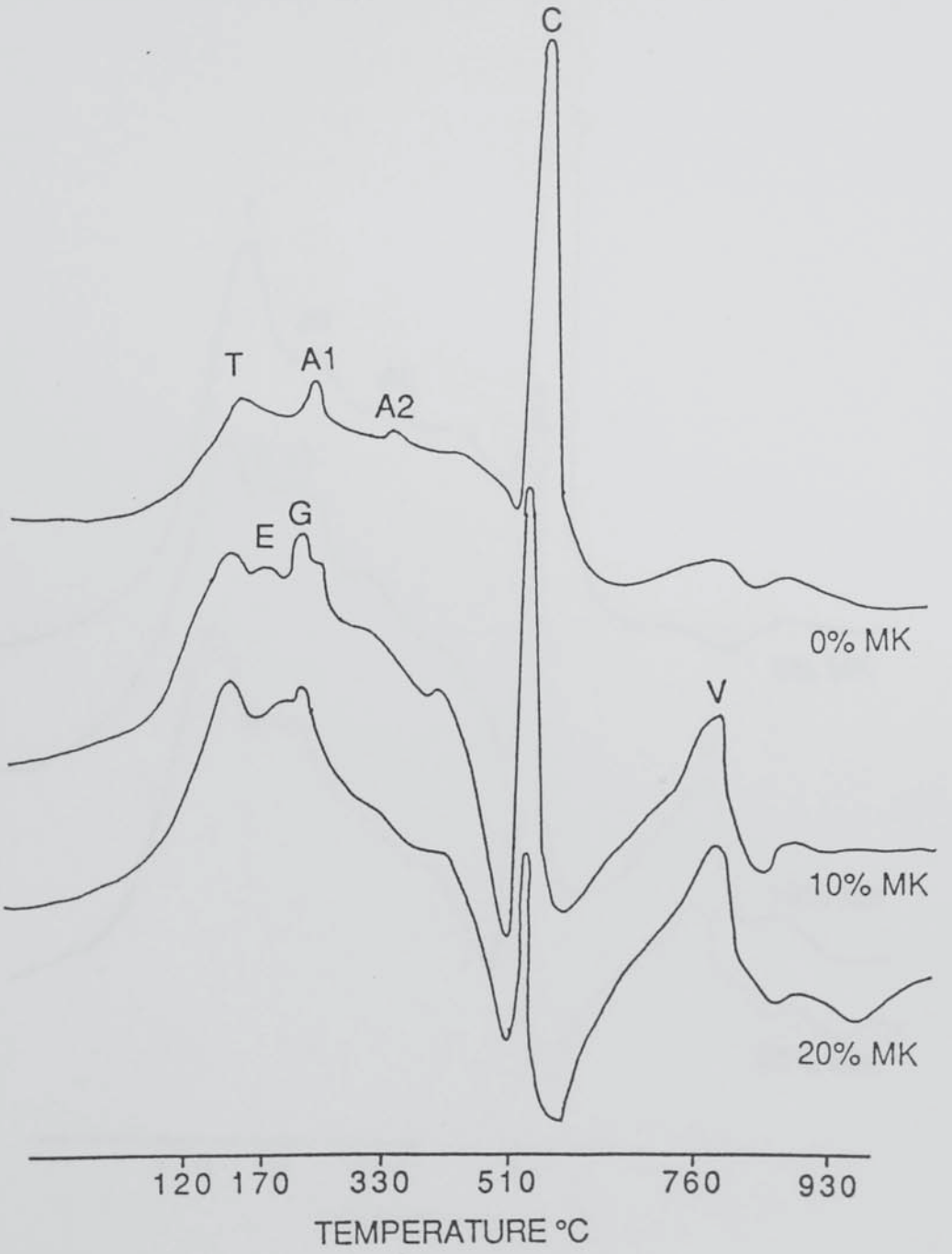

FIGURE 4.8
DTA TRACES OF THE HYDRATION PRODUCTS OF OPC AND METAKAOLIN-BLENDED OPC FOLLOWING A 36 DAY CURING PERIOD

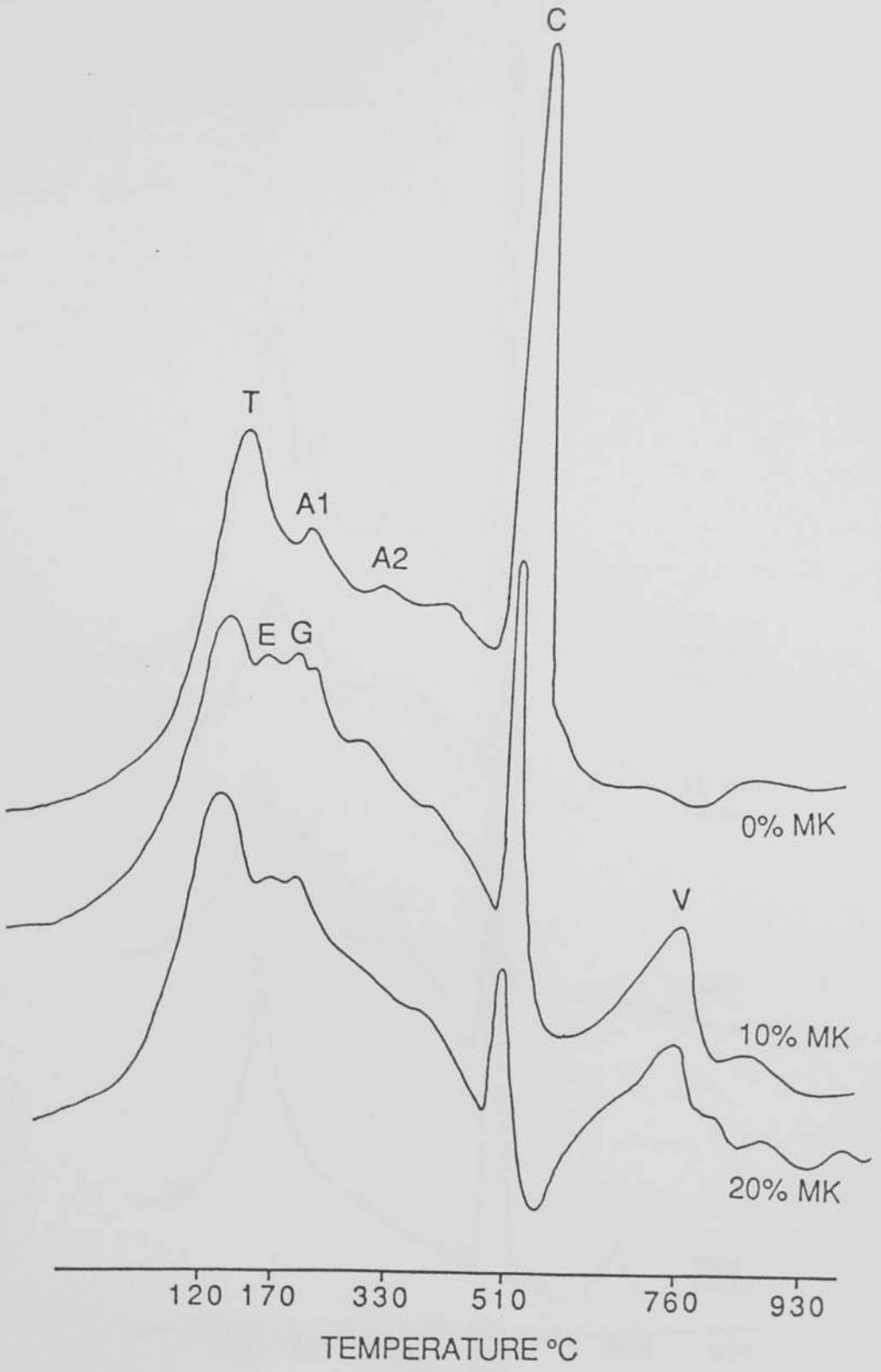

FIGURE 4.9
DTA TRACES OF THE HYDRATION PRODUCTS OF OPC AND METAKAOLIN-BLENDED OPC FOLLOWING A 100 DAY CURING PERIOD

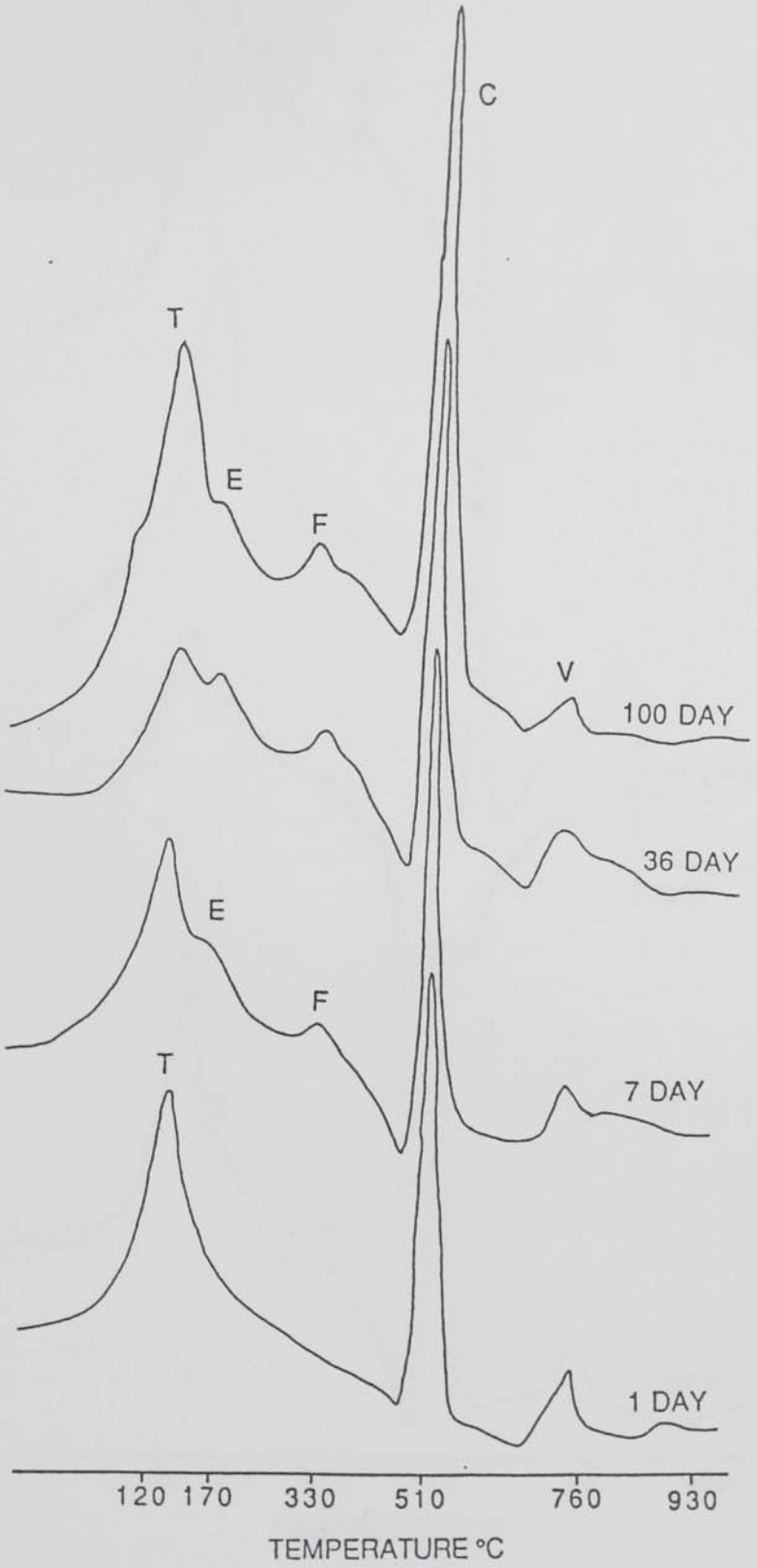

FIGURE 4.10
DTA TRACES OF THE HYDRATION PRODUCTS OF OPC IN THE PRESENCE OF SODIUM CHLORIDE

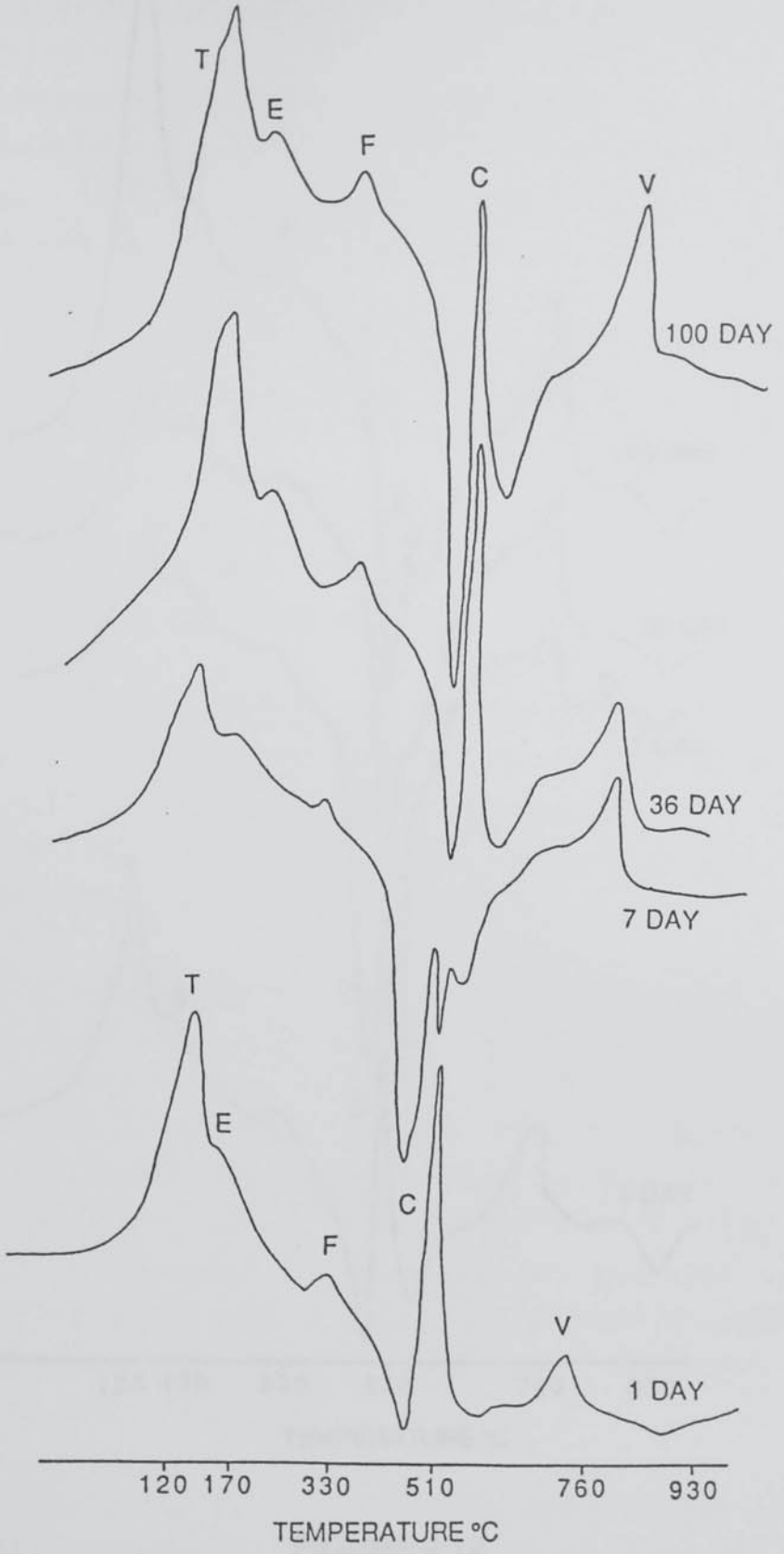

FIGURE 4.11

DTA TRACES OF THE HYDRATION PRODUCTS OF A BLEND OF 90% OPC AND 10% METAKAOLIN IN THE PRESENCE OF SODIUM CHLORIDE

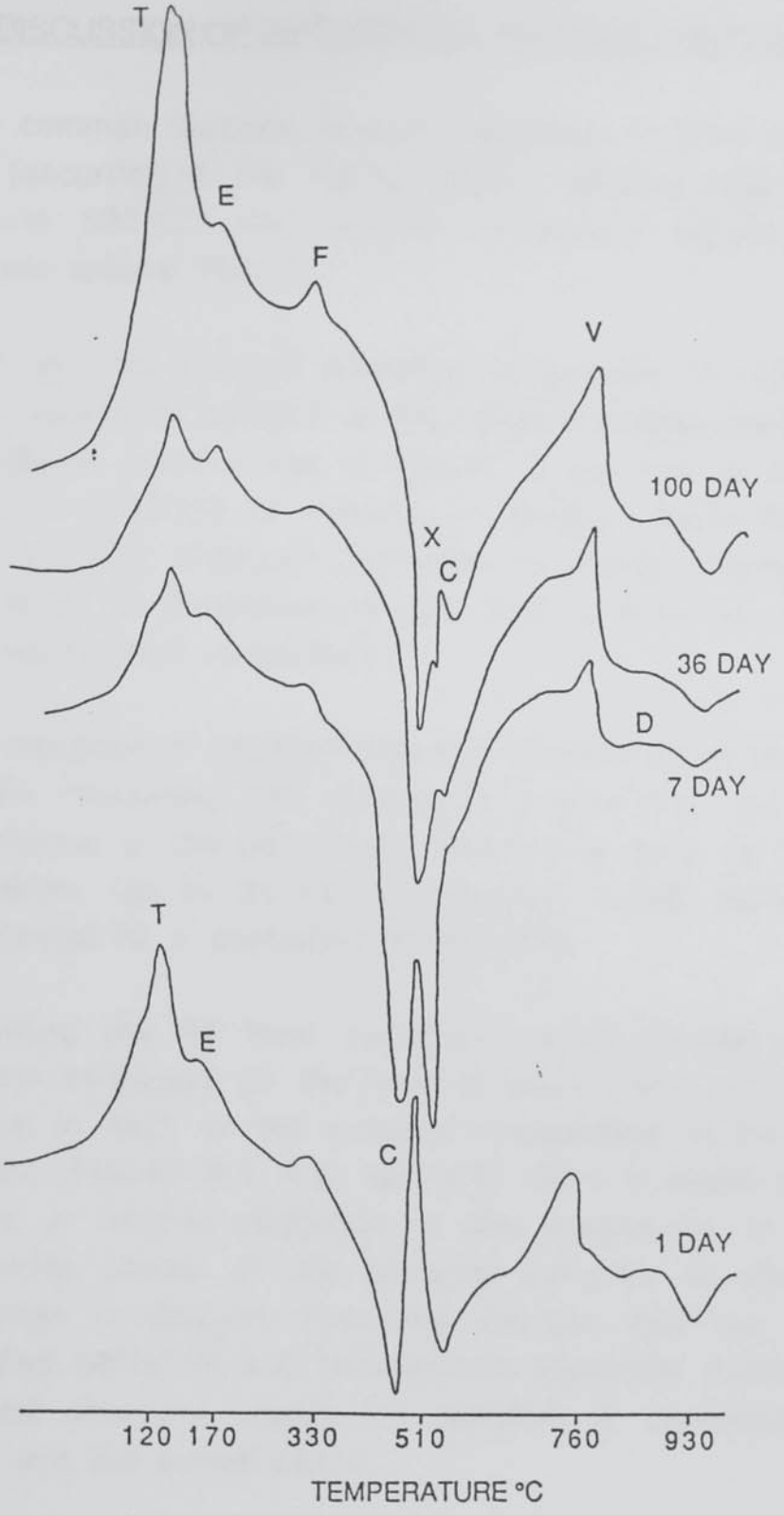

FIGURE 4.12

DTA TRACES OF THE HYDRATION PRODUCTS OF A BLEND OF 80% OPC AND 20% METAKAOLIN IN THE PRESENCE OF SODIUM CHLORIDE

A glossary of the symbols used in Figures 4.5 - 4.12 is located in Appendix 5.

4.6 DISCUSSION OF DIFFERENTIAL THERMAL ANALYSIS RESULTS

The common features of each collection of DTA traces are CSH gel (occurring in the 120°C region), calcium hydroxide (situated around 500°C), and vaterite (μ-calcium carbonate which is centred around 760°C).

CSH gel, the strength rendering component of hydrated cement, is a product of reaction of the calcium silicate phases present in anhydrous cement and is known to be one of the pozzolanic reaction products of metakaolin, calcium hydroxide and water [10, 49, 50]. Calcium hydroxide is mainly liberated from the hydration of tricalcium silicate and vaterite is present as a consequence of carbonation.

The presence of hydrated gehlenite is observed in the one day old sample containing 20% metakaolin (Figure 4.7) and indicates the occurrence of the pozzolanic reaction as early as 24 hours into hydration. Up to 24 hours, however, curing samples are not maintained at a controlled temperature.

Following the 24 hour hydration period, similar quantities of calcium hydroxide (in the form of portlandite) are seen to have formed in each of the samples irrespective of their metakaolin content (Figures 4.5, 4.6, and 4.7). After a seven day hydration period a relative reduction in the magnitude of the calcium hydroxide peaks of the blended samples is observed. This reduction in calcium hydroxide content and the presence of hydrated gehlenite and tetracalcium aluminate hydrate (C_4AH_{13}) indicate that the pozzolanic reaction is significant after one week into the curing period.

Comparison of the calcium hydroxide peaks of the blended and unblended samples in Figures 4.8 and 4.9 illustrates the extent of the pozzolanic reaction after 36 and 100 days respectively. After a 36 day curing period a significant proportion of the calcium hydroxide of the sample containing 10% metakaolin has

reacted and very little calcium hydroxide remains in the sample blended with 20% metakaolin.

These two sets of thermoanalytical curves are remarkably similar indicating that the majority of the hydration chemistry occurs before 36 days. This assumption is supported by the results of the pore solution study which revealed little change in the pore solution compositions (of both the blended and unblended samples) between 36 and 100 days (Figure 3.6).

The fact that a proportion of calcium hydroxide still remains after a curing period of 100 days (even for the sample containing 20% metakaolin) is relevant to the passivity of embedded steel reinforcements. The phenomenon of passivity and an important process known as 'buffering', which is responsible for the maintenance of the pore solution alkalinity, are considered in Chapter 6.

All thermoanalytical curves were obtained within 10 days of sample dehydration with the exception of that of the 7 day unblended OPC sample (Figure 4.5) which was delayed for 40 days. This is a possible explanation for the absence of ettringite and the presence of its thermodynamically more stable decomposition products, tetracalcium aluminate hydrate (C_4AH_{13}), and tetracalcium sulphoaluminate hydrate ($C_3A.CS.12H$). After 36 days any ettringite which may have formed appears to have broken down into the aforementioned species. The decomposition of ettringite is generally expected to occur after a longer hydration period although there is no fixed time at which this reaction takes place since the hydration chemistry of each OPC type differs.

Figure 4.10 illustrates the way in which the addition of sodium chloride modifies the constituents of the solid phase. Primarily, the formation of Friedel's salt begins to occur at some point between one and seven days.

The second effect of the addition of sodium chloride is the prolonged existence of ettringite. No apparent decomposition of ettringite has taken place up to 100 days.

Following a 24 hour hydration period there is no evidence for the formation of either ettringite or Friedel's salt in the unblended OPC sample, however both phases are observed in the thermoanalytical curves of the corresponding metakaolin-blended systems (Figures 4.11 and 4.12) which contain sodium chloride.

It is believed that the absence of hydrated gehlenite indicates that it is operative in the removal and solid state binding of chloride ions from the pore solution. Since no other identifiable phases are seen to be present other than CSH gel, calcium hydroxide and vaterite it is suggested that hydrated gehlenite (possibly in conjunction with tetracalcium aluminate hydrate) combines with chloride ions in the formation of Friedel's salt. Further evidence for this hypothesis and the implications thereof are located in the following chapter and the final discussion in Chapter 7.

An unusual feature of the thermoanalytical curves of samples containing both metakaolin and sodium chloride is the presence of large exothermic troughs which appear in the same region as the calcium hydroxide peaks. Observation of this region of the 7 day and the 100 day sample traces in Figures 4.11 and 4.12, respectively, possibly indicates the presence of a second endothermic peak approximately 10°C away from that of the calcium hydroxide. With the information currently available it is not possible to deduce whether this apparent peak is a consequence of the superposition of the calcium hydroxide peak and the exothermic trough or a signal derived from an actual solid state phase. The presence of the exothermic trough, however, is undoubtedly related to the combined effect of additions of metakaolin and sodium chloride on the solid phase. It does not necessarily represent a discrete phase in the matrix

although it is likely to arise from a solid state reaction in which bond formation is occurring.

The section on future work in this field (Chapter 7) contains suggestions for the further investigation and identification of the phases arising from sodium chloride contamination of metakaolin-blended OPC systems.

4.7 RESULTS OF THE MAS NMR INVESTIGATION

Aluminium-27 and silicon-29 magic angle spinning nuclear magnetic resonance spectroscopy was conducted on 1, 7, 36, and 100 day samples containing 0% and 20%. Spectra were also obtained for anhydrous cement and metakaolin.

The spectra collected during this investigation are presented in Figures 4.13 to 4.22. Chemical shift values corresponding to the spectral resonances are contained in Tables 4.5, 4.6 and 4.7.

	CHEMICAL SHIFT						
SAMPLE TYPE	Q^0	Q^1	Q^3	Q^4	4	5	6
ANHYDROUS OPC	-71.2	-	-	-	97.1 82.0	-	-
METAKAOLIN	-	-	-	AMORPHOUS -101	63.4	52.4	5.4
1 DAY 0%MK	-71.2	-79.9	-	-	7 DAY OPC 0% MK		8.5

(CORRESPONDING WITH FIGURES 4.13, 4.14, 4.15, 4.16, 4.17 AND 4.22)

TABLE 4.5
NMR CHEMICAL SHIFT DATA FOR
ANHYDROUS OPC, METAKAOLIN AND 1 AND 7 DAY OPC

CHEMICAL SHIFT (ppm)

SAMPLE MATURITY (DAYS)	SILICATE TYPE			ALUMINIUM CO-ORDINATION NUMBER		
	Q^0	Q^1	Q^2	4	5	6
1	-71.2	-79.5	-	-	-	13.3
7	-71.3	-78.9	-	-	-	7.58
36	-71.4	-79.2	APPROX. -85	-	-	7.87
100	-71.4	-79.0	APPROX. -86	-	-	7.61

(CORRESPONDING WITH FIGURES 4.18, 4.19)
TABLE 4.6
NMR CHEMICAL SHIFT DATA FOR PLAIN OPC PASTE SAMPLES
(AT VARIOUS STAGES OF HYDRATION)

	CHEMICAL SHIFT (ppm)							
	SILICATE TYPE					ALUMINIUM CO-ORDINATION NUMBER		
SAMPLE MATURITY (DAYS)	Q^0	Q^1	Q^2	Q^3	Q^4	4	5	6
1	-71.2	-81.5	-	-	AMORPHOUS -101	57.2	27.7	8.45
7	-71.5	-82.1	-85.6	SOME SIGNAL IN THIS REGION	AMORPHOUS -103	60.6	-	9.01
36	-71.4	-81.1	-	-	-	60.1	-	8.72
100	-71.2	-80.4	APPROX. -84	-	-	60.6	-	9.04

(CORRESPONDING WITH FIGURES 4.20, 4.21)

TABLE 4.7

NMR CHEMICAL SHIFT DATA FOR SAMPLES CONTAINING 20% METAKAOLIN (AT VARIOUS STAGES OF HYDRATION)

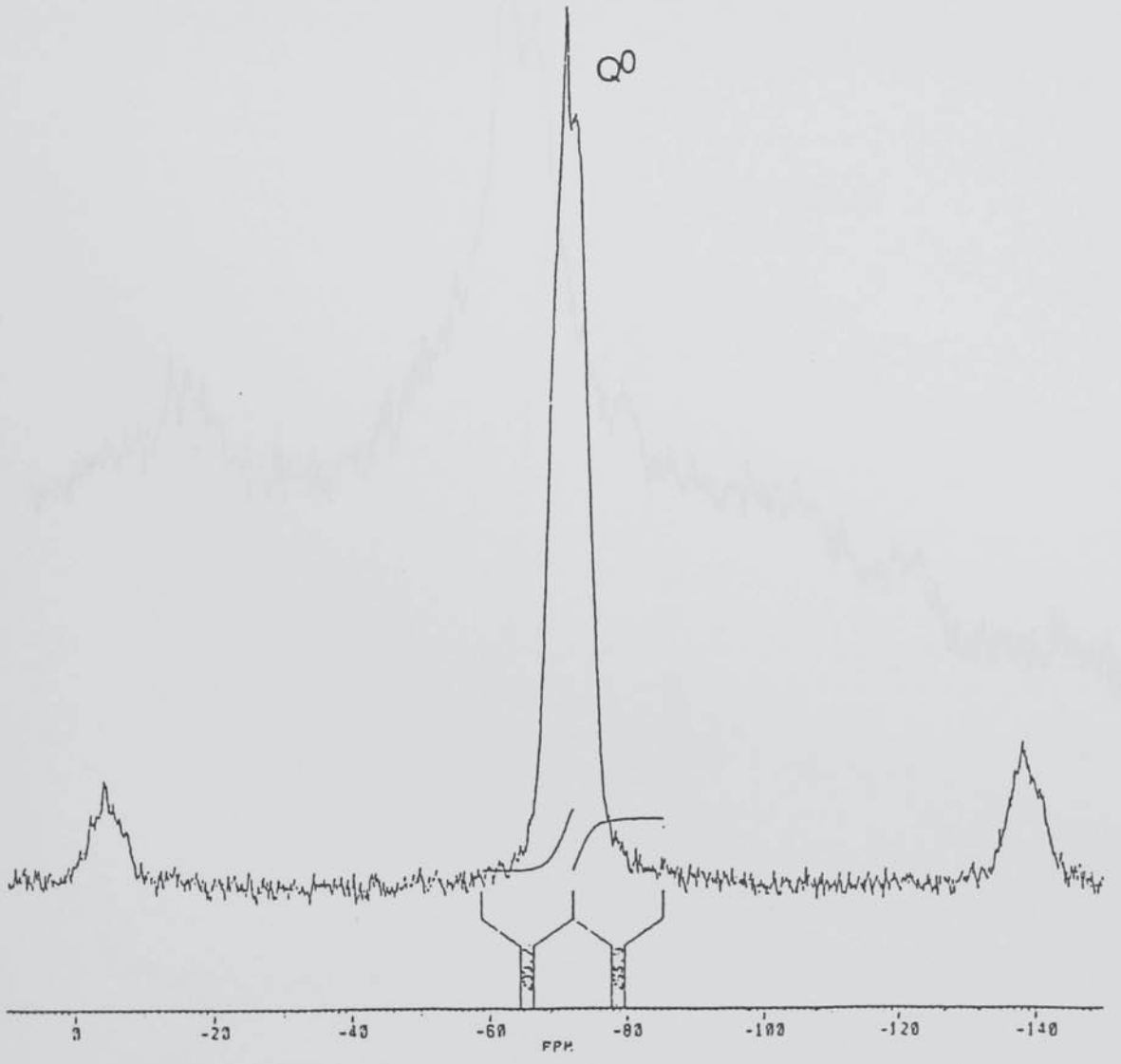

FIGURE 4.13
SILICON-29 MAS NMR SPECTRUM OF
ANHYDROUS OPC

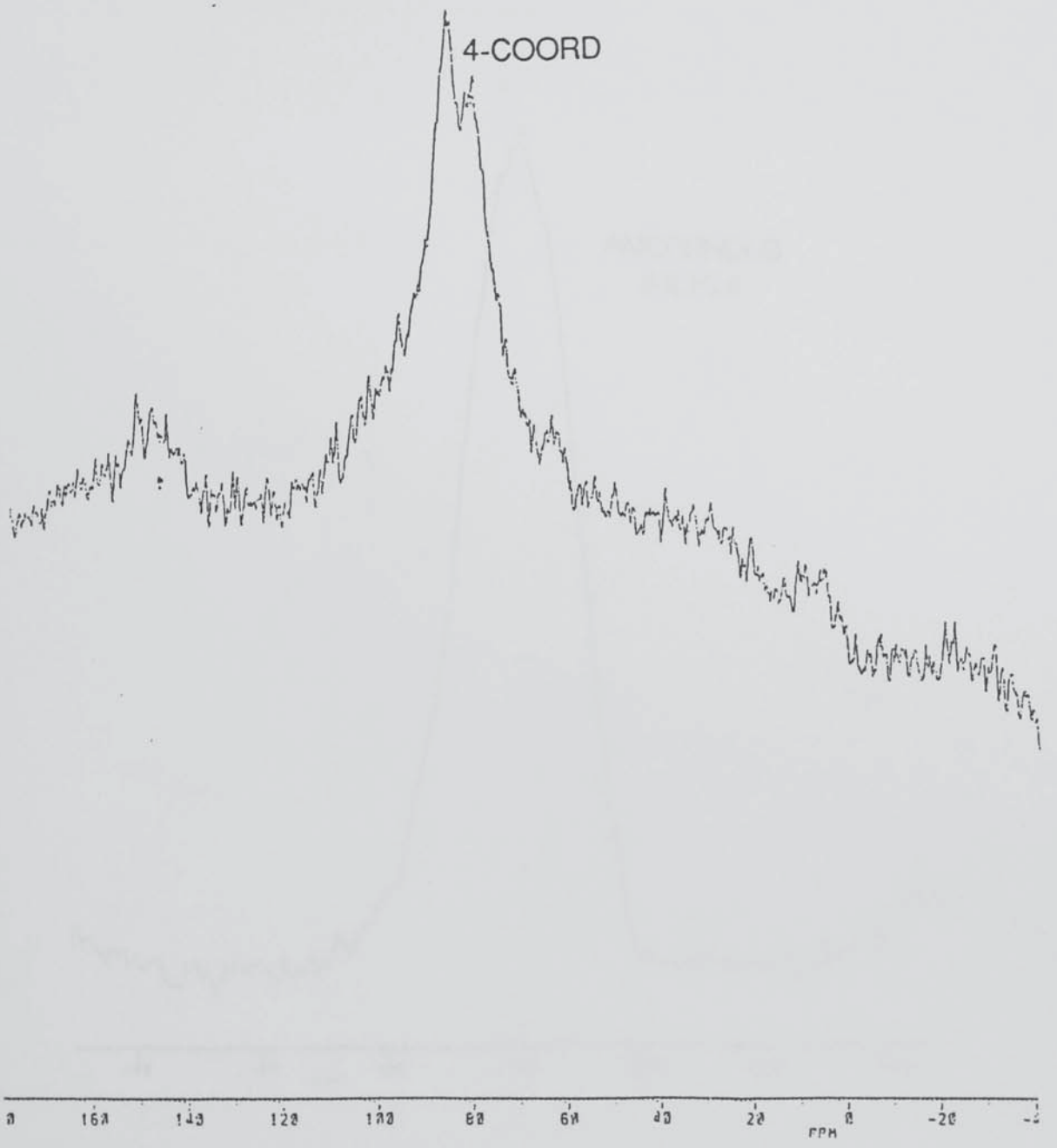

FIGURE 4.14
ALUMINIUM-27 NMR SPECTRUM OF
ANHYDROUS OPC

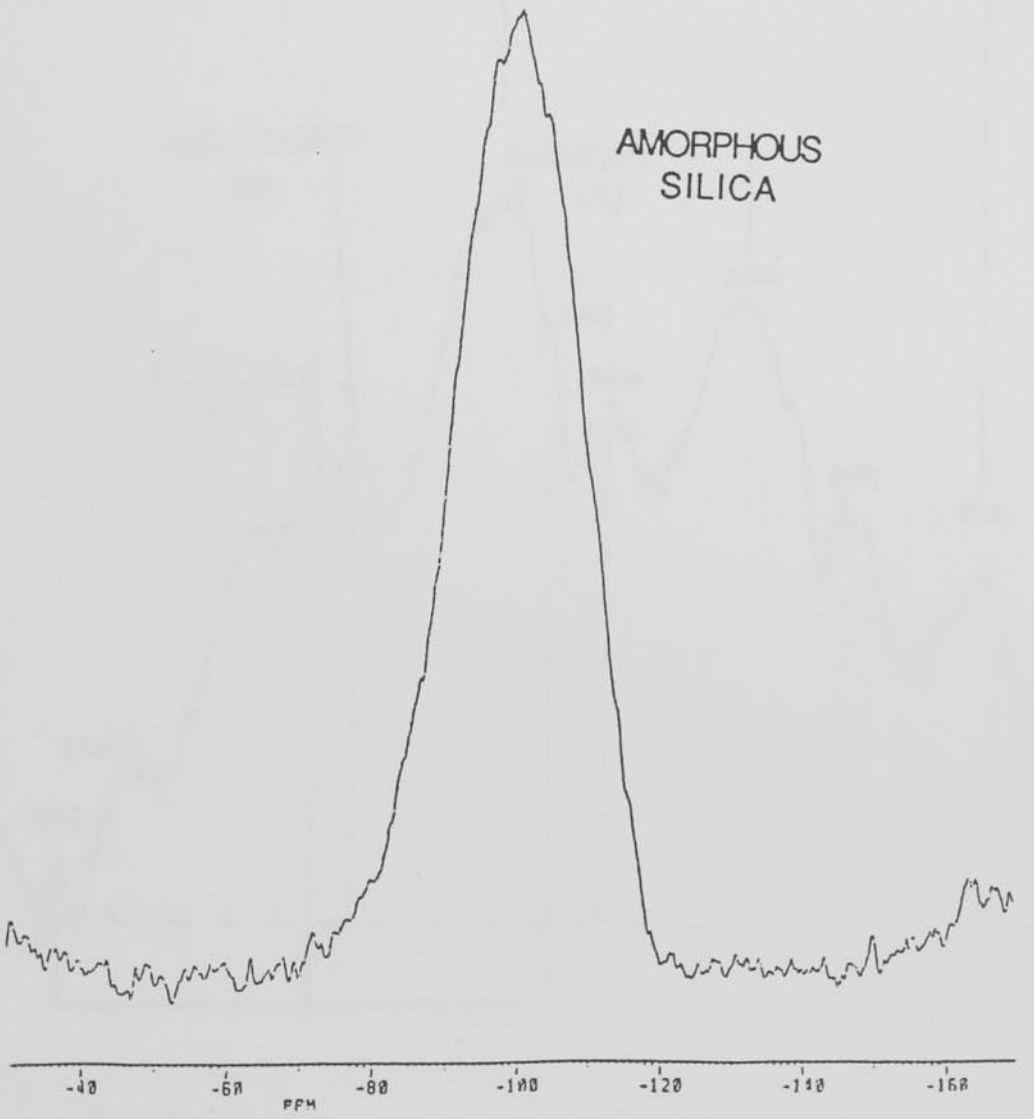

FIGURE 4.15
SILICON-29 MAS NMR SPECTRUM OF
METAKAOLIN

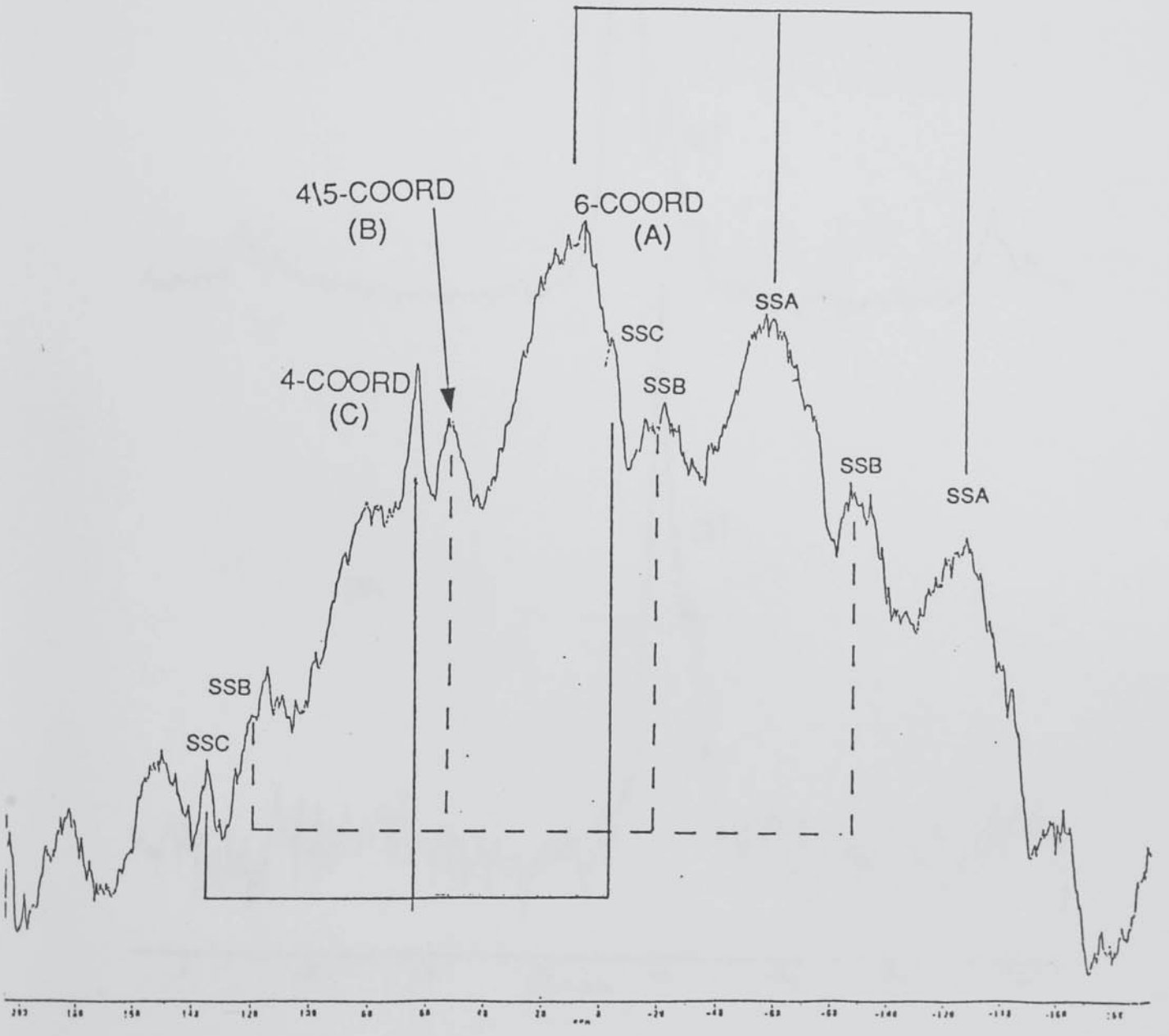

FIGURE 4.16
ALUMINIUM-27 NMR SPECTRUM OF
METAKAOLIN

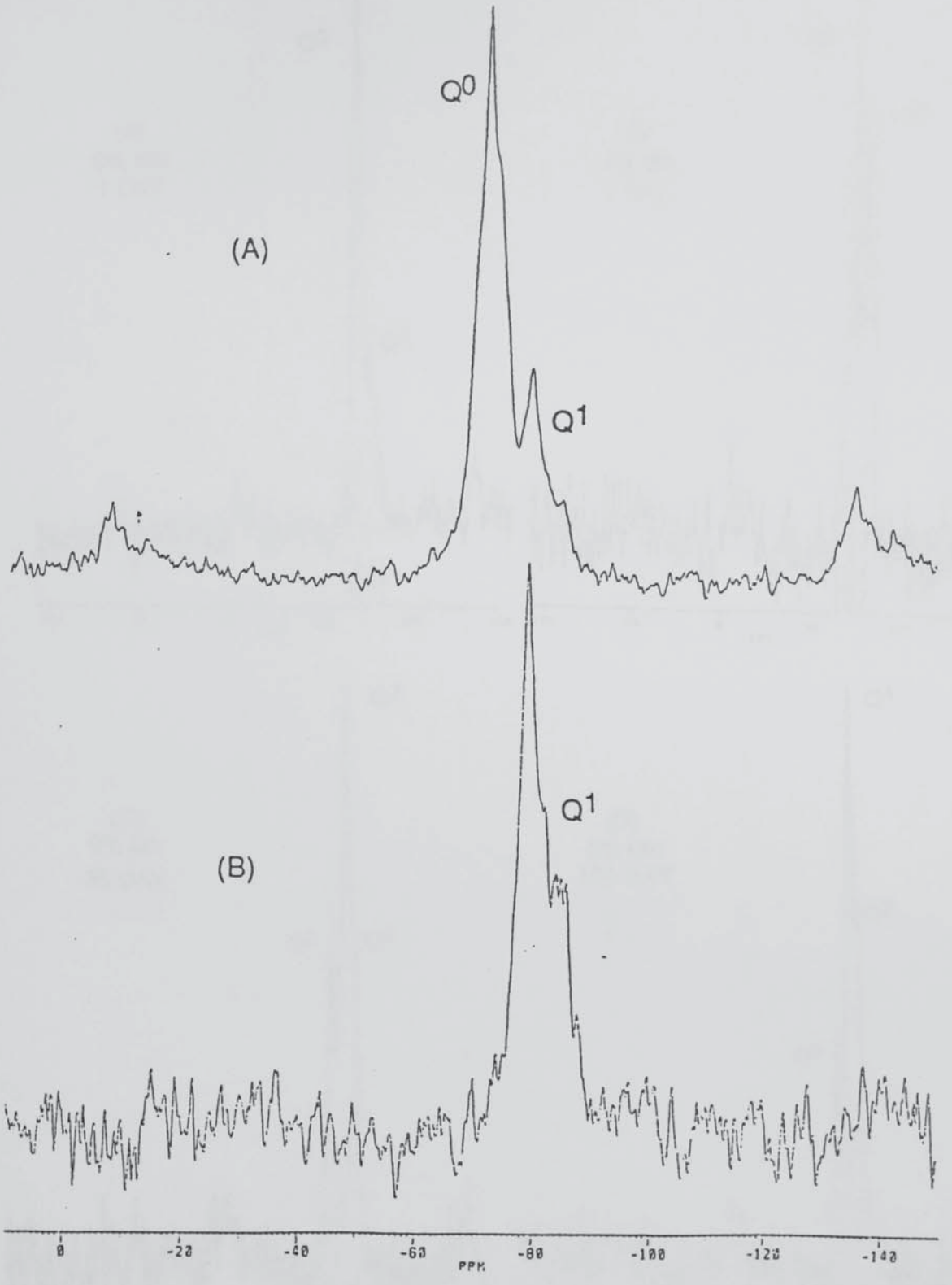

FIGURE 4.17
(A) SILICON-29 MAS NMR SPECTRUM OF
1 DAY, 0% METAKAOLIN SAMPLE
(B) SILICON-29 MAS NMR CROSS POLARISED SPECTRUM OF
1 DAY, 0% METAKAOLIN SAMPLE

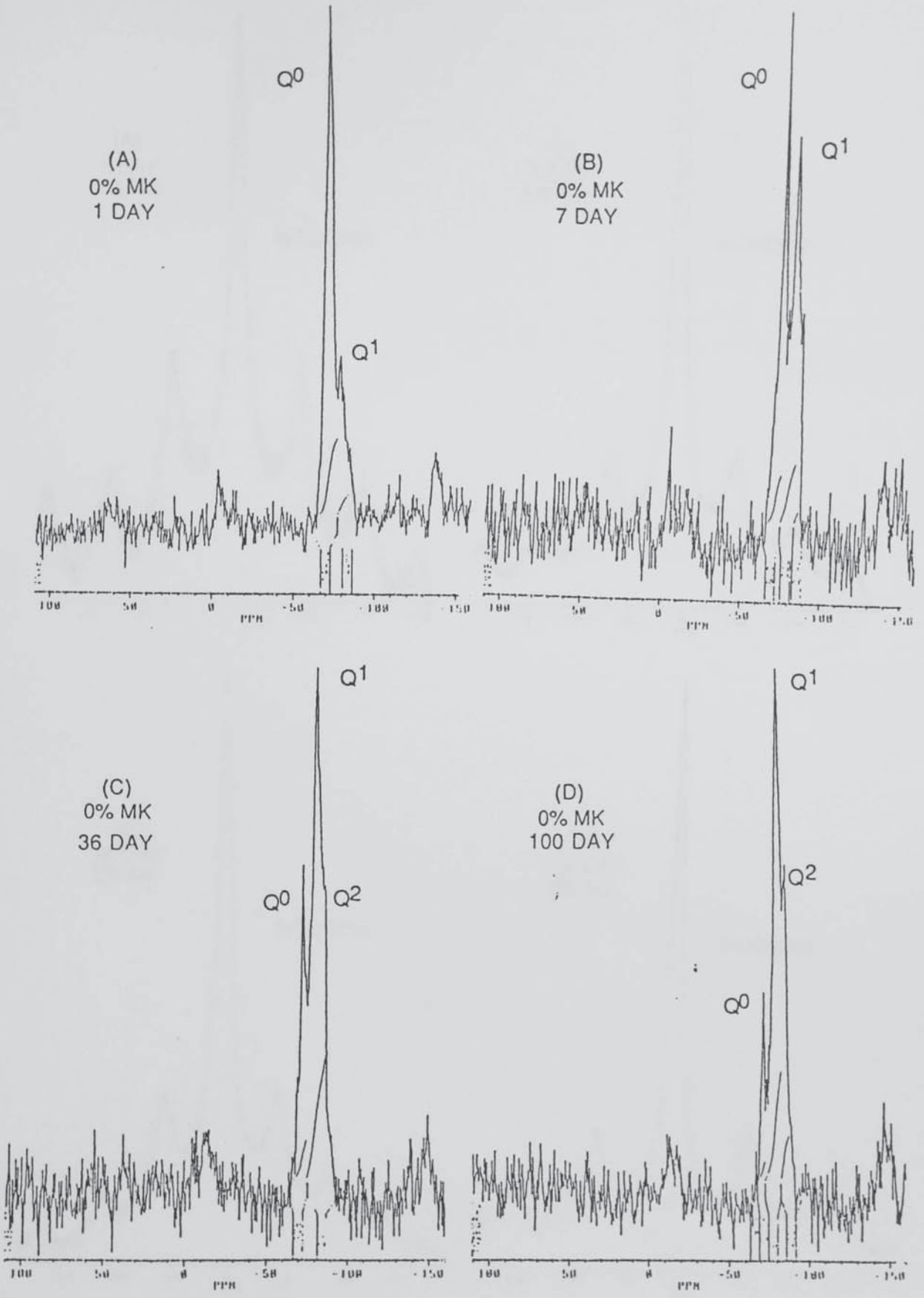

FIGURE 4.18
SILICON-29 MAS NMR SPECTRA OF
1, 7, 36, AND 100 DAY 0% METAKAOLIN SAMPLES

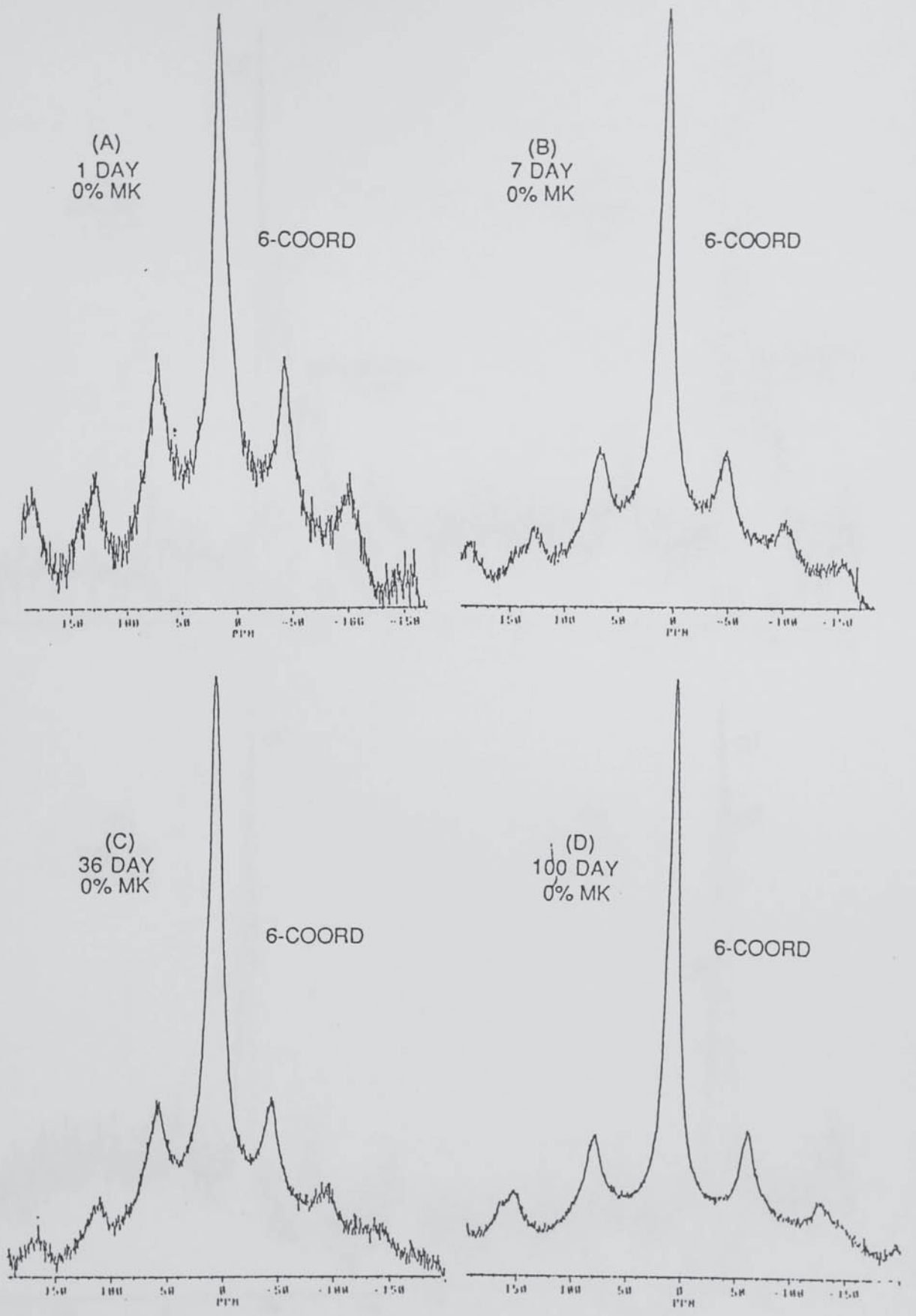

FIGURE 4.19
ALUMINIUM-27 NMR SPECTRA OF
1, 7, 36, AND 100 DAY 0% METAKAOLIN SAMPLES

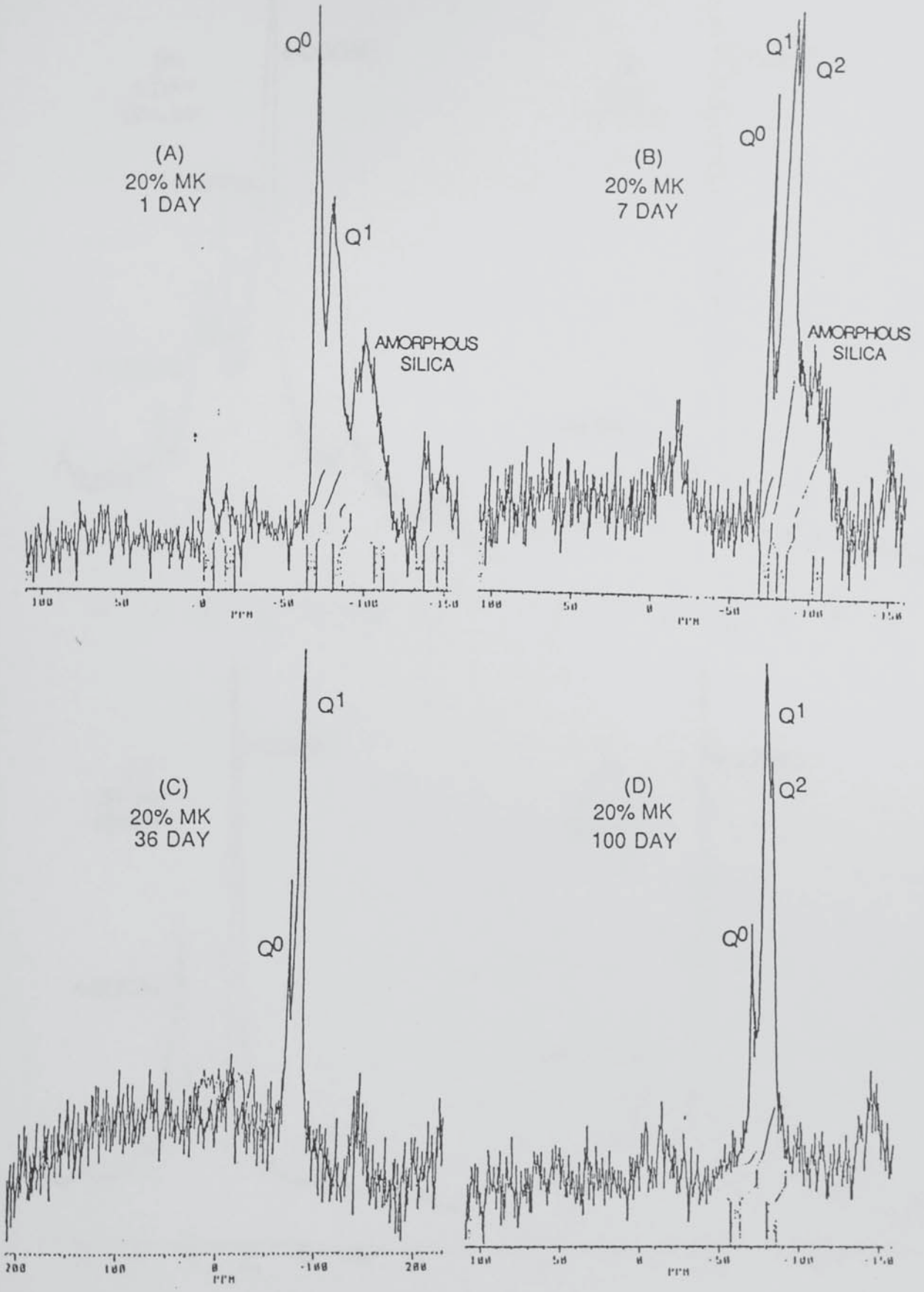

FIGURE 4.20
SILICON-29 MAS NMR SPECTRA OF
1, 7, 36, AND 100 DAY 20% METAKAOLIN SAMPLES

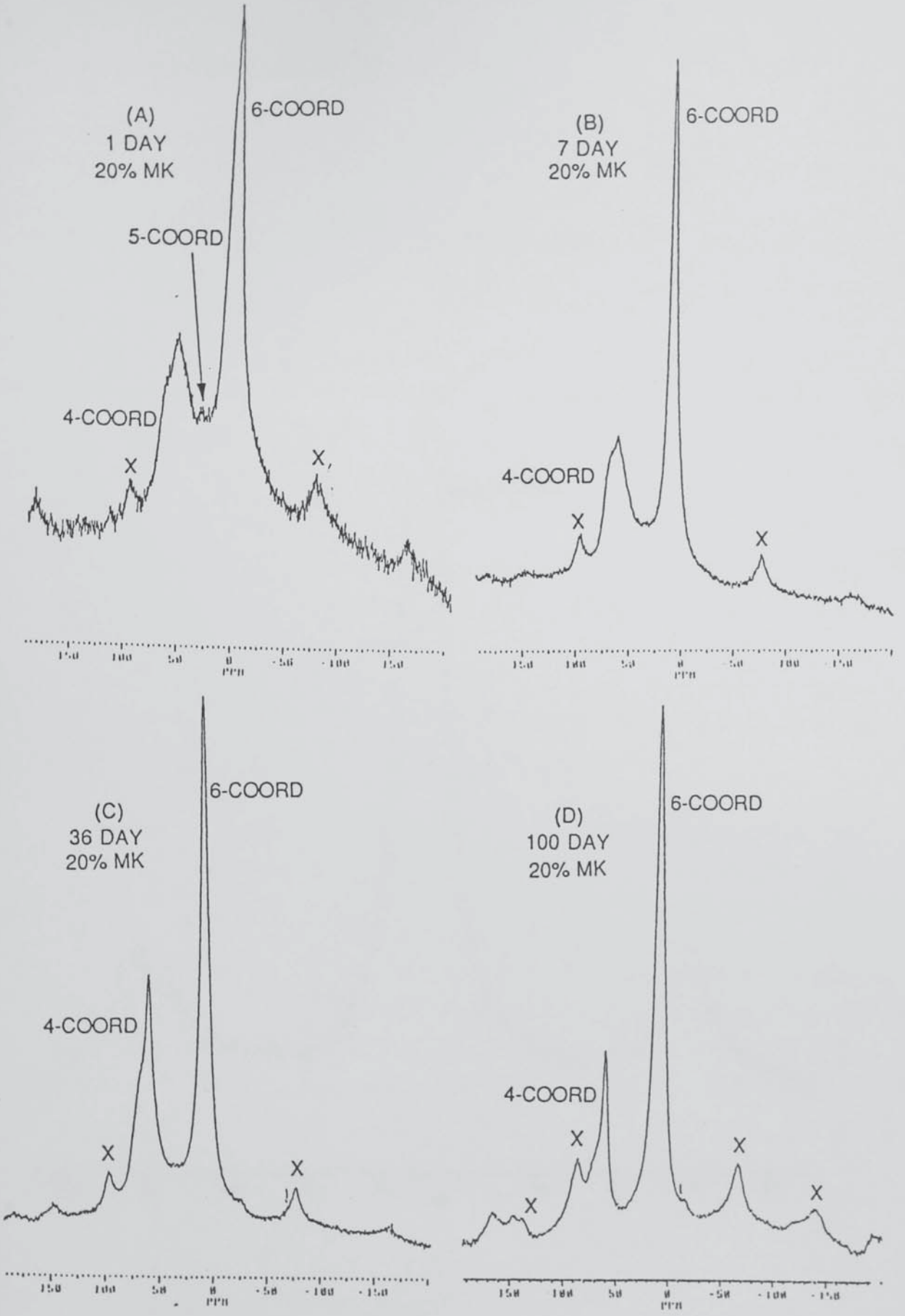

FIGURE 4.21
ALUMINIUM-27 NMR SPECTRA OF
1, 7, 36, AND 100 DAY 20% METAKAOLIN SAMPLES

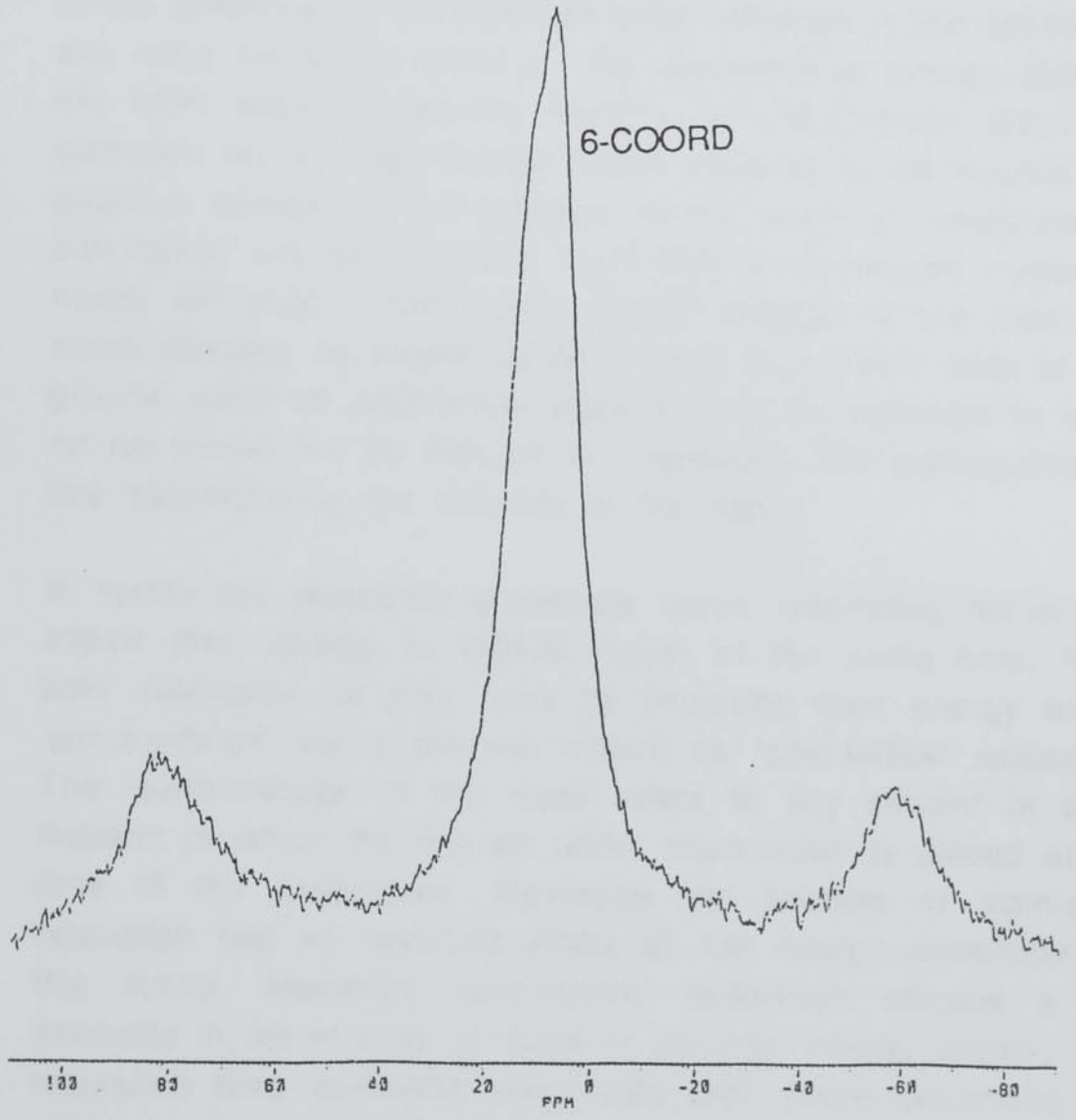

FIGURE 4.22
ALUMINIUM-27 NMR SPECTRUM OF
7 DAY, 0% METAKAOLIN SAMPLE

4.8 DISCUSSION OF MAS NMR RESULTS

It must be noted that the silicon-29 spectra presented in Figures 4.13 and 4.15 were obtained using a relaxation delay time of 3.5 seconds. That is, the duration between each radio frequency pulse which causes the nuclei to resonate was 3.5 seconds. Whereas all other silicon-29 spectra were recorded using a relaxation delay of 50 seconds.

In the presence of the magnetic field, although in the absence of any radio frequency radiation, the population of energy states of the NMR active nuclei will conform to a Boltzmann distribution (between two or more energy states dictated by the nuclear spin quantum number of the nucleus). In the event of resonance this distribution will be disturbed such that an increased number of nuclei will exist in the higher energy state(s). If the resonating nuclei possess no means by which they may 'relax' back to their ground state an equilibrium situation will be achieved in which no net nuclei will be brought to resonance. The consequence of this 'saturation' is the collapse of the signal.

In reality two relaxation processes occur; resonating nuclei may impart their energy to vicinial nuclei of the same kind, 'spin-spin' relaxation, or may relax by imparting their energy to the 'surroundings' via a process known as 'spin-lattice' relaxation. The 'surroundings' in this case refers to any solvent or other medium in which the sample under observation is placed at the time of the experiment. Obviously the process of 'spin-spin' relaxation has no resultant effect on the energy distribution of the nuclei. However 'spin-lattice' relaxation causes a net decrease in the number of nuclei in the high energy state(s). The relaxation time constants associated with these processes are assigned the symbols T_2 and T_1 respectively (and are fairly analogous with the time constants associated with the charging and uncharging of capacitors).

Hence, for the acquisition good spectra a time period of five times T_1 should elapse in between radio frequency pulses.

Originally all silicon spectra were obtained using a relaxation delay time of 3.5 seconds. It was discovered that the metakaolin yielded a disproportionately small signal when spectra of blended cement paste systems were observed. (The actual spectra have not been included in this thesis.) This absence of any signal arising from the metakaolin was correctly assumed to be due to an insufficiently small relaxation delay time which allowed the species derived from the cement to appear on the spectra but which caused the signal from the metakaolin to become 'saturated'. As demonstrated by figure 4.15 metakaolin itself does yield a signal if a relaxation delay of 3.5 seconds is used. A problem arises when a quantitative analysis of components from the metakaolin, cement and pozzolanic or hydration reactions is required. In such cases it must be ensured that, either the relaxation delay time is at least five times longer than the largest T_1 value, or, that the integrals of saturated signals are multiplied by a factor (dependent on T_1 and the relaxation delay) to give that value which would have been obtained if that component had had sufficient time to relax in between pulses.

Spin-lattice relaxation time may depend upon crystallinity, vicinial paramagnetic species (e.g. Fe ions) and the presence of bonded hydroxyl groups or water as a close neighbour. In general, a high degree of crystallinity results in a long T_1; short T_1 values are expected for nuclei having vicinial paramagnetic species, bonded hydroxyl groups or water. Justnes et al. report that the Q^4 signal from silica fume (containing 1.9% Fe_2O_3) in OPC had to be multiplied by a factor of 1.5 when a relaxation delay time of 10 seconds was used despite the significant iron content [52]. They found that silica fume of a lower iron content (0.5% Fe_2O_3) in a slightly acidic slurry gave a full signal under the same conditions.

All subsequent silicon-29 spectra were obtained with a relaxation delay time of 50 seconds allowing both signals from the cement and metakaolin to appear. This delay time was

arrived at following discussion with other workers having investigated similar silicate compounds.

Reference was made in the introduction to this chapter to a method for obtaining information on the degree of hydration and the extent of the pozzolanic reaction. Unfortunately insufficient time was available during this research to measure T_1 values for the metakaolin and cement species. It is for this reason that such spectral analysis has been omitted here.

All aluminium-27 spectra were obtained with a relaxation delay time of 0.1 seconds except for those in Figures 4.14 and 4.22 which were recorded with a relaxation delay of 1.0 second. The similarities and differences arising from this ten-fold difference in relaxation times are discussed later in this section.

The experimental preference for the smallest relaxation delay time possible is based on the amount of time required to produce each NMR spectrum considering that, sometimes, several thousand pulses are required to obtain solid state spectra having an acceptable signal to noise ratio of nuclei of low abundance.

The two resonances at -71.2 and -72.6 ppm comprising the silicon-29 spectrum of anhydrous OPC (Figure 4.13) appear to indicate two Q^0 silicate environments. These signals, however, are believed to arise from the superposition of resonances from C_2S and C_3S [63]. Pure C_3S is known to give rise to between six and nine resonances in the region -66.5 and -74.5 ppm whereas C_2S exhibits a maximum at around -71.5 ppm [56,64,65]. The presence of 'impurities' and paramagnetic species in OPC enhance the line broadening of the signals making the definition of the resonances of the individual phases currently impossible. This spectrum compares well with that obtained by Parry-Jones et al. [66] which showed a main peak at -71 ppm with a pronounced shoulder at -73 ppm.

A doubly peaked resonance at 97.1-82.0 ppm is noted in the aluminium-27 spectrum of anhydrous cement (Figure 4.14). Recent work of Skibsted et al. [67] provides compelling evidence for the view that the two sharp resonances in the tetrahedral region probably arise from Al for Si substitution in the silicate phases alite (C_3S) and belite (C_2S); the very broad resonance underlying the sharp signals arises in all probability from the C_3A phase which may be broadened due to paramagnetic impurities, e.g. iron (iii). The C_4AF phase is paramagnetic and is therefore not believed to give a signal.

The single broad resonance of the silicate species of metakaolin (Figure 4.15) is centred around -101 ppm. This resonance signifies (Q^4) amorphous or pseudo-amorphous silica. The frequency width of this resonance at half maximum peak height (FWHM) is approximately 1250 Hz (21 ppm at 59.63 MHz) which compares well with that obtained by Rocha et al. [58] (FWHM of 1590-1670 Hz, 20-21 ppm at 79.5 MHz). The narrower line width indicates a comparatively higher degree of order in the metakaolin used in this study.

The most striking feature of the aluminium-27 spectrum of metakaolin is the predominance of the spinning side bands. It has already been stated that spinning side bands can be considered as harmonics of the resonance from which they arise. The frequency at which the rotors are spun (during the collection of the spectrum) dictates the frequency at which the spinning side bands occur.

The aluminium-27 spectrum of metakaolin was obtained with rotors spinning at 5200Hz. Hence each of the primary sets of spinning side bands occur at 5200Hz on either side of the resonance from which they arose. Secondary sets of spinning side bands will occur at 10400Hz away from the central signal and so on. For this particular system 5200Hz is equivalent to approximately 63 ppm on the spectrum.

The location and identification of the actual resonance signals of this spectrum were conducted by considering the spinning side band progression in the region from -20 to -140 ppm in which no aluminium resonances are expected. It was noted that this progression was composed of two sets of harmonics (labelled 'SSA' and 'SSB') which were traced back to their original resonances (A and B, respectively) by measuring along the spectrum in 63 ppm intervals.

The third signal of this spectrum (denoted by the letter C) was identified by its sharp line shape and its location in the 4-coordinate region. The position of one sharp similarly shaped spinning side band 63 ppm away from this resonance also aided its identification. On closer inspection it was noted that a second primary harmonic associated with this resonance appears at approximately 3 ppm. This harmonic is less well defined than the other due to overlap with the 6-coordinate (A) resonance.

The chemical shift of signal B, 52.4 ppm, suggests that it has arisen from a 4-coordinate aluminium species. The signal appears at the end of the 4-coordinate range towards the 5-coordinate region. However Figure 4.21A comprises the aluminium-27 spectrum of a 1 day old cement system containing 20% metakaolin in which an equivalent signal (known to have arisen from the metakaolin as hydrated cement does not resonate in this region (see Figures 4.19 and 4.22)) is seen to occupy the 5-coordinate region of the spectrum. Rocha [58] also reported the presence of a 5-coordinate aluminium species in metakaolin (from more well defined spectra in which the harmonic signals are less intense) which was found to be the most highly reactive centre for the rehydration of metakaolin back to kaolin.

Hence, irrespective of the apparent resonance position of signal B, the aluminium species from which it arose is believed to be 5-coordinate. It is possible that the superposition of the actual resonance signal with background noise and/or harmonic signals could cause a shift in the apparent position of the resonance

signal maximum. The aluminium species from which this signal originates shall henceforth be referred to as possessing 5-coordinate symmetry.

It is reasonable to infer from the sharp, comparatively narrow line shape of signal C (63.4 ppm) that the 4-coordinate aluminium species from which it arose is in a more highly symmetrical environment than the 6-coordinate species which gave rise to a considerably broader, asymmetrical signal. Obviously the 5-coordinate species does not possess high symmetry.

The presence of paramagnetic species (e.g. iron) is known to enhance the intensity of spinning side bands. Since the spinning side bands associated with resonances A and B are of significantly greater intensity than those arising from resonance C it is likely that the species containing iron in the metakaolin are in some way associated with the 6- and 5-coordinate aluminium species although not with the 4-coordinate species.

Suggestions for the production of superior aluminium-27 NMR spectra are located in the section on further work in the final chapter.

Figure 4.17 has been included in the study to demonstrate the phenomenon of cross polarization which was mentioned in the introduction to this chapter.

The silicon-29 spectrum in Figure 4.17A clearly indicates the presence of Q^1 silicate species which are present in unblended OPC after one day of hydration. As mentioned previously in this discussion, the Q^0 signal should be considered as a composite arising from the superposition of resonances from C_2S and C_3S. Figure 4.17B shows the cross polarized spectrum of the same sample. As described in the introduction to this chapter, only silicate species possessing vicinial protons will yield a signal on a cross polarized spectrum. This phenomenon is demonstrated

by the fact that no signal arises from the anhydrous cement species whereas the hydrated Q^1 resonance can be seen.

The silicon-29 spectra of OPC at various stages of curing, shown in Figures 4.18A-D, indicate the increase in the Q^1/Q^0 ratio as hydration proceeds. The splitting of the Q^1 signals (seen most clearly in Figures 4.17B and 4.18B) indicates the presence of (at least) two different silicate environments. One of which is known to be attributed to the resonance of silicate from the CSH gel. It is, however, not possible to assign the split signal to any two (or more) specific silicate species without further experimentation due to the number of possibilities available. For example it may be that the signals arise from any combination of different silicate environments of the CSH gel or carbonated silicate species.

(i) Silicate tetrahedra in the CSH gel may be associated with other silicon tetrahedra, calcium or aluminate species. Different vicinial species will influence the chemical shift.

(ii) During the process of carbonation (the reaction of CO_2 with cement) all of the basic cement constituents are at least partly neutralised. Justnes et al. [52] cite (without reference) that 'studies of the carbonation of concrete may be performed by ^{13}C NMR (also silicon)...' indicating that ^{29}Si resonance signals arising from carbonated CSH gel differ in some respect from those arising from non-carbonated CSH gel.

According to Pietersen and co-workers [63] both literature and laboratory findings indicate the occurrence of Q^2 silicate species in the chemical shift region of -83 to -85 ppm. This is in contradiction to the categorisations published by Lippmaa [59] which are tabulated in Table 4.3. One explanation for this anomaly is that Lippmaa worked with relatively pure silicate compounds in his construction of the relationship between NMR chemical shift and silicate-type. Vicinial species in cements may influence the chemical shifts by a process known as deshielding. Lippmaa et al. [59] observed the deshielding effect

of aluminium on the Q^3 and Q^4 resonances of aluminosilicates in the same paper, however, the effect on Q^1 and Q^2 species was not examined. Other workers have noted that each substitution of Al for Si in various silicates results in a deshielding of about 5 ppm [68,69].

In view of this, the shoulder occurring at approximately -85 ppm in Figure 4.18C and the peak occurring at approximately -86 ppm in Figure 4.18D may be attributed to the existence of Q^2 silicate species present in the CSH gel. Pietersen et al. [63] employed silicon-29 MAS NMR to study the hydration of OPC pastes of water:cement ratio 0.4 (although did not specify the curing conditions so no direct comparison of the timescale of hydration reactions in that and this study can be made).

Pietersen et al. [63] conducted spectral deconvolution and simulation using gaussian line shapes in an attempt to distinguish between signal intensities arising from Q^1 and Q^2 silicate species (which, due to line-broadening and deshielding effects, overlap creating difficulties in the interpretation and analysis of such spectra). These spectra are shown in Figure 4.23.

The results obtained by Pietersen indicate the presence of a shoulder (similar to that found in this study), rather than a distinct peak, arising from Q^2 silicate species after curing for 28 days. After 90 days, however, a discrete signal arising from the Q^2 species is noted although a significant extent of overlap between the Q^1 and Q^2 signals still exists. Again, in this respect the results obtained by Pietersen are not dissimilar from those found here.

During cement hydration Q^1 species arise from Q^0 species as the anhydrous (Q^0) calcium silicate phases combine, initially, to form units comprised of two silicon 'atoms', i.e. (Q^1) di-silicate units. With the progression of hydration, Q^2 species form as more mono-silicate units combine with the existing di-silicate units.

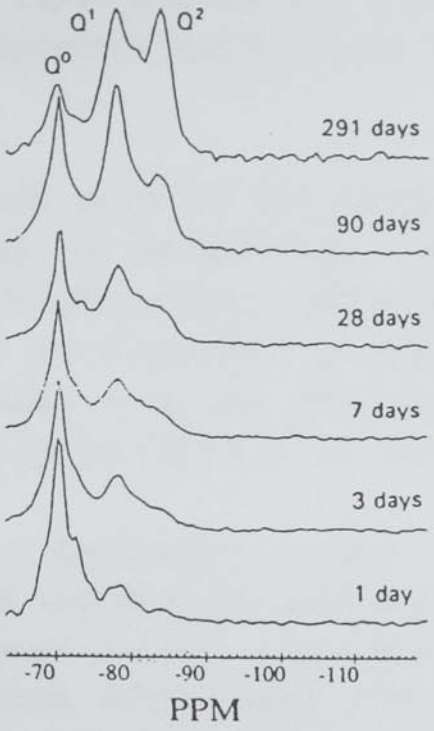

FIGURE 4.23

SILICON-29 MAS NMR SPECTRA OF OPC SAMPLES OF W:S OF 0.4 (AFTER PIETERSEN [63])

In the silicon-29 NMR spectra of mature cement paste the Q^0 signals represent the remaining unhydrated cement, the Q^1 and Q^2 signals represent the end groups and middle groups (respectively).

Comparison of Figures 4.14 and 4.19A-D, which show the aluminium-27 spectra for anhydrous and hydrating cement respectively, indicates a change in symmetry of the aluminium species present in cement on hydration. Initially 4-coordinate aluminium species are present in anhydrous cement. However as little as 24 hours into hydration all of the 4-coordinate species appear to have been transformed into 6-coordinate species. Some 4-coordinate aluminium may still exist which has been masked by the spinning side bands from the 6-coordinate species. It is unlikely that a significant quantity of 4-coordinate aluminium

remains since the spinning side bands on either side of the 6-coordinate signal appear to be of similar intensity. The 'smoothing' of the signal (Figures 4.19 A, B, and C) indicates an increasingly homogeneous aluminium environment as hydration progresses.

Each spinning side band of the spectra of Figure 4.19 is asymmetrical about the vertical axis. There are two possible explanations for this phenomenon; either the spinning side bands are 'folding back' on themselves through space with a slight shift or there actually exist two aluminium environments which are not observable by the nature of the main resonance.

Aluminium-27 is a quadrupolar nucleus which tends to relax fairly rapidly. This explains why the relaxation delay times of the silicon-29 spectra are 500 times greater than those of the aluminium-27 spectra. Even though their T_1 values tend to be low it is still possible that an aluminium species in a particular chemical environment in the cement matrix is not 'allowed' sufficient time to relax in between pulses and is therefore not featuring as a discrete signal on the main spectrum.

The aluminium-27 spectrum shown in Figure 4.22 again possesses asymmetrical spinning side bands and also exhibits an asymmetrical resonance signal. The relaxation delay of this signal is ten times that of the other aluminium-27 spectra in which symmetrical signals are observed. This supports the postulate that two 6-coordinate aluminium environments are in existence although is not conclusive evidence since the asymmetrical line shape may arise from an effect of the quadrupolar nature of the nucleus.

One way to test this postulate would be to conduct a line shape study of spectra obtained at angles which deviate slightly from the Magic Angle. An investigation of this nature is suggested in the final chapter in the section on further work.

After one day of hydration the chemical shift value for the 6-coordinate aluminium species is 13.3 ppm (Figure 4.19) which is seen to differ from those of the more mature samples which occur at around 7.6 to 7.9 ppm. This is indicative of a change in the chemical environment of the aluminium species. This change possibly corresponds with the formation of ettringite and its associated tetracalcium (sulpho)aluminate phases which have been shown by DTA (previous section) to form during this period of hydration. Any further changes in chemical environment of the aluminium (up to 100 days), for example the breakdown of ettringite into thermodynamically more stable species, are not seen to significantly influence the chemical shift of the aluminium.

The increase in the Q^1/Q^0 ratio with curing time of the silicon-29 NMR spectra of samples containing 20% metakaolin in Figure 4.20 demonstrates the progression of hydration.

Semiquantitative comparison of the ratios of the Q^1/Q^0 peaks of the corresponding 1 and 7 day samples containing 0% and 20% metakaolin (Figures 4.18 and 4.20, spectra A and B) suggests that the initial rate of hydration of the calcium silicate phases in metakaolin-blended OPC is greater than that of unblended OPC. This kinetic effect has already been documented in a paper by Pietersen et al. [63]. The effective increase in water:cement ratio in blended cements is believed to be the primary reason for an initial increase in the rate of hydration.

The resonance centred around -101 ppm in Figure 4.20A arises from the Q^4 amorphous silica of metakaolin. Comparison of the two such signals in Figures 4.20A and B demonstrates the depolymerisation of the metakaolin silicate species as hydration proceeds and the pozzolanic reaction occurs. The depolymerisation of the silica is denoted by the 'spreading' of the signal through the Q^3 range towards and into the Q^2 and Q^1 regions of the spectrum. Depolymerisation occurs as the siloxane linkages between the silicate species are cleaved in the highly alkaline conditions associated with the cementitious system.

The pozzolanic reaction is known to commence, in OPC samples bound with 20% metakaolin, during the first 24 hours of curing since one of the products of pozzolanic reaction, hydrated gehlenite, was identified after this period by DTA (see Section 4.6). Owing to the fact that one of the hydration reaction products of the calcium silicates (calcium hydroxide) is consumed by pozzolanic reaction a further increase in the overall rate of hydration is expected. Hence, it is likely that the increase in the Q^1/Q^0 ratio of the metakaolin-blended systems is due to the combined effect of the depolymerisation of the Q^4 silicate species originally present in the metakaolin and an accelerated rate of hydration of the anhydrous calcium silicates.

On the basis that signals arising from Q^2 silicate species can occur in the -83 to -86 ppm region of the NMR spectrum the 7 day 20% metakaolin-blended sample appears to possess an high proportion of such silicate species (-85.64 ppm) whereas no apparent Q^2 species is noted for the same sample-type after a 36 day hydration period. Again, after 100 days hydration, the presence of Q^2 species is acknowledged.

Similarly the silicon-29 MAS NMR spectra of 28 and 197 day samples, containing 20%, 'activated kaolinite' (metakaolin) obtained by Pietersen and co-workers [63] (Figure 4.24) indicate the presence of a shoulder on the Q^1 signal arising from Q^2 species although no such definition exists for the spectrum of the 90 day sample (even though all spectra were obtained under the same conditions with approximately the same number of scans). As previously stated, unfortunately the water:cement ratio of the Pietersen samples, 0.4, differs from that of the samples in this study. Also the temperature at which they were cured is not published. Water:cement ratio and curing temperature both affect the rate of hydration (and in severe circumstances, the products of reaction) hence no direct comparison of the timescale of hydration reactions of the aforementioned results and those published here can be made. Pietersen et al. [63] attribute the lack of distinction between

the Q^1 and Q^2 signals to a deshielding effect caused by the abundance of aluminium from the metakaolin.

The author considers that the effect of deshielding by the increased proportion of aluminium would operate similarly on both Q^1 and Q^2 silicates species causing a relatively similar downfield shift in the signals arising from each and that, therefore, the absence of (a significant quantity of) Q^2 species at some point during hydration is, in fact, real. Also any changes in the environment of the aluminium species between 7 and 100 days are seen (by NMR later in this section) to be negligible. Hence, one would not expect a significant change in the effect of the deshielding of the aluminium on the silicate species during this period.

This postulate operates on the basis that the silica of the metakaolin depolymerises initially to form Q^3, Q^2 and finally Q^1 species (some of) which are then repolymerised as components of the CSH gel (and some of which will remain in the form of (Q^1) hydrated gehlenite as demonstrated by DTA in the previous section). The absence of Q^2 species derived from the hydration of the anhydrous calcium silicates (from the cement) at this point (considering that Q^2 species are present in the unblended counterpart after 36 days of curing) is attributed to the following:

The initial reaction products of the blended system which form at a comparatively increased rate, due to the effective increase in water:cement ratio etc., act to 'block' the pore system and restrict the transport of pore water at later stages of hydration [63]. The effect of this is observed in a comparatively reduced rate of hydration during the later stages of curing. Hence, it is possible that, after 36 days of hydration, the calcium silicates of the cement, in metakaolin-blended systems, have not yet engaged in the formation of silicate species whose extent of polymerisation is greater than Q^1.

Another question naturally arises from this postulate; if the metakaolin depolymerises to form Q^2 species, then why are these not incorporated into the CSH gel instead of depolymerising further only to repolymerise? An answer to this question possibly lies in the morphology of the two Q^2 silicate species.

Q^2 silicate species arising from the depolymerisation of metakaolin are derived from the alkaline cleavage of the siloxane linkages of the amorphous 'parent' system. Hence, it is reasonable to suppose that the Q^2 depolymerisation products of metakaolin will also be amorphous. Whereas Q^2 silicate species arising from the hydration of the anhydrous calcium silicates of OPC are known to possess some degree of crystallinity. (The belief that CSH gels are regarded to possess a degree of crystallinity is reported in the literature [2,4] and denoted by the fact that CSH gels render X-ray diffraction patterns whereas amorphous silicates e.g. metakaolin, do not).

Thus any progressive depolymerisation of Q^2 species derived from metakaolin followed by the their recombination into Q^2 constituents of CSH gel can be explained in terms of a possible difference in morphology between the two silicate types.

Parry-Jones et al. [70] observed a linear relationship between degree of hydration and compressive strength of cement paste systems. Increases in the proportion of Q^2 species present were found to "disproportionately" increase the compressive strength. Increases in Q^2 components relative to Q^1 components in CSH gel indicate an increase in the mean chain length of the silicate polymer system. Thus it might be assumed that, in the event of the metakaolin depolymerisation postulated above, an accompanying strength loss would occur. However this is not necessarily believed to be the case.

If the Q^2 product of depolymerisation is amorphous and not incorporated into the semi-crystalline, rigid CSH gel then there is no more reason for a significant loss in strength than would

be associated with the initial Q^4 to Q^3, or Q^3 to Q^2 depolymerisation processes.

Neither of the hypotheses presented by Pietersen or the author are conclusive although both are available for testing by experimentation of the kind suggested in the further work section in the final chapter.

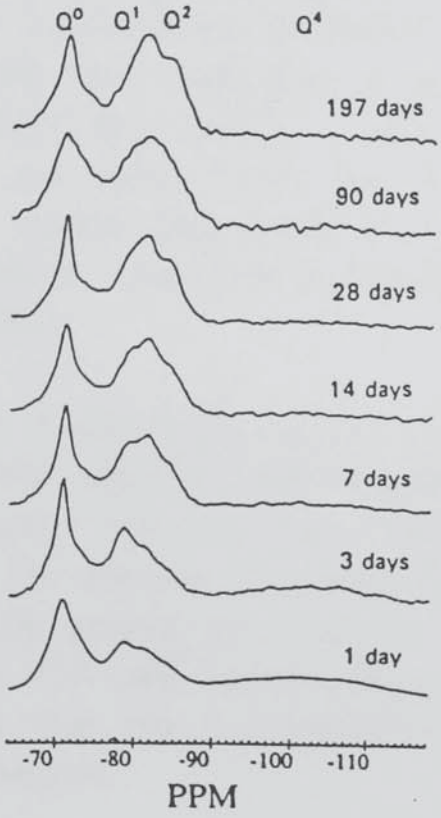

FIGURE 4.24

SILICON-29 MAS NMR SPECTRA OF OPC SAMPLES
CONTAINING 20% MK AT A W:S OF 0.4 (AFTER PIETERSEN [63])

The absence of a distinct signal arising from the activated kaolinite in the spectra in Figure 4.24 should be noted. The only evidence of the presence of activated kaolinite is a very slight camber in the -100 ppm region. An assumption in the production of the NMR spectra is stated to be that "As all materials contained significant levels of iron, T_1 relaxation times for all minerals studied were less than one second" and consequently relaxation delay times of 5 to 10 seconds were employed. No explanation of the absence of a Q^4 amorphous signal is given so

it must be assumed that it has either been omitted in the representation of the spectra or that insufficiently long relaxation delay times were, in fact, used in obtaining those spectra.

An interesting feature of the aluminium-27 spectra of 20% metakaolin-blended samples presented in Figure 4.21 is the relatively rapid disappearance of the 5-coordinate aluminium species. After a curing period of 7 days a negligible concentration of 5-coordinate aluminium remains. Rocha [58] employed the MAS NMR technique to assess the hydrothermal rehydration (at 155°C and 200°C) of metakaolin to kaolinite and discovered that the signal from the 5-coordinate aluminium decreased at a substantially faster rate than that of the 4-coordinate aluminium. (Kaolinite is comprised of 6-coordinate aluminium only [58].)

The fate of the 5-coordinate aluminium species cannot be ascertained by NMR alone as the integrals of the signals from quadrupolar nuclei are not in linear relation to the concentrations of the species from which they arise. During the first 24 hour curing period the formation of hydrated gehlenite has been noted by DTA (see previous section) although it does not necessarily follow that the 5-coordinate aluminium species is engaged in this reaction.

In both Rocha's study and the research reported in this thesis the 5-coordinate aluminium species is seen to be a reactive site. This is unsurprising since the symmetry of that complex is lower than that of the other aluminium species present.

Again the spinning side bands arising from the central 6-coordinate signal are asymmetrical. These spinning side bands have been marked with the symbol 'X' so as to distinguish them from those arising from the other resonances. The same discussion as given (previously in this chapter) for the aluminium-27 spectra of the unblended OPC samples applies.

The problems associated with the production of 'good' spectra of cementitious materials and the ambiguities arising in the interpretation of such have been highlighted in this chapter. Nonetheless it is still a powerful technique for the analysis of the solid phase of cements (especially effective when used in conjunction with other techniques). It may be possible to elucidate further the mechanisms of pozzolanic reaction of metakaolin with results from an MAS NMR synthetic binder project similar to that proposed in the section on further study in the final chapter. A summary of the results of the solid phase study of metakaolin-blended OPC is also included in the discussion in Chapter 7.

CHAPTER 5 THE DIFFUSION OF CHLORIDE IONS THROUGH THE CEMENT MATRIX

5.1 INTRODUCTION

In service many cementitious materials are exposed to attack from aggressive agents such as sea water and deicing salts. One example of this is the penetration of chloride ions which may result in the depassivation and corrosion of embedded steel reinforcements (see Chapter 6).

Embedded steel is usually protected from corrosion by the formation of a passive ferric oxide film. Once chloride ions are within the matrix (in 'sufficient' concentration and in the presence of oxygen) they tend to depassivate embedded steel by locally breaking down this protective oxide layer which is normally stabilised by the highly alkaline environment provided by the electrolyte phase. Sites of intense anodic activity form and develop into 'pits' which may continue to grow if the chloride ion concentration is maintained above a critical level. Anodic corrosion is a volume expansive reaction. (Increases in volume by a factor of seven have been reported [71].) The effect of this volume increase is that stresses are created within the cement matrix, which may, ultimately, result in cracking and spalling.

The rate and extent of corrosive failure of this kind are related to a number of cement matrix variables and environmental factors; the composition of the electrolyte phase (in particular, pH and the ability of the system to 'buffer' the pore solution), chloride binding capacity and the composition of the solid phase, pore structure (porosity, pore size distribution, pore geometry and interconnectivity of pores), the chloride ion concentration of the surroundings, depth of concrete cover and the occurrence of cracks and fissures in the structure.

There exist three possible modes of entry of chloride ions (or other deleterious species) into a structure, which are classified as primary, secondary, and tertiary [72].

Primary chlorides are those introduced via contaminated mix water, accelerating admixtures, aggregates or sand during the mixing stage. Secondary chlorides are categorised as those which penetrate the structure (from the service environment) via the capillary pores. Chloride ions which enter the structure via cracks and fissures (possibly arising from shrinkage and thermal expansion) are referred to as tertiary chlorides.

In the U.K. BS 8110:Part1:1985 limits the chloride ion content of concrete (to below 0.4, 0.2, or 0.1% relative to the mass of cement, and depending on the nature and curing conditions of that cement). Hence, for a concrete structure produced in compliance with this standard, having insignificant cracks and fissures, the only possible mode of entry of chloride ions is via the pore network (i.e. secondary chloride ingress).

The penetration of chloride ions into structures is a diffusion controlled process which was shown, by Sorensen and Maahn [71], to obey Fick's Second Law of diffusion. They studied the chloride penetration of (15-20 years old) marine structures by analysing concrete cores at varying heights above the water level.

Pore structure is seen to be the most influential matrix variable in the diffusion of species through mature hydrated cement pastes [73]. The particular pore structure of a cement is dependent on curing conditions (e.g. temperature, humidity), nature and proportion of admixtures (e.g. pozzolans and plasticisers), water:cement ratio and the presence, within the system, of interfacial zones of segregation.

Pozzolanically-blended cements (in comparison with plain OPCs) tend to provide a greater resistance to the ingress of aqueous agents due to the enhanced subdivision of the capillary pores by a relatively increased proportion of CSH gel.

It was reported in Section 4.4 that the total porosities of (10 and 20%) metakaolin-blended OPC paste samples are lower than those of their unblended counterparts. Literature citations of the

diminished permeability and 'finer' pore structure of metakaolin-blended cement pastes compared with those of plain OPC pastes have also been noted in the introduction to the previous chapter [11,15].

Page, Short, and El Tarras [73] suggested that the effect of chloroaluminate hydrate formation may be of secondary importance with respect to chloride diffusion kinetics compared with the influence of the factors determined by pore structure. Metakaolin-blended samples were found to exhibit superior chloride binding capacities (Chapter 3) which are likely to enhance the resistance of attack from chloride ion penetration.

From these results it can be inferred that additions of metakaolin to ordinary Portland cement paste are likely to cause favourable reductions in the rates at which chloride ions diffuse into the matrices. This postulate has been tested by comparing the diffusion characteristics of metakaolin-blended and plain OPC pastes in an unsteady state chloride diffusion investigation, the results of which are presented in this chapter.

There are two commonly employed techniques for studying the penetration of chloride ions into cement pastes. One is a steady-state technique which produces diffusion coefficients which do not actually resemble any 'in service' situations. This approach is widely used as results may be obtained after a relatively short period of time.

The technique involves the diffusion of the species under investigation through a thin section of cement paste (or mortar) secured between two reservoirs, one of which contains a relatively high concentration of that species. As diffusion occurs the concentration increase of the lower concentration reservoir is monitored. Fick's first law is then used to obtain diffusion coefficients. Many researchers have employed this approach (or similar) to obtain diffusion coefficients enabling the comparison of diffusion characteristics between different cement paste types, curing regimes, admixtures etc. [73,74,75,76].

The non-steady state method which has been adopted in this study to assess the rates of diffusion of chloride ions through plain and metakaolin-blended OPC systems (of water:cement ratios 0.4, 0.5, and 0.6) involves the penetration of chloride ions through the flat surface of a cylinder of cement paste exposed to a saline solution.

The exposure period of such an investigation is usually around 100 days. In general, this is considerably longer than the time required to complete the steady state diffusion investigation. The advantage of the unsteady state diffusion system is that the diffusion coefficients obtained also relate to 'in service' situations and, hence, may be used to calculate the rate of chloride ion penetration through a structure. Such estimates enable the prediction of the depth of concrete cover required to 'protect' steel reinforced systems from chloride ion ingress (for a given service life).

5.2 EXPERIMENTAL PROCEDURE

The mix proportions of samples prepared for the purpose of the diffusion investigation are shown in Table 5.1 (overleaf). Five replicates of each sample type were prepared as described in Section 2.2 and allowed to cure at 22 $\pm$ 2°C for 28 days (since the majority of the hydration chemistry is believed to have taken place by this time). Metakaolin MK 501 was used for all blended systems.

Following the 28 day curing period the samples were demoulded and prepared for immersion in molar saline solution as described in Section 2.2.2. The immersed cylinders were incubated at a constant temperature of 22 $\pm$ 2°C in sealed polypropylene containers.

The saline solution was prepared from a 'background' solution of 0.034M sodium hydroxide, which is of the same pH as saturated calcium hydroxide solution. The purpose of this was to inhibit the leaching and dissolution of the portlandite present in the

cement paste samples. The use of a background solution of saturated calcium hydroxide itself would be unsuitable in this investigation due to the possibility of pozzolanic reaction between the metakaolin and the solution constituents.

W:S RATIO	% METAKAOLIN	AGE {DAYS}
0.4	0, 10, 20	28
0.5	0, 10, 20	28
0.6	0, 10, 20	28

TABLE 5.1
MIX PROPORTIONS OF OPC SAMPLES FOR NON-STEADY STATE CHLORIDE DIFFUSION INVESTIGATION.

No more than ten cylinders were immersed in 4 dm^{-3}. This relatively large volume of solution was required to ensure minimal changes in chloride ion concentration as diffusion progressed.

Following the requisite exposure period the waxed cylinders were retrieved as documented in Section 2.2.2. The various exposure periods are listed in Table 5.2. Three of each cylinder type were then sectioned into discs taken at 7mm intervals along the axis from the exposed surface. The remaining two samples of each type were again cut into 7mm sections but with the first disc cut at 3.5mm to achieve an 'overlapping' effect as indicated in Figure 5.1. The different sets of disc types were labelled 'A' and 'B' respectively.

One set of discs from group 'A' of each sample type was broken into pieces approximately 7mm in diameter. Around 4 grammes from each disc was then subjected to evaporable and non-evaporable water determination as described in Section 2.6. Evaporable and non-evaporable water content values were required for the calculations of total chloride ion concentration (see Sections 2.5 and 2.6).

WATER:CEMENT RATIO	EXPOSURE PERIOD {DAYS}
0.4	79
0.5	64
0.6	79

TABLE 5.2
EXPOSURE PERIOD OF CEMENT PASTE SAMPLE CYLINDERS
TO SALINE SOLUTION

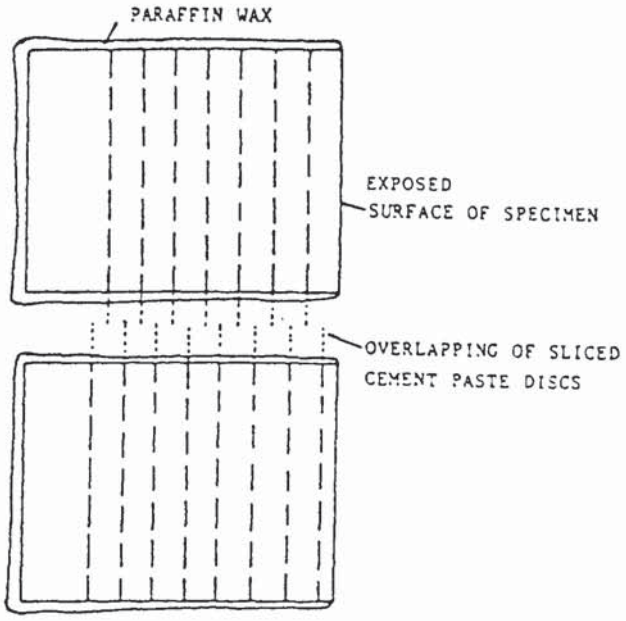

FIGURE 5.1
THE SECTIONING SCHEME OF SPECIMENS FOR
TOTAL CHLORIDE ANALYSIS

Data and worked examples of evaporable and non-evaporable water contents and total chloride ion concentration calculations are located in Appendices 1, 2, and 3. The remaining portion of each disc was oven dried at 105°C in preparation for solid phase analysis by DTA (see Section 2.7.2).

All of the remaining sample discs (two each from groups 'A' and 'B') were ground, graded to 150μm, oven dried and analysed for total chloride ion concentration as described in Section 2.5. The initial absorbence readings taken from the spectrophotometer were corrected (prior to further calculation) to account for the base reading registered when a chloride-free cement paste sample is analysed in the same way.

5.3 RESULTS

The results of the total chloride ion determinations are presented in Tables 5.3, 5.4, and 5.5 with the corresponding graphical profiles in Figures 5.2, 5.3, and 5.4. Each data point represents an average of two experimental results obtained from the analyses of discs from the two sample cylinders of each of the groups 'A' and 'B'. The chloride ion diffusion coefficients derived from the data in Tables 5.3, 5.4, and 5.5 are located in Tables 5.6, 5.7 and 5.8. The data points marked with an asterisk have been omitted from the calculations of the diffusion coefficients. The basis for disregarding these data points is discussed in Appendix 6. DTA profiles (comparing the changes in solid phase composition on exposure to chloride ion ingress) of samples containing 0% and 10% metakaolin, of water:cement ratio 0.5 appear in Figures 5.5 and 5.6.

CHLORIDE ION PENETRATION DEPTH x (mm)	0% MK TOTAL CHLORIDE CONC. mM/g	10% MK TOTAL CHLORIDE CONC. mM/g	20% MK TOTAL CHLORIDE CONC. mM/g
1.75	0.630	0.604	0.323
3.5	0.516	0.395	0.183
7.0	0.265	0.035	0.007
10.5	0.105	0.010	0.006*
14.0	0.031	-	-

TABLE 5.3

TOTAL CHLORIDE ION CONCENTRATIONS

(EXPRESSED AS THE NUMBER OF MOLES PER UNIT MASS OF 'DRY' CEMENT)

FOR SAMPLES OF WATER:CEMENT RATIO 0.4

CONTAINING 0%, 10%, AND 20% METAKAOLIN

CHLORIDE ION PENETRATION DEPTH x (mm)	0% MK TOTAL CHLORIDE CONC. mM/g	10% MK TOTAL CHLORIDE CONC. mM/g	20% MK TOTAL CHLORIDE CONC. mM/g
1.75	0.866	0.876	0.598
3.5	0.696	0.537	0.470
7.0	0.510	0.079	-
10.5	0.290	0.016	0.008
14.0	0.207	-	-
17.5	0.080	0.005*	0.003*
21.0	0.038	-	-
24.5	0.015	-	-
28.0	0.003*	-	-
35.0	0.002*	-	-

TABLE 5.4

TOTAL CHLORIDE ION CONCENTRATIONS

(EXPRESSED AS THE NUMBER OF MOLES PER UNIT MASS OF 'DRY' CEMENT)

FOR SAMPLES OF WATER:CEMENT RATIO 0.5

CONTAINING 0%, 10%, AND 20% METAKAOLIN

CHLORIDE ION PENETRATION DEPTH x (mm)	0% MK TOTAL CHLORIDE CONC. mM/g	10% MK TOTAL CHLORIDE CONC. mM/g	20% MK TOTAL CHLORIDE CONC. mM/g
1.75	1.068	1.217	0.980
3.5	0.891	0.988	0.624
7.0	0.598	0.393	0.223
10.5	0.513	0.125	0.027
14.0	0.341	0.048	0.005
17.5	0.238	0.004*	-
21.0	0.140	-	-
24.5	0.079	-	-
31.5	0.022*	-	-

TABLE 5.5

TOTAL CHLORIDE ION CONCENTRATIONS

(EXPRESSED AS THE NUMBER OF MOLES PER UNIT MASS OF 'DRY' CEMENT)

FOR SAMPLES OF WATER:CEMENT RATIO 0.6

CONTAINING 0%, 10%, AND 20% METAKAOLIN

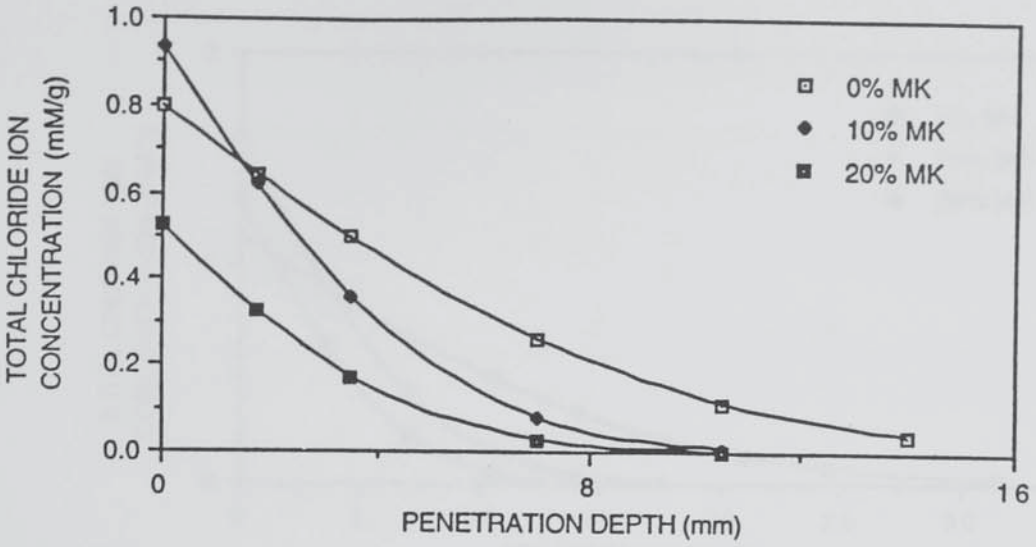

FIGURE 5.2
TOTAL CHLORIDE ION CONCENTRATION PENETRATION PROFILES FOR CEMENT PASTE SAMPLES OF WATER:CEMENT RATIO 0.4 CONTAINING 0%, 10%, AND 20% METAKAOLIN

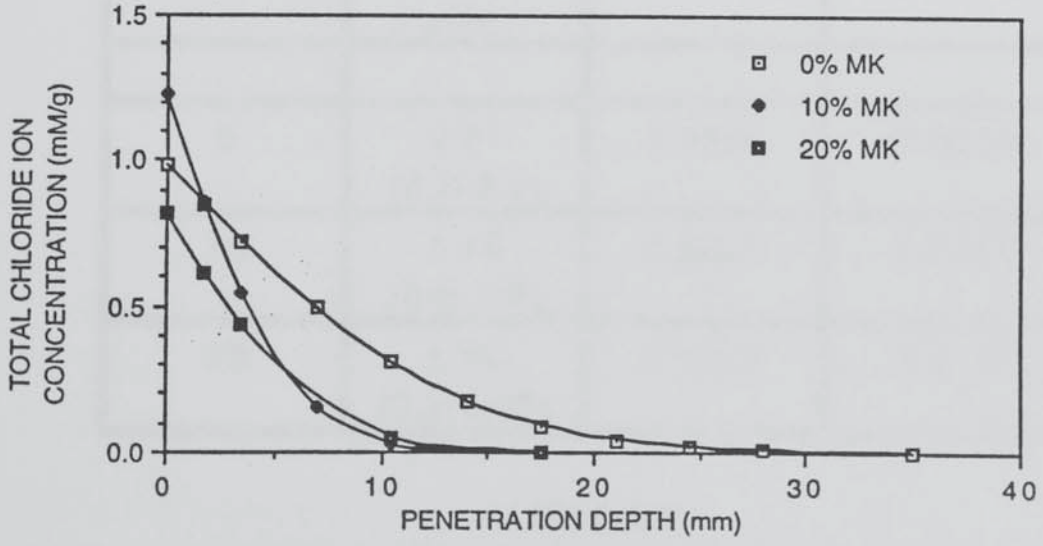

FIGURE 5.3
TOTAL CHLORIDE ION CONCENTRATION PENETRATION PROFILES FOR CEMENT PASTE SAMPLES OF WATER:CEMENT RATIO 0.5 CONTAINING 0%, 10%, AND 20% METAKAOLIN

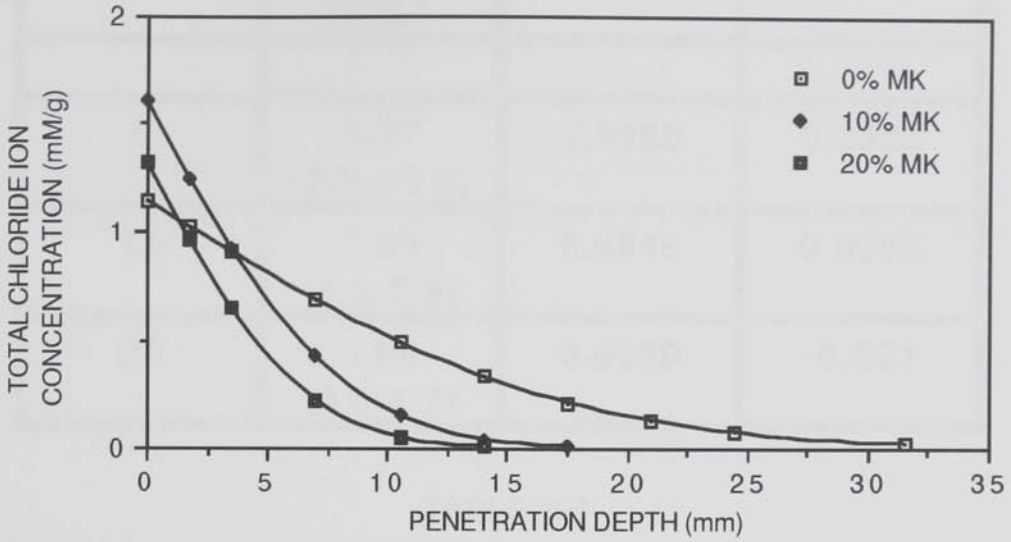

FIGURE 5.4
TOTAL CHLORIDE ION CONCENTRATION PENETRATION PROFILES FOR CEMENT PASTE SAMPLES OF WATER:CEMENT RATIO 0.6 CONTAINING 0%, 10%, AND 20% METAKAOLIN

% METAKAOLIN	D ($\times 10^8$) $cm^2 s^{-1}$	r	INTERCEPT cm
0	3.51 (3.8-3.2)	0.9990	-0.0028
10	1.16 (0.8-1.8)	0.9808	-0.0039
20	1.50 (0.9-2.85)	0.9929	-0.0117

TABLE 5.6
EFFECTIVE DIFFUSION COEFFICIENTS, D, FOR THE PENETRATION OF CHLORIDE IONS INTO CEMENT PASTES OF WATER:CEMENT RATIO 0.4 CONTAINING 0%, 10%, AND 20% METAKAOLIN (AT 22°C). THE FIGURES IN BRACKETS ARE THE 95% CONFIDENCE INTERVALS FOR THE DIFFUSION COEFFICIENTS.

% METAKAOLIN	D(x10^8) cm^2s^{-1}	r	INTERCEPT cm
0	9.37 (8.8-10.0)	0.9980	0.0029
10	1.85 (1.3-2.8)	0.9849	0.0068
20	1.66 (0.8-4.7)	0.9950	-0.021

TABLE 5.7
EFFECTIVE DIFFUSION COEFFICIENTS, D, FOR THE PENETRATION OF CHLORIDE IONS INTO CEMENT PASTES OF WATER:CEMENT RATIO 0.5 CONTAINING 0%, 10%, AND 20% METAKAOLIN (AT 22°C). THE FIGURES IN BRACKETS ARE THE 95% CONFIDENCE INTERVALS FOR THE DIFFUSION COEFFICIENTS.

% METAKAOLIN	D(x10^8) cm^2s^{-1}	r	INTERCEPT cm
0	13.43 (12.4-14.6)	0.9964	0.0008
10	2.86 (2.6-3.2)	0.9966	0.0010
20	1.58 (1.5-1.7)	0.9982	0.0016

TABLE 5.8
EFFECTIVE DIFFUSION COEFFICIENTS, D, FOR THE PENETRATION OF CHLORIDE IONS INTO CEMENT PASTES OF WATER:CEMENT RATIO 0.6 CONTAINING 0%, 10%, AND 20% METAKAOLIN (AT 22°C). THE FIGURES IN BRACKETS ARE THE 95% CONFIDENCE INTERVALS FOR THE DIFFUSION COEFFICIENTS.

W:S / %MK	0%	10%	20%
0.4	0.80	0.93	0.54
0.5	1.00	1.23	0.78
0.6	1.17	1.61	1.32

TABLE 5.9
CHLORIDE ION 'SURFACE CONCENTRATIONS' OF CEMENT PASTE SAMPLES OF WATER:CEMENT RATIOS 0.4, 0.5, AND 0.6 AND 0%, 10%, AND 20% REPLACEMENT METAKAOLIN.

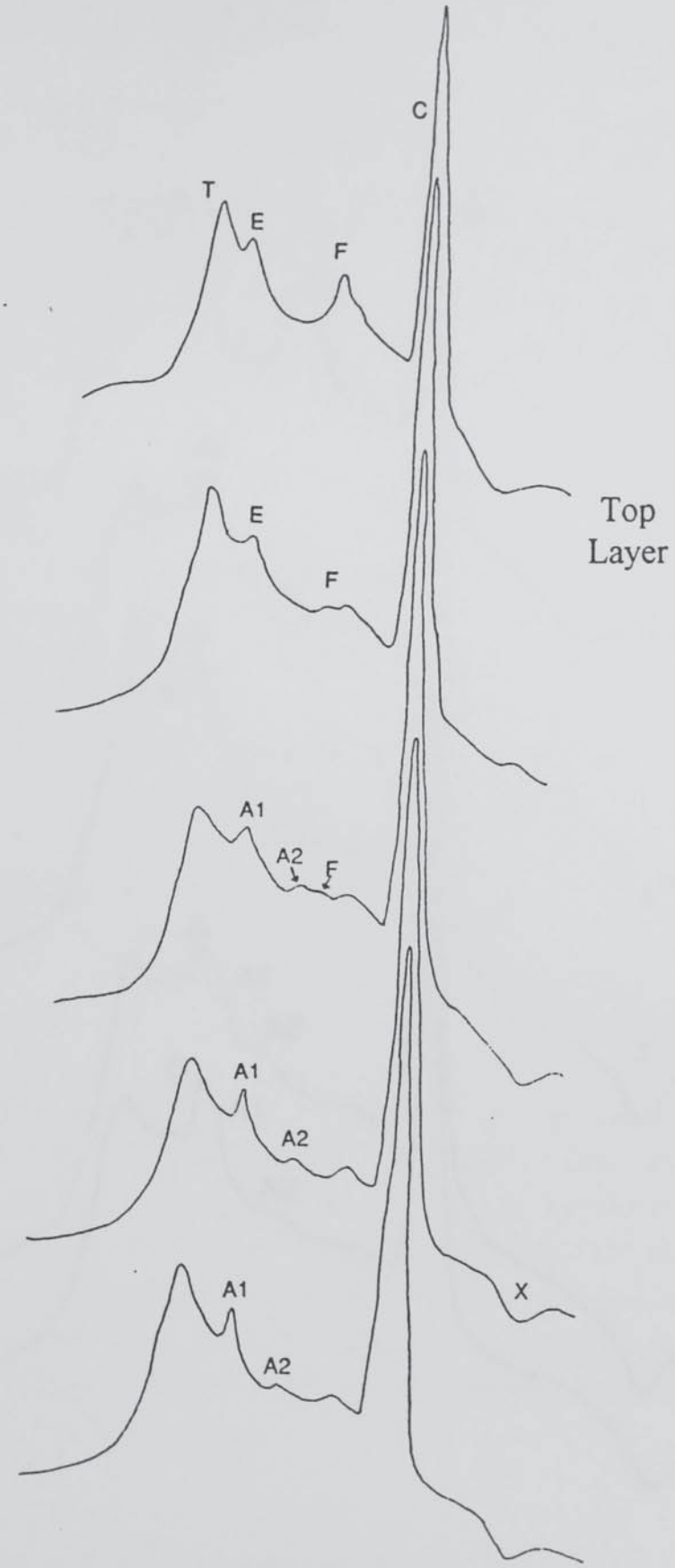

FIGURE 5.5
DTA TRACES OF PLAIN OPC PASTES
(OF WATER:CEMENT RATIO 0.5) AT INCREASING DEPTHS AFTER
EXPOSURE TO MOLAR SODIUM CHLORIDE SOLUTION FOR 64 DAYS

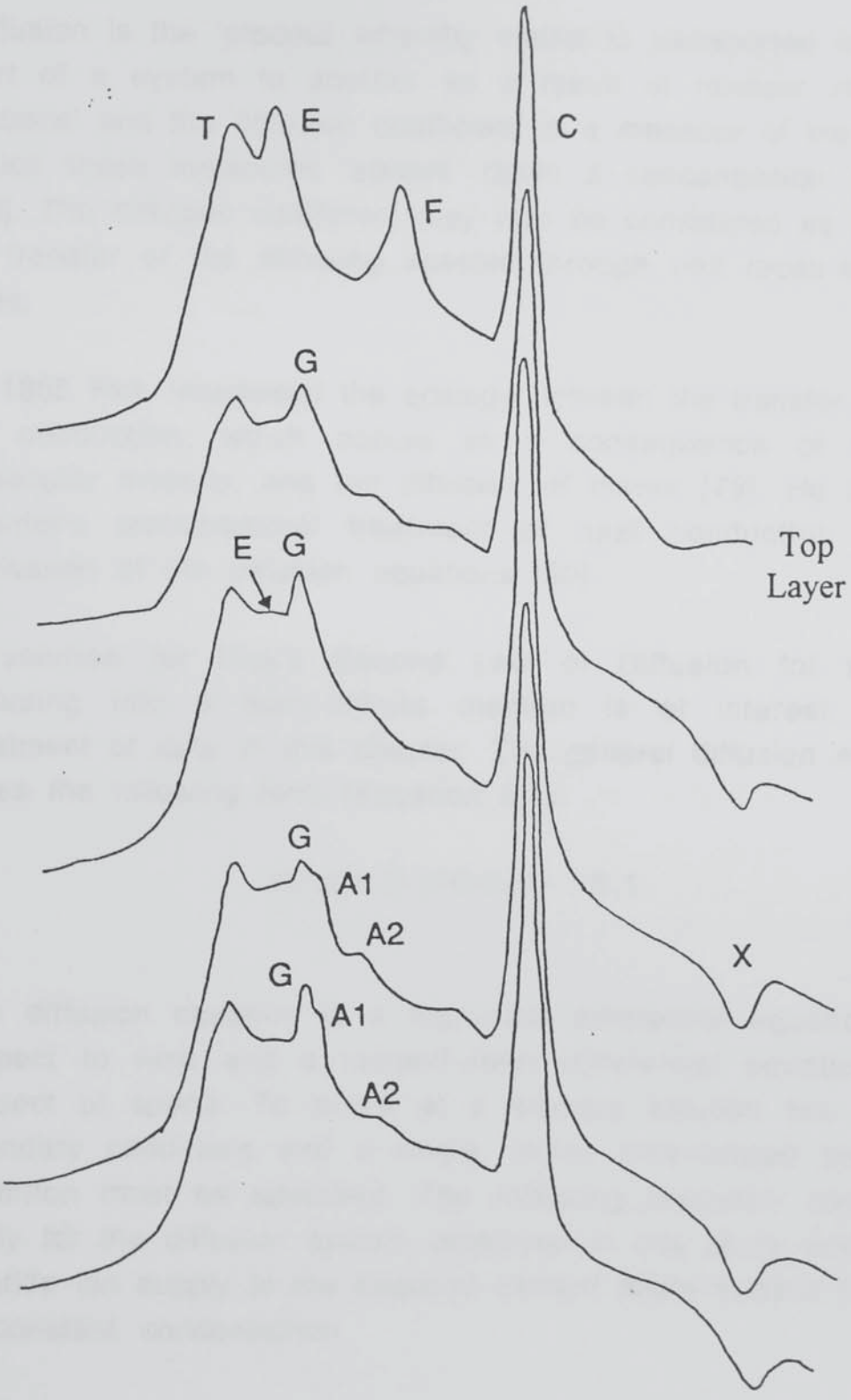

FIGURE 5.6
DTA TRACES OF 10% METAKAOLIN-BLENDED OPC PASTES (OF WATER:CEMENT RATIO 0.5) AT INCREASING DEPTHS AFTER EXPOSURE TO MOLAR SODIUM CHLORIDE SOLUTION FOR 64 DAYS

5.4 EXAMINATION OF THE MATHEMATICAL TREATMENT OF RESULTS

Diffusion is the 'process whereby matter is transported from one part of a system to another as a result of random molecular motions' and the diffusion coefficient is a measure of the rate at which those molecules 'spread' down a concentration gradient [78]. The diffusion coefficient may also be considered as the rate of transfer of the diffusing species through unit cross-sectional area.

In 1855 Fick recognised the analogy between the transfer of heat by conduction, which occurs as a consequence of random molecular motions, and the diffusion of matter [79]. He adapted Fourier's mathematical treatment of heat conduction in the derivation of the diffusion equations [80].

A solution for Fick's Second Law of Diffusion for species diffusing into a semi-infinite medium is of interest in the treatment of data in this chapter. The general diffusion equation takes the following form (Equation 5.1):

$$\partial C/\partial t = D\ \partial^2 C/\partial x^2 \quad \cdots\cdots 5.1$$

The diffusion equation is a first-order differential equation with respect to time and a second-order differential equation with respect to space. To arrive at a working solution two spatial boundary conditions and a single, initial, time-related boundary condition must be specified. The following boundary conditions apply for the diffusion system employed in this study where the chloride ion supply at the exposed cement paste surface (x=0) is of constant concentration.

$$C_x = 0 \text{ at } x > 0 \text{ and } t = 0$$

$$C_x = C_s \text{ at } x = 0 \text{ and } t > 0$$

$$C_x = C_0 \text{ at } x = \infty$$

$$C_x = C_{(x,t)} \text{ at } x > 0 \text{ and } t > 0$$

The following expression is the solution to Fick's Second Law for the boundary conditions defined above (Equation 5.2):

$$C_x = C_s - \{(C_s - C_0)\ \text{erf}(y)\} \cdots\cdots 5.2$$

where $y = \{x/[2(Dt)^{1/2}]\}$, and since $C_0 = 0$, the expression reduces to:

$$C_x/C_s = 1 - \text{erf}(y) \cdots\cdots 5.3$$

where,

C_x = chloride ion concentration within the paste at distance x from the exposed surface.

C_0 = the original chloride ion concentration of the cement paste.

C_s = the chloride ion concentration at the exposed surface.

x = the distance (into the cement paste) from the exposed surface (cm).

t = exposure time (seconds).

D = the (effective) diffusion coefficient (cm^2s^{-1}).

erf(y) = Gaussian error function

Expression 5.3 may be used to calculate effective diffusion coefficients for the penetration of chloride ions into cement pastes. Various assumptions are made about the diffusion

coefficient and the experimental conditions in the derivation of Expression 5.3:

(i) The medium into which diffusion occurs is assumed to be semi-infinite and homogeneous. On a relatively small scale (i.e. a μm scale) this is obviously not true for a cement paste system which is composed of interconnected pore networks containing the electrolyte phase through which the (hydrated) chloride ions diffuse. Surface interaction takes place between the pore walls (which are composed of CSH gel, portlandite, and various alumino-silicate species) and the chloride ions. However, on a macro-scale (the cross-sectional area exposed to saline solution in this investigation is approximately 18.9cm^2) the system may be considered to possess the same bulk properties in all directions.

(ii) The value of the diffusion coefficient is presumed to be constant and independent of concentration at this (1 molar) dilution.

(iii) The chloride ion concentration at the exposed surface is considered to be constant. The results and diffusion coefficients derived from this investigation are based on total chloride ion concentration measurements. The total chloride ion concentration is the sum of the bound and unbound chloride ion contents, which are both assumed to be constant (at the surface) since the chloride ion concentration of the saline solution is constant. Theoretically, the concentration of the unbound chloride ions at the surface will attain the same value as that of the saline solution a short while after the diffusion process is initiated, and once the initial binding of chloride ions has occurred it is reasonable to regard its level as fixed (since the concentration of the external saline solution does not change).

It should be noted that the diffusion coefficients estimated in this study are referred to as 'effective' diffusion coefficients since the pores through which the actual diffusion takes place

only constitute a proportion of the total bulk volume of the cement paste sample under investigation.

Since all of the diffusion investigations in this study took place under the same experimental conditions (especially at the same temperature) the resulting diffusion coefficients can be regarded as a measure of the resistance of the different cement matrices to chloride ion penetration. Obviously, the smaller the diffusion coefficient, the greater the resistance to penetration.

The dimensions of the diffusion coefficient are independent of the units of the concentration of the chloride ion reservoir and total chloride ion content of the cement paste. Hence any consistent units may be used in the calculations of the diffusion coefficients.

An example of the mathematical treatment described above is given in Appendix 6.

5.5 DISCUSSION

The diffusion coefficients for the penetration of chloride ions into mature cement pastes calculated from the data collected in this investigation (Tables 5.6, 5.7, and 5.8) are of the same orders of magnitude and compare well with those of other workers using similar experimental techniques [71, 82, 83]. A correlation coefficient, r, of unity and a zero intercept indicate that the mechanism of diffusion is as described by Fick's Second Law.

The accuracy of the diffusion coefficients calculated for some of the systems containing metakaolin are comparatively low as a consequence of an inadequately long exposure period. The research schedule allowed a maximum immersion period of 79 days as opposed to 100 days which would ordinarily elapse during such investigations. The result of this reduced immersion period was that relatively few data points could be collected for the sample systems of particularly low porosity (i.e. those of

low water:cement ratio and high metakaolin content) which did not allow sufficiently extensive penetration of chloride ions. That the chloride ion penetration into the metakaolin-blended cement pastes was seen to be less extensive than that of their unblended counterparts gives a qualitative indication that metakaolin-blended cements offer more resistance to chloride ion ingress than do plain OPC pastes (of the same water:cement ratio).

The diffusion coefficients for the diffusion of chloride ions in plain OPC pastes are all significantly higher than those for the corresponding samples blended with 10 and 20% metakaolin. The differences between the diffusion coefficients of the blended and unblended systems are more marked at higher water:cement ratios. The diffusion coefficient of 3.51×10^{-8} cms^{-1} obtained for the permeation of chloride ions into unblended OPC of water:cement ratio 0.4 is three and twice times those of pastes blended with 10 and 20% metakaolin respectively. The diffusion coefficient for the unblended OPC system of water:cement ratio 0.6 is approximately five and eight times those of the systems blended with 10 and 20% metakaolin respectively.

The chloride ion 'surface concentration' values (Table 5.9) were calculated from the total chloride ion profile data (using a software package). The surface concentration is the chloride ion concentration of the first layer of infinitesimal depth which had been exposed to the saline solution. This value (when derived from total chloride ion analysis data) gives an indication of the extent of the chloride binding capacity of a cementitious system.

An high surface ion concentration is indicative of an high chloride binding capacity. At the exposed surface the free chloride ion concentration is, theoretically, equivalent to the chloride ion concentration of the saline reservoir i.e. all cement paste samples should possess the same concentration of free chloride ions in the pore solution phase at the exposed surface. The 'surface concentration' is the sum of the free and bound chloride ion concentrations at the surface. Hence, any difference

in surface concentration must be due to a difference in the quantities of chloride ions which are bound in the solid phase. This argument is based on the assumption that the bound and unbound water contents are similar for all samples of the same water cement ratio irrespective of metakaolin content. The bound and unbound water contents of all samples observed in this study are tabulated in Appendix 2 and indicate that this assumption is reasonable.

The chloride ion surface concentration values for all of the paste samples blended with 10% replacement metakaolin are higher than those of the corresponding, unblended, plain OPC pastes. This (as described above) indicates that the chloride binding capacities of the metakaolin-blended pastes are greater than those of their unblended counterparts.

It is surprising to note that the surface concentrations of the samples containing 20% metakaolin are the lowest of each set of values for samples of water:cement ratios 0.4 and 0.5 (and relatively low for those of water:cement ratio 0.6), since it was discovered that samples blended with 20% replacement metakaolin containing 'internal' chloride ions, possessed the highest chloride binding capacities (Chapter 3).

There exist two possible explanations for this apparent discrepancy. The surface concentrations for the samples containing 20% metakaolin have been derived from data of low accuracy (as previously discussed) so it is possible that more precise data collection and analysis would produce a contrary result. If, however, the chloride binding capacities of the samples containing 20% metakaolin are, in actual fact, lower than those of either the unblended pastes or pastes extended with 10% metakaolin (for samples of water:cement ratios 0.4 and 0.5) this phenomenon may be accounted for by considering the availability of 'binding sites'.

It is possible that the low porosity of the samples blended with 20% metakaolin (of water:cement ratios 0.4 and 0.5) has caused a

relative decrease in the availability of binding sites along the pore walls with which solvated chloride ions may combine in an insoluble form (owing to the general reduction in the total (pore wall) surface area which accompanies a reduction in porosity). This possible reduction of available binding sites would obviously be irrelevant when considering chloride binding capacities based on investigations involving the addition of 'internal' chlorides which are introduced at the mixing stage (as documented in Chapter 3). The surface concentration of the sample blended with 20% metakaolin of water:cement ratio 0.6, which is undoubtedly more porous than the corresponding samples of water:cement ratios 0.4 and 0.5, is of an intermediate (as opposed to being the lowest) value. This result is in evidence of the above postulate.

DTA thermoanalytical curves of samples (of water:cement ratio 0.5) containing 0% and 10% metakaolin at increasing depths after exposure to the saline reservoir are located in Figures 5.5 and 5.6 respectively.

The presence of Friedel's salt up to a depth of (approximately) 21mm (i.e. the top three layers) from the exposed surface is observed for both sample sets. Chloride ions, however, are known to be present at greater depths (see Table 5.5). It is possible that Friedel's salt is present in the lower two layers but not in sufficient concentration to allow detection.

Comparison of the surface and subsequent layers of each set of thermoanalytical curves indicates relative reductions in the proportion of calcium hydroxide (portlandite). This is due to the dissolution and leaching of the calcium hydroxide from the pastes during the immersion period. Leaching, although inhibited by the sodium hydroxide background solution of the same pH as aqueous saturated calcium hydroxide, cannot be completely eliminated.

As noted in Section 4.6 the prolonged existence of ettringite in the presence of chloride ions is again observed. The

thermoanalytical curves of Figure 5.5 (0% metakaolin) indicate that the two uppermost layers, which possess a relatively high proportion of chloride species, also possess quantities of ettringite, which, in lower layers (of lower 'chloride' content) has decomposed into its thermodynamically more stable constituents: tetracalcium sulphoaluminate hydrate and tetracalcium aluminate hydrate. The presence of ettringite is also observed in the exposed and third layers of the paste containing 10% metakaolin (Figure 5.5). It is likely that the second layer also contains a proportion of ettringite, the corresponding signal of which is masked by that of hydrated gehlenite.

Hydrated gehlenite (one of the products of pozzolanic reaction) is observed in all but the exposed layer of the thermoanalytical curves of the pastes containing 10% metakaolin. The DTA thermoanalytical curves of samples (of water:cement ratio 0.5) containing 10% and 20% metakaolin and 1.0% 'internal chloride' species (Figures 4.11 and 4.12) indicate the absence of hydrated gehlenite.

This is suggestive of the role of hydrated gehlenite in the enhancement of chloride binding capacity as postulated in Section 4.6. Hence the absence of hydrated gehlenite in the exposed layer (i.e. that layer which contains the highest proportion of chloride species) further implies its participation in the solid state binding of chloride ions.

Unfortunately the DTA set-up utilised in this study was intended to give a 'fingerprint' of each cement paste composition and does not allow quantitative analysis thus it is not possible from these results alone to assess the relative proportions of Friedel's salt and hydrated gehlenite. However, considering the absence of hydrated gehlenite in both metakaolin-blended sample systems containing chloride ions and the absence of any other identifiable phases other than CSH gel and calcium hydroxide it is believed that hydrated gehlenite is operative in the removal and solid state binding of chloride ions from the pore solution.

(As a matter of interest, the large exothermic peaks present in the thermoanalytical curves of samples containing both metakaolin and 'internal chlorides' are not present in the thermoanalytical curves of the chloride-contaminated mature pastes of the diffusion investigation. The difference in method of chloride ion entry or sample preparation for DTA analysis may be accountable for this dissimilarity.)

In conclusion, the diffusion coefficients obtained in this study indicate that OPC pastes containing replacement metakaolin exhibit superior chloride ion diffusion characteristics in comparison with those of plain OPC pastes of the same water:cement ratio (for the water:cement ratio range observed). In addition, it is known that metakaolin-blended OPC pastes, in general, possess higher chloride binding capacities compared with those of their unblended counterparts (Sections 3.4, 4.6 and above). This indicates that their actual performances in the resistance to chloride ion penetration are likely to be better than those reflected by the diffusion coefficients which have been derived from total chloride ion analysis since the proportion of free chloride present in their electrolyte phases is likely to be lower.

CHAPTER 6 THE CHLORIDE-INDUCED CORROSION BEHAVIOUR OF STEEL EMBEDDED IN METAKAOLIN-BLENDED CEMENT PASTES

6.1 INTRODUCTION

The corrosion of steel in concrete exposed to chloride-rich environments (e.g. highway and marine structures) presents a major problem to bridge and concrete engineers. Many large-scale, premature failures of reinforced concrete structures (often requiring costly refurbishment or complete replacement) are attributed to the corrosion of the reinforcing steel components [84,85]. The problem of corrosive failure of steel in concrete exposed to chloride species has been acknowledged and investigated since the beginning of this century [86].

Several parameters determine the corrosion characteristics of embedded steel reinforcements - the composition and surface condition of the steel, the composition of the electrolyte, the portlandite content and 'buffering' ability of the solid phase - and consequently many varied approaches to the inhibition of reinforcement corrosion exist - galvanisation and protective epoxy coating of steel reinforcements, impregnation of hardened concrete with polymers and waxes, cathodic protection, and the addition of chemical inhibitors (e.g. calcium nitrite) to the cement phase [87,88,89,90].

The corrosion of embedded steel in concrete is an electrochemical phenomenon. Steel is normally protected from corrosion in dense concrete by the formation of a passive oxide film similar in composition to γ-Fe_2O_3 [30]. This oxide film is stabilised in the highly alkaline environments usually associated with the pore electrolyte phase (owing to the insolubility of the oxide layer in basic solution). The loss of alkalinity (by leaching or carbonation) or the presence of aggressive anions such as chloride ions are capable of destroying the passive oxide film.

With sufficiently oxygenated pore solution and in the absence of aggressive anions, should the passive film breakdown, anodic

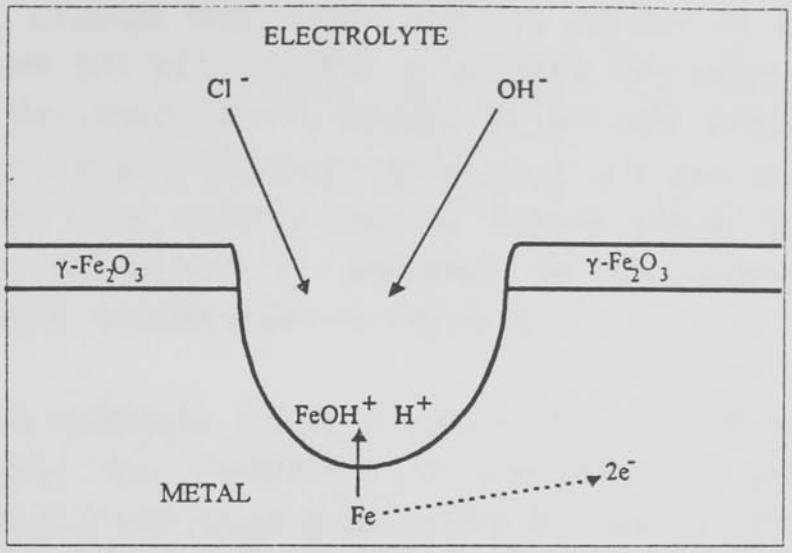

Figure 6.1
Schematic Diagram of Developing Pit

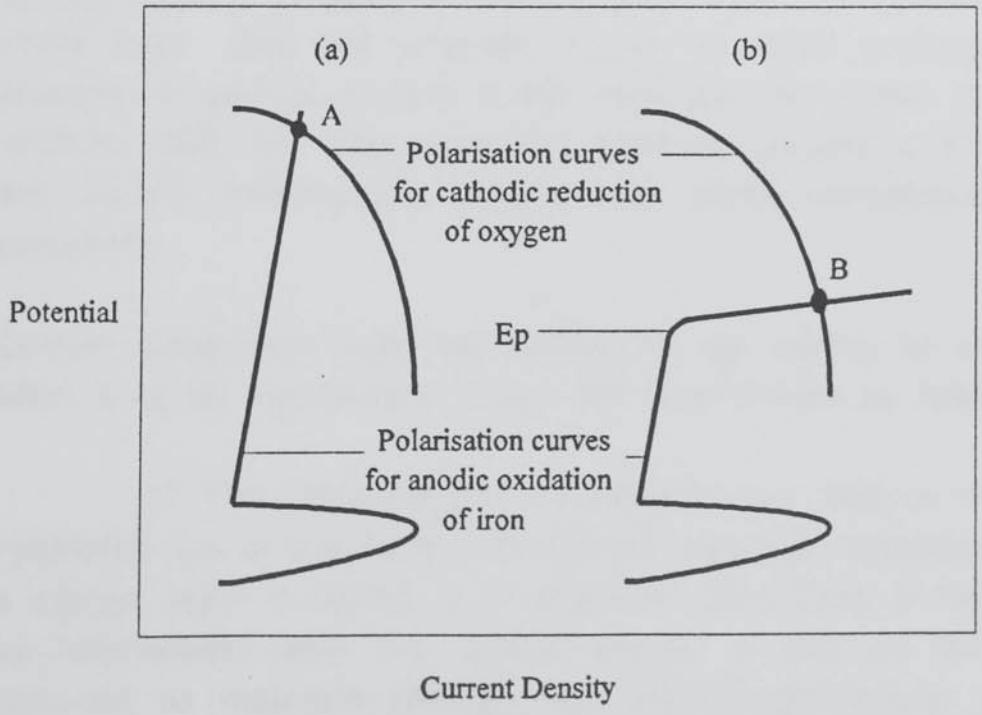

Figure 6.2
The schematic Polarization Curves for:
(a) Passive Iron and (b) Pitting Iron

dissolution of iron II ions is likely to be followed by the formation of more iron III oxide which repairs the active site.

However, chloride ions, which may be present in the solution phase (from mix contamination or chloride rich environments, as noted in the introduction to Chapter 5) are able to penetrate the oxide layer causing localised reduction of pH and breakdown of the passive layer creating sites of intense anodic activity. This localised breakdown is referred to as pitting and is demonstrated schematically in Figure 6.1.

The Evans diagrams shown in Figure 6.2 (a) and (b) indicate, respectively, the conditions of passive and pitting steel embedded in a well oxygenated cement or concrete specimen. The corrosion potential (E_{CORR}) and corrosion rate (i_{CORR}) are represented by the Cartesian co-ordinate values of the points of intersection (i.e. the points at which the rates of the anodic and cathodic reactions are equal), A and B, of the anodic and cathodic polarization curves in each case.

E_{CORR} values for passive steel (Figure 6.2a) are generally more noble than -250 mV whereas those for steel undergoing the process of pitting (Figure 6.2b) normally fall within the range -350 to -500 mV. The corrosion currents associated with pitting are usually considerably greater than those corresponding with passivity.

Certain conditions must be fulfilled if the pitting of embedded steel is to be maintained. These are summarised as follows:

(i) The concentration of chloride ion relative to that of hydroxide ion in the vicinity of the pit must be maintained above a certain level if pitting is to proceed. This ratio is believed to be interrelated with the 'critical depth' of the pit (that depth required to maintain pitting) and the concentrations of many other aqueous species present (e.g. Fe^{2+}, $FeOH^{+}$, $Fe(OH)_2$ and H^{+}) [34]. It should be noted that, as anodic dissolution occurs, the developing pit becomes progressively more acidic as a

consequence of the dissociation of water during the hydrolysis of iron II ions. Hausmann [43] proposed a critical $[Cl^-]/[OH^-]$ ratio of 0.6 based upon mild steel corrosion tests in calcium hydroxide solution of pH 12.5. A critical ratio of this kind, above which pitting occurs, is not applicable to embedded steel in concrete owing to the influence of other factors. The $[Cl^-]/[OH^-]$ ratio can, however, provide a simple index for the comparison of the relative risks of chloride induced depassivation leading to pitting corrosion of steel in different types of concrete.

(ii) Since the anodic reaction is coupled with the cathodic reduction of molecular oxygen, a sufficient oxygen supply is required to sustain pitting at values of E_{CORR} more noble than the pitting potential (denoted in Figure 6.2b by 'Ep'). For a given steel alloy and surface preparation procedure, the pitting potential is a function of the composition of the electrolyte. The pitting potential decreases with increasing chloride ion concentration. As the oxygen supply is restricted the cathodic polarization curve becomes progressively more steep causing the point of intersection of the two polarization curves to occur below Ep in the region of passivity [93].

The formation of portlandite around embedded steel reinforcements is considered to act, not only as an hydroxyl ion replenisher, but is also believed to constitute a physical barrier against the further diffusion of chloride ions to a developing pit [94]. This process of hydroxide ion replenishment of the electrolyte at the expense of the portlandite of the solid phase is referred to as 'buffering'.

The presence of pozzolans, such as metakaolin, may reduce the effectiveness of both the buffering phenomenon and the portlandite barrier owing to the consumption of portlandite during pozzolanic reaction. However, the increased subdivision of the pore structure in pozzolanically-blended cement pastes is thought to cause a reduction in the net 'mobility' of the chloride ions. Since a flux of chloride ions is required to sustain the pitting process the provision of a relatively increased barrier to

chloride ion transport in pozzolanically-blended pastes is undoubtedly advantageous [91].

The application of metakaolin as an high quality, pozzolanic, cement supplement is a relatively recent one. Its influence on the long-term behaviour and durability of reinforced structures is not known. The superior chloride binding capacities of metakaolin-blended cement pastes with respect to those of OPC have already been reported in Chapter 3. This characteristic is obviously favourable when considering the chloride-induced corrosion of embedded steel. However, metakaolin-blended OPCs are known to contain a relatively reduced proportion of portlandite in comparison with their unblended counterparts.

The purpose of the investigation documented in this chapter is to present a relative assessment of the corrosion characteristics of mild steel embedded in plain OPC and metakaolin-blended cement pastes. Gravimetric and linear polarisation techniques (see Section 2.9) were used to monitor the extent of corrosion of the steel embedded in cement paste specimens containing 0, 10, and 20% metakaolin and 0, 0.4, and 1.0% internal chloride ions.

6.2 EXPERIMENTAL PROCEDURE

The mix proportions of samples prepared for the purpose of chloride-induced corrosion analysis are presented in Table 2.4. Four replicates of each sample type were prepared as described in Section 2.2.3.

The mild steel electrodes were masked with a white cement and styrene-butadiene rubber paste prior to the application of a cold curing epoxy resin in an attempt to inhibit crevice corrosion which may otherwise occur at the steel/epoxy resin interface.

The linear polarization technique and experimental procedure are outlined in Section 2.9. E_{CORR} measurements were made relative to a saturated calomel electrode. Contact between the calomel

electrode and samples was made via a small section of sponge moistened with deionized water.

Within hours of the final linear polarization measurement the steel electrodes were recovered from the cement pastes and subjected to an electrolytic cleaning procedure. They were each immersed in Clark's solution for 15 minutes, scrubbed with a soft bristle brush, and successively rinsed with deionised water and acetone.

The use of Clark's solution provides an effective method for removing oxide coatings formed on iron and steel. The removal of some solid metal, which would result in error in the determination of the corrosion rate, is unavoidable. As a measure against this, several cleaned and weighed specimens were recleaned by the same method and reweighed. The loss due to this second treatment was then used as a correction to that indicated by the first weighing.

Following the cleaning procedure, the mass of each electrode was then recorded, corrected, and compared with that prior to embedding in the cement paste.

The extent of corrosion determined by this method was then compared with that determined by linear polarization.

6.3 RESULTS

The results of measurements of E_{CORR} versus time are shown in Figures 6.3, 6.4, and 6.5. The points on the graph represent averaged values of the four replicates in each case. The corrosion rate profiles (obtained by the linear polarization technique) are presented in Figures 6.6, 6.7, and 6.8. The i_{CORR} values were calculated using the Stern-Geary equation (equation (x) Section 2.9) with the assumption that the anodic and cathodic Tafel constants are equal and have a value of 120 mV [29].

The average electrode mass losses of each sample type which were determined by gravimetric analysis are shown in Table 6.1. Each calculation of the average mass loss according to the linear polarization data was made by estimating the total surface charge which flowed throughout the investigation (i.e. estimating the area under the corrosion rate versus time curve) and converting this value to a loss in mass (on the basis that the anodic oxidation of iron is a 2 electron transfer process). The average mass losses calculated by this method are located in Table 6.2.

The suite of numerical data obtained during this investigation is located in Appendix 7. The results for each set of replicate specimens showed considerable scatter, however this is common for E_{CORR} and i_{CORR} measurements of this type [30].

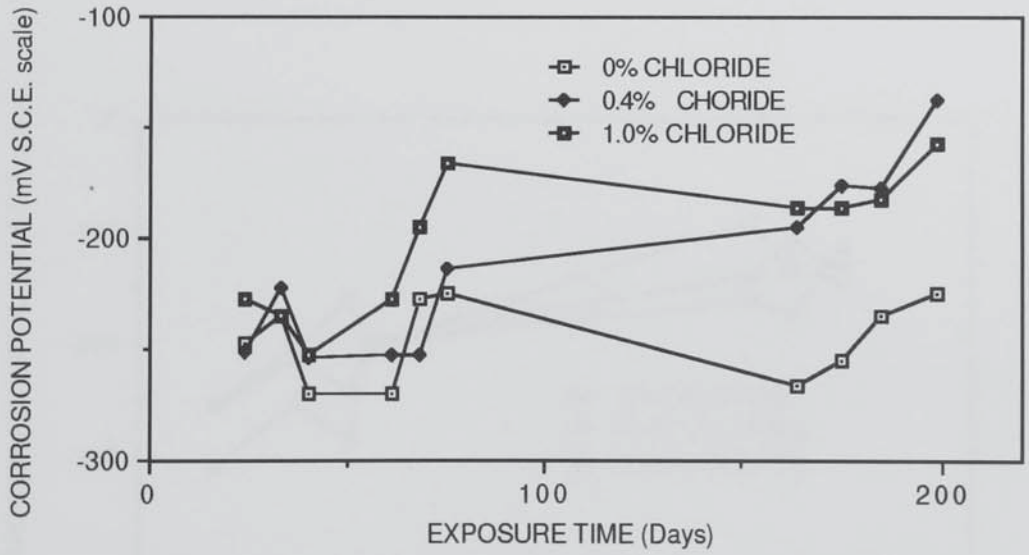

FIGURE 6.3
CORROSION POTENTIAL PROFILES FOR MILD STEEL IN PLAIN OPC SPECIMEN PASTES

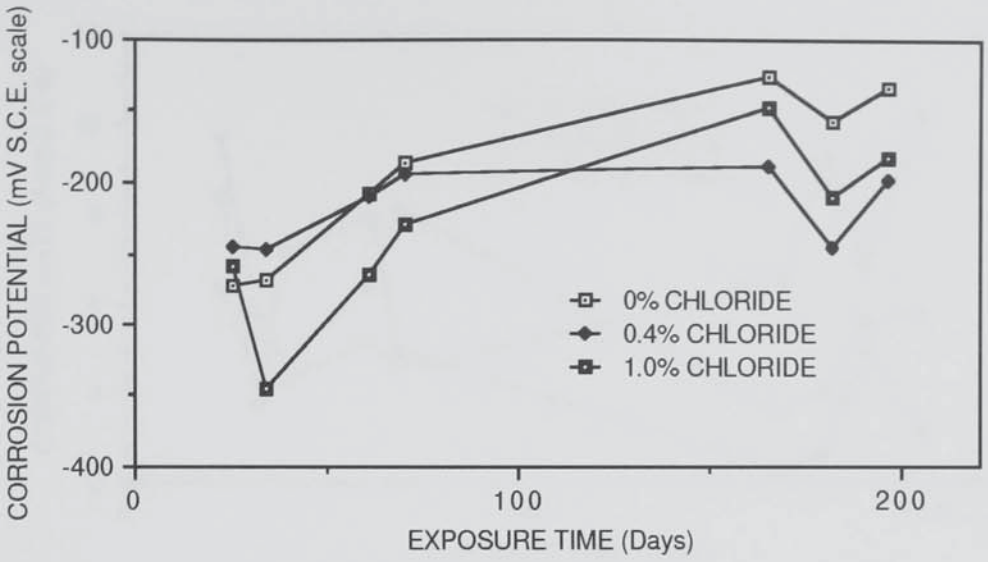

FIGURE 6.4
CORROSION POTENTIAL PROFILES FOR MILD STEEL IN OPC SPECIMEN PASTES CONTAINING 10% METAKAOLIN

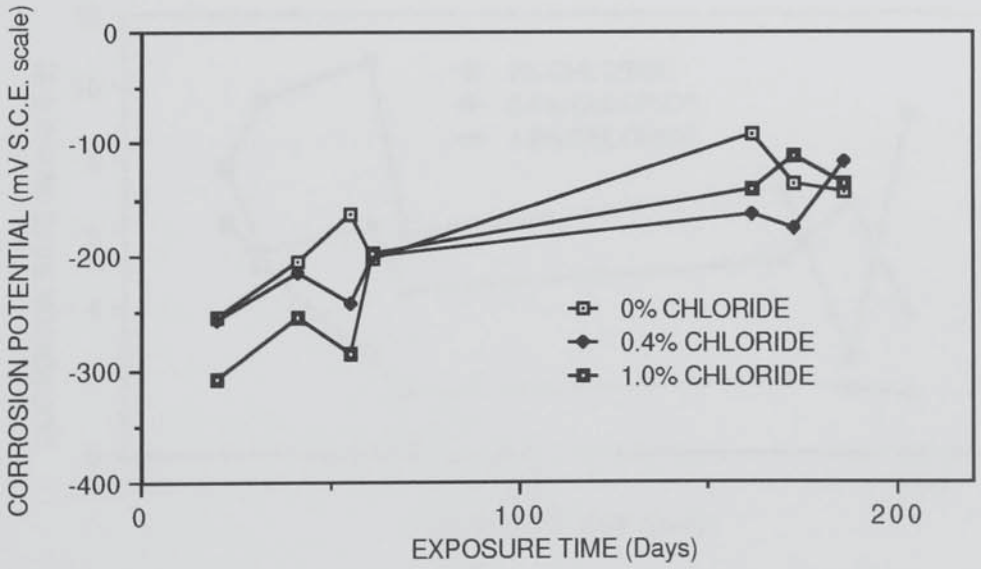

FIGURE 6.5
CORROSION POTENTIAL PROFILES FOR MILD STEEL IN OPC SPECIMEN PASTES CONTAINING 20% METAKAOLIN

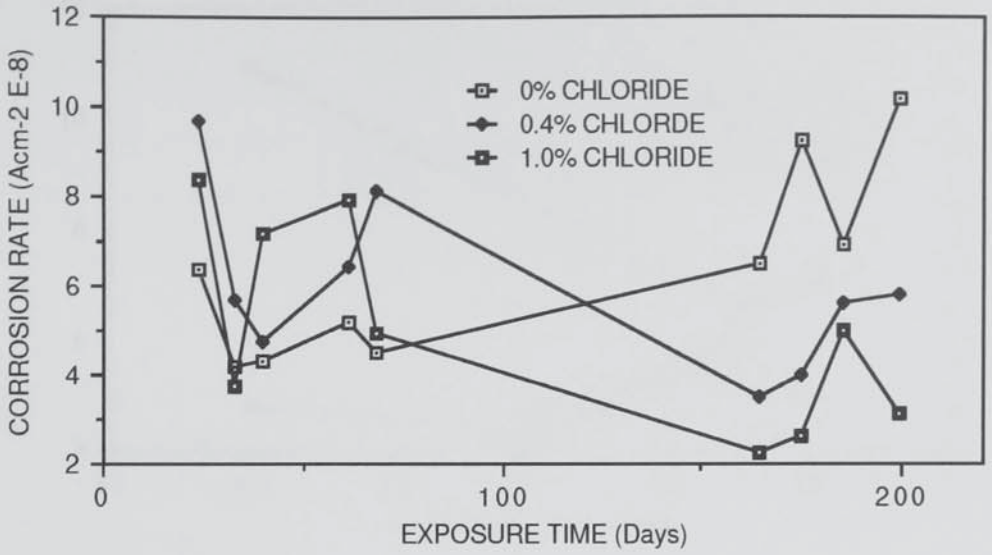

FIGURE 6.6
CORROSION RATE PROFILES FOR MILD STEEL IN
PLAIN OPC SPECIMEN PASTES

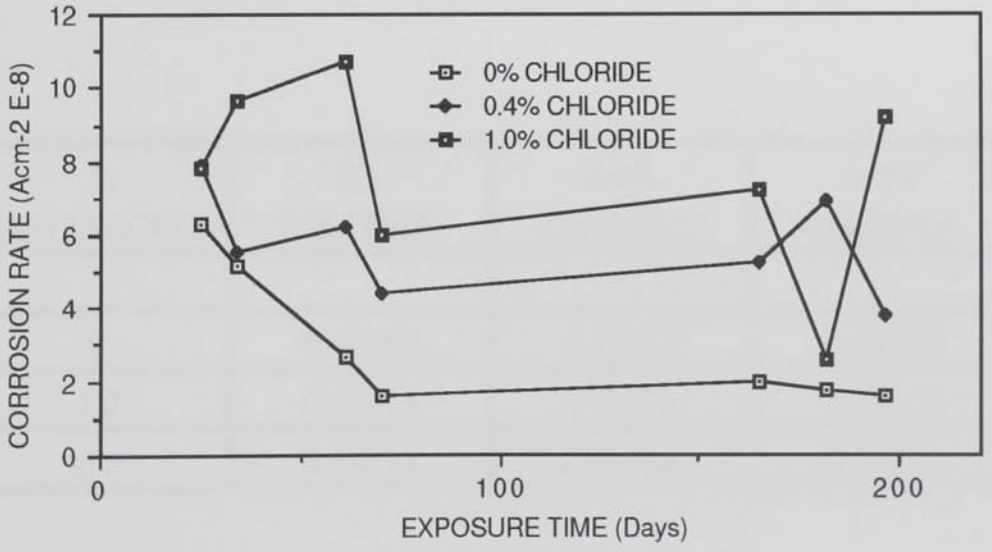

FIGURE 6.7
CORROSION RATE PROFILES FOR MILD STEEL IN
OPC SPECIMEN PASTES CONTAINING 10% METAKAOLIN

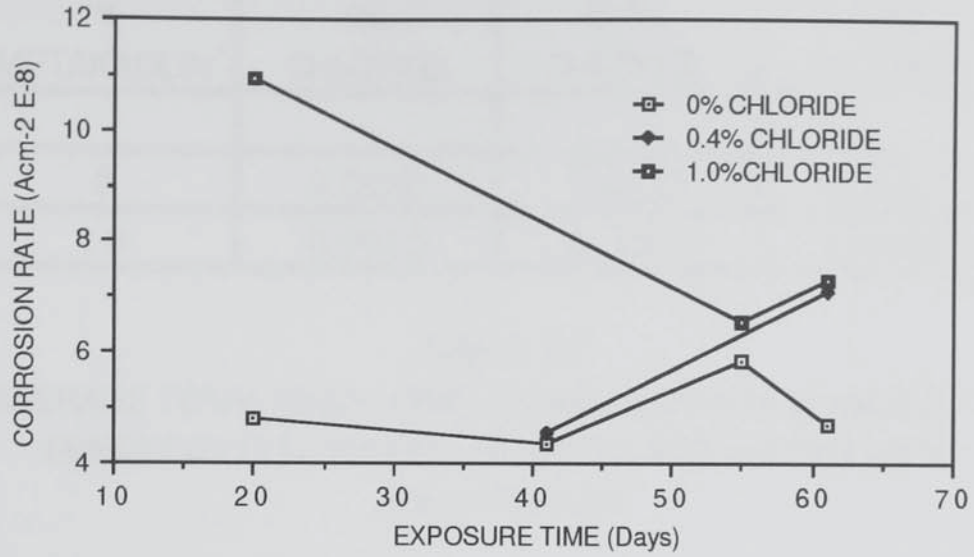

FIGURE 6.8
CORROSION RATE PROFILES FOR MILD STEEL IN
OPC SPECIMEN PASTES CONTAINING 20% METAKAOLIN

% METAKAOLIN	0% CHLORIDE	0.4% CHLORIDE	1.0% CHLORIDE
0	0.0049	0.0043	0.0023
10	0.0014	0.0014	0.0035
20	0.0014	0.0008	0.0015

TABLE 6.1
AVERAGE TOTAL MASS LOSSES (EXPRESSED IN GRAMMES) OF
EMBEDDED ELECTRODES AS DETERMINED BY GRAVIMETRIC
ANALYSIS

% METAKAOLIN	0% CHLORIDE	0.4% CHLORIDE	1.0% CHLORIDE
0	0.0023	0.0023	0.0017
10	0.0010	0.0017	0.0026

TABLE 6.2
AVERAGE TOTAL MASS LOSSES (EXPRESSED IN GRAMMES) OF EMBEDDED ELECTRODES AS CALCULATED FROM LINEAR POLARISATION

One of the electrodes which had been embedded in a plain cement paste specimen containing 1.0% chloride ions had visibly corroded over the entire region exposed to the chloride contaminated paste. This corrosion took place on the surface of a counter electrode and, consequently, was not registered by the linear polarization technique. By inspection, all other electrodes embedded in plain cement paste specimens appeared not to have corroded.

On recovery of the electrodes, which had been embedded in the cement pastes containing 10% metakaolin, no corroded regions were observed (although the surfaces of the electrodes were dull).

Three of the electrodes embedded in pastes containing 20% metakaolin (one of each chloride ion concentration) were seen to have undergone crevice corrosion. No other corrosion was observed on visual inspection.

6.4 DISCUSSION

The absence of linear polarization data (and hence, no corresponding total loss in mass values) for specimens containing 20% metakaolin after approximately 7 weeks is believed to be due to small cavity (0.5-1mm dia.) formation in

the paste surrounding the electrodes. It is presumed that the cavities formed during the introduction of the electrodes.

Replacement of OPC by metakaolin causes an increase in the stiffness of the resultant cement paste. It is thought that both the plain cement pastes and those containing 10% replacement metakaolin were sufficiently fluid to allow the insertion of electrodes into the pastes without significant cavity formation. It is presumed that, initially, sufficient pore solution was available to fill the cavities with the conducting fluid. As hydration progressed the linear polarization scans developed spurious data points (appearing as spikes along the curve) eventually making an accurate determination of the gradient of the scan impossible.

All chloride free samples, irrespective of metakaolin content, possessed E_{CORR} values which were more noble than -273 mV. According to ASTM C876-87 the probability of anodic pitting occurring at these potentials is less than 5% (i.e. they are indicative of passive steel).

The corresponding corrosion rates of the chloride-free samples were all below 10.20 x 10^{-8} Acm^{-2}, (typically values of around 3 x10^{-8} Acm^{-2} were obtained) again indicating the condition of passivity.

Hence, for the 10 and 20% metakaolin-blended specimens the reduction in calcium hydroxide (as a consequence of pozzolanic reaction) had not caused the pH to fall to a potentially dangerous level. The lowest pore solution pH value observed during the pore solution investigation (Chapter 3) was 13.15 (for paste samples containing 20% metakaolin having been cured for 100 days). In the absence of other aggressive agents steel is expected to show passivity in solutions of pH 11.5 and higher [30]. Thus the E_{CORR} values obtained here are consistent with the results of the pore solution investigation.

Both the corrosion potentials (all values more noble than -258 mV) and rates (all values below 9.67 $x10^{-8}$ Acm^{-2}) obtained for paste specimens containing 0.4% chloride ions again indicate that the embedded steel electrodes were in a state of passivity.

The corrosion potential values for samples containing 0 and 10% metakaolin and 1.0% chloride ions are all more noble than -265 mV and the corresponding corrosion rates were lower than 10.72 $x10^{-8}$ Acm^{-2} (typically values of around 6 x 10^{-8} Acm^{-2} were obtained). Samples containing 20% metakaolin and 1.0% chloride ions were initially found to possess 'borderline' potentials of -309 and -287 mV. After 8 weeks, however, the corrosion potential values reflected the existence of passive steel (although corrosion rate data was not available to support the corrosion potential data in this case).

The average total mass loss values calculated from the linear polarization technique (Table 6.2) are of the same order of magnitude as those obtained from gravimetric analysis (Table 6.1).

Those values derived from the linear polarization technique are subject to error arising from the use of estimated Tafel constants. Error arising from this assumption could possibly affect estimates of i_{CORR} by a factor of two (which is considered acceptable for these purposes) [30]. These results were also monitored at intervals over a period of time. The elapse of 100 days between the two sets of readings at the beginning and end of the investigation constitutes another source of error. Inaccuracies will also arise from the fact that the re-weighing of the electrodes took place nearly 200 days after their initial weighing (even though the same balance was employed both times).

Satisfactory agreement between the two corrosion monitoring methods is considered to have been obtained.

In conclusion, no significant corrosion has been observed by either monitoring technique, indicating that sufficient pore solution alkalinity is maintained after pozzolanic reaction to prevent the chloride to hydroxide ion ratio from reaching potentially dangerous values at levels of chloride ion addition of up to 1.0%. Although the specimens containing 20% replacement metakaolin and 1.0% chloride ions are believed to be on the 'borderline' of passive and corrosive behaviour.

CHAPTER 7 GENERAL DISCUSSION AND CONCLUSIONS

7.1 PORE SOLUTION CHEMISTRY, CORROSION BEHAVIOUR AND CHLORIDE DIFFUSION CHARACTERISTICS OF METAKAOLIN-BLENDED CEMENT PASTES

The incorporation of metakaolin into OPC has been seen to result in substantial changes in the chemical compositions of both the pore electrolyte and solid state phases of the hydrated product.

A relative reduction in pore electrolyte pH (as a consequence of pozzolanic reaction) has been observed for cement pastes containing 10 and 20% replacement (MK 501 and MK 505) metakaolin (Figures 3.6 and 3.7). In general, this reduction in pore solution alkalinity compared favourably with that of PFAs, was superior to that of GBFSs although was not as great as that found for silica fumes [35,45]. The timescale of the reductions in pore solution alkali concentration of metakaolin-blended pastes was seen to be intermediate between those (reported by other workers) of pozzolanic cement systems containing silica fume [35] and PFA [45].

This reduction in pore solution pH is considered to be relevant to the ability of metakaolin-blended cements to reduce the risk of expansive alkali aggregate reaction in concrete. A reduction in the extent of expansion by AAR in metakaolin-blended systems has been reported by other workers [33].

Long term pH values recorded in the range 13.4 to 13.5 for 10% metakaolin specimens and 13.1 to 13.2 for 20% metakaolin specimens were well in excess of the minimum pH required to cause passivation of steel in reasonably well-oxygenated concrete. Hence, the reduction in pore solution alkali concentration as a consequence of the incorporation of 10 and 20% replacement metakaolin is believed to have very little direct effect on the stability of the passive film that provides corrosion protection to embedded steel. These speculations have been corroborated by the results of the investigation into the

corrosion behaviour of mild steel embedded in metakaolin-blended cement pastes (Chapter 6) which are discussed later in this section.

The incorporation of metakaolin into OPC pastes has also been found to result in an increase in the extent to which chloride ions, introduced via the mix water, are excluded from the electrolyte phase (Figures 3.8 and 3.9). The possibility that this phenomenon could be attributed to a 'dilution' effect has been dismissed on the basis that experimentally determined, average, evaporable water content values (derived from Tables A2.4, A2.5, and A2.6 in Appendix 2) for mature (92 days) paste samples of water:cement ratio 0.5, having 0, 10, and 20% replacement metakaolin, compare to within 5%.

Both metakaolin types (MK 501 and MK 505) caused substantial reductions in the concentrations of free chloride ions retained in the pore solution phase of paste specimens containing 1.0% chloride ions (by weight of total solids). This effect was also observed for specimens made from MK 501 metakaolin with 0.4% chloride. In specimens containing 0.1% chloride ions the capacity of the cement hydration products to bind chloride ions was such that the concentration of chloride remaining in the pore solution after 36 days had fallen to around 10 $mmoldm^{-3}$ irrespective of the metakaolin content.

It has been suggested that the increase in chloride binding capacity observed for metakaolin-blended cement paste samples may, at least in part, be attributed to the participation of hydrated gehlenite (a product of pozzolanic reaction) in the formation of Friedel's salt (or other solid phase product). Hydrated gehlenite was seen to be absent from DTA thermoanalytical curves of metakaolin-blended cement pastes containing 'internal' chloride ions and those of the surface of paste cylinders exposed to saline solutions (Figures 4.11, 4.12 and 5.6). The fact that it was absent from the specimens irrespective of whether contamination took place during the mixing stage or some time after the majority of the hydration

chemistry had occurred suggests that it is involved in the removal and solid phase binding of chloride ions from the pore solution. Superior sorptive properties of the CSH gel of the blended specimens may also contribute to the solid phase binding of free chloride ions.

The ratio of the concentrations of chloride to hydroxide ions in the pore solution phase, $[Cl^-]/[OH^-]$, provides a simple index for the comparison of the relative risks of chloride-induced depassivation leading to pitting corrosion of steel in different types of concrete. This ratio is one of many factors which influence the corrosion behaviour of steel in concrete; it is for this reason that a critical $[Cl^-]/[OH^-]$ ratio, above which pitting occurs, is not applicable. In general, low values of $[Cl^-]/[OH^-]$ ratio are associated with passive steel. The $[Cl^-]/[OH^-]$ ratios determined in this study indicate only marginal differences between the expected risks of corrosion associated with a given dosage of chloride as mix contaminant in the pastes containing 0, 10, and 20% metakaolin (Table A4.25). Hence, the effect of chloride binding in metakaolin-blended specimens counteracted the reduction in pH of the pore solution phase. Thus the risks of chloride-induced corrosion of embedded steel are expected to be affected relatively little by the inclusion of up to 20% metakaolin in OPC-blended cement concretes.

The $[Cl^-]/[OH^-]$ ratios of metakaolin cement pastes were found to be significantly lower than those reported previously for silica fume cement pastes [30,37,38]. $[Cl^-]/[OH^-]$ ratios obtained by other workers for cements having replacement PFA [42] were similar to those obtained here for replacement metakaolin, however the presence of blast furnace slag investigated by Al-Amoudi et al. [38] was seen to have a marginally more favourable effect on both chloride binding and $[Cl^-]/[OH^-]$ ratio than did metakaolin.

The difference in reactivity with respect to pore solution pH modification and the exclusion of chloride ions from the solution

phase, between the two metakaolin types (MK 501 and MK 505) investigated, was found to be negligible.

As predicted from the results of the pore solution investigation, the reduction in pore electrolyte pH associated with the replacement of 10 and 20% metakaolin by weight of OPC (for systems of water:cement ratio 0.4) did not adversely affect the passivity of mild steel embedded in paste specimens (in the absence of other deleterious factors, e.g. carbonation and chloride ion contamination). The introduction of up to 1.0% internal chloride ions as a mix water contaminant during the preparation of specimen pastes did not result in significant corrosion of embedded mild steel. However specimens blended with 20% metakaolin were believed to be on the 'borderline' of passive and corrosive behaviour.

The reduced porosity observed, by mercury intrusion porosimetry, (Sections 4.3 and 4.4) for 10 and 20% metakaolin-blended systems not only favours the restriction of the ingress of deleterious agents, such as chloride ions, from the external environment but also serves to reduce the mobility, and thus, restrict the flux of chloride ions (in the vicinity of developing pits) which are required to sustain the pitting process.

The diffusion coefficients obtained in this study indicate that OPC pastes containing 10 and 20% replacement metakaolin exhibit superior chloride ion diffusion characteristics in comparison with those of plain OPC pastes of the same water:cement ratio (for the water:cement ratio range observed). In addition, it is known that metakaolin-blended OPC pastes, in general, possess higher chloride binding capacities compared with those of their unblended counterparts (Sections 3.4, 4.6 and 5.5). This indicates that their actual performances in the resistance of chloride ion penetration are likely to be better than those reflected by the diffusion coefficients which have been derived from total chloride ion analysis since the proportion of free chloride present in their electrolyte phases is likely to be lower.

7.2 THE SOLID STATE HYDRATION CHEMISTRY OF METAKAOLIN-BLENDED CEMENT PASTES

The two main methods of investigation of the solid phase employed in this research were differential thermal analysis (Sections 2.7.2, 4.5, 4.6, 5.3, and 5.5) and nuclear magnetic resonance spectroscopy (Sections 2.7.3, 4.7, and 4.8).

The extent of pozzolanic reaction has been illustrated by the relative reduction in the magnitude of the calcium hydroxide peaks of the thermoanalytical curves of metakaolin-blended specimens (Figures 4.8 and 4.9). Following a 36 day curing period a significant proportion of the calcium hydroxide of the specimen containing 10% replacement metakaolin had reacted and very little remained in the specimen blended with 20% metakaolin. All thermoanalytical curves obtained after 100 day curing periods were remarkably similar to those obtained after 36 days indicating that the majority of the hydration chemistry occurs within the first 36 days of curing. This is also illustrated by the similarities between 36 and 100 day pore solution analyses. The fact that a proportion of calcium hydroxide remained in the specimen blended with 20% metakaolin after a curing period of 100 days is relevant to the maintenance of passivity of embedded steel reinforcements.

The prolonged existence of ettringite in the presence of chloride ions has been observed (Sections 4.6 and 5.5). Ettringite was seen to be present in the DTA thermoanalytical curves of 36 and 100 day plain OPC paste specimens contaminated with 1.0% chloride ions (from the mix water) (Figure 4.10) whereas the thermoanalytical curves of the uncontaminated specimens of the same ages showed that ettringite had decomposed into its thermodynamically more stable constituents: tetracalcium sulphoaluminate hydrate and tetracalcium aluminate hydrate. The thermoanalytical curves of plain OPC paste cylinders exposed to saline solution (Figure 5.5) indicate that the two 'uppermost' layers (up to 14 mm from the exposed surface), which possess a relatively high proportion of chloride species, also possess

quantities of ettringite. Tetracalcium sulphoaluminate hydrate and tetracalcium aluminate hydrate were observed in the lower layers (containing lower levels of chloride ion contamination) from which ettringite is absent.

Similarly, additions of replacement metakaolin have also been seen to inhibit the decomposition of ettringite (Figures 4.7 and 4.8).

As mentioned in the previous section, the results of differential thermal analysis are indicative of the participation of hydrated gehlenite in the removal and solid state binding of chloride ions from the pore solution (Sections 4.6 and 5.5).

4-coordinate species are present in anhydrous OPC; a change in symmetry from 4- to 6-coordinate aluminium during the first 24 hours of hydration has been noted. Other workers have reported similar symmetry changes for a variety of hydrating cement systems [56,57]. A change in the aluminium chemical shift from 13.3 ppm for 1 day OPC specimens to the region 7.6 to 7.9 ppm for more mature samples represents a change in environment of the aluminium species.

4-, 5- and 6-coordinate aluminium species are present in metakaolin. The relatively rapid disappearance of the 5-coordinate aluminium species of the metakaolin during hydration has been noted. That the 5-coordinate aluminium was seen to be a reactive site is unsurprising since the symmetry of that complex is lower than that of the other aluminium species present. After 100 days hydration a significant proportion of 4-coordinate aluminium, originating from the metakaolin, remained in the blended paste specimens.

The initial accelerating effect of metakaolin on the rate of hydration of the cement pastes has been observed by NMR and was denoted by a comparative increase in the Q^1/Q^0 signal intensity ratios of metakaolin-blended specimens during the early stages of hydration (Section 4.8).

The depolymerisation of the amorphous silicate structure of metakaolin during pozzolanic reaction has also been observed and was denoted by the 'spreading' of the signal through the Q^3 range and into the Q^2 and Q^1 regions of the spectrum. Depolymerisation occurs as the siloxane linkages between the silicate units of the metakaolin are cleaved in the highly alkaline conditions associated with the cementitious system. It is suggested that the mechanism of pozzolanic reaction of metakaolin is such that the Q^4 silica depolymerises to Q^1 species (some of) which are then 'repolymerised' as components of CSH gel (and some of which will remain in the form of Q^1 hydrated gehlenite).

7.3 SUGGESTIONS FOR FURTHER WORK

(i) In view of the reduction in pore solution alkali content of metakaolin-blended cement specimens an investigation into the effect of additions of metakaolin on the extent of expansion caused by the alkali aggregate reaction is suggested. In a previous study on the effect of alkali aggregate reaction Walters and Jones [33] discovered negligible expansion using reactive chert although Sibbick et al. [95] found silurian siltstone to be a more reactive aggregate. Hence an investigation into the expansion of metakaolin-extended samples containing silurian siltstone may prove to be a worthwhile project.

(ii) The demagnetisation of metakaolin or the production of metakaolin from kaolin having low or zero iron content would reduce the intensity of the spinning side bands which are remarkably prominent in the aluminium-27 NMR spectrum of metakaolin. The collection of spectra at higher spin speeds would also shift the spinning side bands out of the region in which the resonance signals occur.

(iii) Aluminium-27 NMR spectra have been obtained in which the spinning side bands were non-symmetrical about the vertical axes. This is a possible consequence of the quadrupolar nature of the aluminium nucleus but may have arisen from the presence of two different aluminium species which were not

sufficiently resolved to appear as two separate signals in the spectrum. It is proposed that the technique of dynamic-angle spinning NMR may be used to obtain information on the number of different aluminium species present (where the degree of spectral resolution is insufficient to make the distinction) [96]. There exist four possible sets of pairs of complimentary angles at which the spectra may be obtained. The collected spectra are then superimposed; the point of intersection of the two signals denotes the isotropic chemical shift. The existence of two aluminium environments gives rise to two points of intersection. This technique may be employed with any quadrupolar nuclei.

(ix) To further investigate the role of hydrated gehlenite in the exclusion of chloride ions from the pore solution phase a synthetic binder study is suggested as an area of further study. The analysis of the products of reaction of water, calcium hydroxide, and metakaolin in the presence and absence of sodium chloride by DTA should indicate whether hydrated gehlenite engages in reaction with sodium chloride to form a solid phase product.

It is thought that the mechanism of pozzolanic reaction would be more clearly observed (by silicon-29 MAS NMR) in the synthetic binder than in OPC paste specimens.

REFERENCES

[1] West A.R., "Solid State Chemistry and its Applications", John Wiley and Sons, 1984, p 638.

[2] Neville A.M., and Brooks J.J., "Concrete Technology", Longman Scientific and Technical, 1987, p8.

[3] Double D.D., "New Developments in Understanding the Chemistry of Cement Hydration", Phil. Trans. R. Soc., London, A 310, 1983, pp. 53-66.

[4] Diamond S., "Cement Paste Microstructure", Conference on Hydraulic Cement Pastes: Their Structure and Properties, Proceedings of the Cement and Concrete Association, Sheffield 1976, pp. 2-30.

[5] Longuet P., Burglen L. and Zelwer A., "La Phase Liquide du Ciment Hydraté", Revue Matériaux de Construction et Travaux Publics, 676, 1973, pp. 35-41.

[6] Barneyback R.S. Jr. and Diamond S., "Expression and Analysis of Pore Fluids from Hardened Cement Pastes and Mortars", Cement and Concrete Research 11, 1981, pp. 279-285.

[7] Murat M., Ambroise J. and Pera J., "Investigations on Synthetic Binders Obtained by Middle Temperature Thermal Dissociation of Clay Minerals", 87th Annual Meeting of the American Ceramic Society, Cincinnati (U.S.A), 5-9 May, 1985.

[8] Sayanam R.A., Kalsotra A.K., Mehta S.K., Singh R.S. and Mandal G., "Studies on the Thermal Transformation and Pozzolanic Activities of Clay from the Jammu Region (India)", Journal of Thermal Analysis 35, 1989, pp. 99-106.

[9] Thiery J., Vautrin A. and Francios-Brazier J., "High Density Glass-Fibre Reinforced Modified Cementitious Matrix", Materials Research Society Symposium Proceedings, 211, 1991, pp. 79-91.

[10] Murat M., "Hydration Reaction and Hardening of Calcined Clays and Related Materials. {1} Preliminary Investigation of Metakaolin", Cement and Concrete Research 13, 1983, pp. 259-266.

[11] Bijen J.M. and Larbi J.A., "Metakaolinite, a Potential Superior Pozzolan in Concrete", Institute of Materials "The Microstructure of Cement and Concrete.", Oxford, 19-20 September, 1990.

[12] Palomo A. and Glasser F.P., "Chemically-Bonded Cementitious Materials Based on Metakaolin", British Ceramic Transactions and Journal, 91, No. 4, 1992, 107-112.

[13] Davidovitz, "Mineral Polymers and Methods of Making Them", U.S. Patent 4349386, Sept. 1982.

[14] Davidovitz, "Early High Strength Mineral Polymer", U.S. Patent 45009985, April 1985.

[15] Bredy P, Chabannet M. and Pera J., "Microstructure and Porosity of Metakaolin-Blended Cements", Materials Research Society Symposium, 137, 1983, pp. 431-436.

[16] Dunster A.M., Parsonage J.R. and Thomas M.J.K., "The Pozzolanic Reaction of Metakaolinite and its Effects on Portland Cement Hydration", Journal of Materials Science, 28, 1993, 1345-1350.

[17] Tamas F.D., Sarkar A. and Roy D. "Conference Proceedings", Maxwell P.V., ed., Cement and Concrete Research Association, Slough, 1976, p 55.

[18] Dunster A.M. and Parsonage J.R. Cement and Concrete Research, 18, 1988, 758.

[19] Ambroise J., Dejean J., Foumbi J. and Pera J., "Metakaolin Blended Cements Improve GRC Durability and Ductility", Construction and Building Materials 3(2), 1989, pp. 73-77.

[20] Oriol M. and Pera J., "Pozzolanic Activity of Metakaolin Under Microwave Treatment", Cement and Concrete Research, 25, No. 2, 1995, 265-270.

[21] Everett L.H. and Treadaway K.W.J., "Deterioration due to Corrosion in Reinforced Concrete", Building Research Establishment Information Paper IP 12/80, 1980.

[22] Neville A.M. and Brooks J.J., "Concrete Technology", Longman Scientific and Technical, Harlow, 1987, p 101.

[23] British Standard 4550: Part 2: Section 13.2, "Loss-on-Ignition", 1970.

[24] Tyrer M., "Hydration Chemistry of Blended Portland Blast Furnace Slag Cements for Radioactive Waste Encapsulation", PhD. Thesis, Aston University, U.K., 1991, p. 78.

[25] Day R.L. and Marsh B.K., "Measurement of Porosity in Blended Cement Pastes", Cement and Concrete Research, 18, 1988, pp. 63-67.

[26] Eldman, R.F. and Beaudoin J.J., "Pretreatment of Hardened Cement Pastes for Mercury Intrusion Measurements", Cement and Concrete Research, 21, 1991 pp. 297-308.

[27] Akitt J.W., "NMR and Chemistry", Second Edition, Chapman and Hall, London.

[28] Washburn E.W., "Porosity I. Purpose of Investigation II. Porosity and the Mechanism of Absorption", Journal of the American Ceramic Society, 4, 1921, pp. 916-922.

[29] Andrade C. and Gonzalez J.A., "Quantitative Measurement of Corrosion Rate of Reinforcing Steels Embedded in Concrete using Polarization Resistance Measurements", Werkstoffe und Korrosion, 29, 1978, pp. 515-519.

[30] Page C.L. and Havdahl J., "Electrochemical Monitoring of Corrosion of Steel in Microsilica Cement Pastes", Matériaux et Constructions, 18, 103, 1985, pp. 41-47.

[31] Stern M. and Geary A.L., "A Theoretical Analysis of the Shape of Polarization Curves", Journal of the Electrochemical Society, 104, 1957, pp. 56-63.

[32] Nixon P. and Page C.L., "Pore Solution Chemistry and Alkali Aggregate Reaction", American Concrete Institute, Special Publication 100-94, pp. 1833-1862.

[33] Walters G.V. and Jones T.R., "Effect of Metakaolin on Alkali-Silica Reaction (ASR) in Concrete Manufactured with Reactive Aggregate", International Conference on Durability of Concrete, Montreal, Canada, August 1991.

[34] Galvele J.R., "Transport Processes in Passivity Breakdown II. Full Hydrolysis of the Metal Ions". Corrosion Science, 21, No.8, 1981, pp. 551-579.

[35] Page C.L. and Vennesland O., "Pore Solution Composition and Chloride Binding Capacity of Silica Fume Cement Pastes", Materials and Structures, 16, 1983, pp. 19-24.

[36] Trittart J., "Chloride Binding in Cement II. The Influence of the Hydroxide Concentration in the Pore Solution of Hardened Cement Paste on Chloride Binding", Cement and Concrete Research, 19, 1989, pp. 683-691.

[37] Rasheeduzzafar, Hussain S.E. and Al-Gahtani A.S. "Pore Solution Composition and Reinforcement Corrosion Characteristics of Microsilica Blended Cement Concrete", Cement and Concrete Research, 21, 1991, 1035-1048.

[38] Al-Amoudi O.S.B., Rasheeduzzafar, Maslehuddin M. and Abduljauwad S.N., "Influence of Sulfate Ions on Chloride-Induced Reinforcement Corrosion in Portland and Blended Cement Concretes", Cement, Concrete and Aggregates, 16, June 1994, 3-11.

[39] Byfors K., Hansson C.M. and Tritthart J., "Pore Solution Expression as a Method to Determine the Influence of Mineral Additives on Chloride Binding", Cement and Concrete Research, 16, 1986, 760-770.

[40] Andrade C. and Page C.L., "Pore Solution Chemistry and Corrosion in Hydrated Cement Systems Containing Chloride Salts: A Study of Cation Specific Effects", British Corrosion Journal, 21, 1986, 49-53.

[41] Hussain S.E., "Mechanisms of High Durability Performance of Plain and Blended Cements, PhD. Thesis, King Fahad University of Petroleum and Minerals, Dhahran, Saudi Arabia, 1991.

[42] Kayyali O.A., Kawamura M. and Haque M.N., "Fly Ash and Cation Effects on Free Cl^- and OH^- Concentrations in Mortar", ASCE Journal of Materials in Civil Engineering, 3, May, 1991, 113-125.

[43] Hausmann D.A., "Steel Corrosion in Concrete", Materials Protection, 6, No.19, Nov. 1967, 19-23.

[44] Glasser F.P. and Marr J., "The Effect of Mineral Additives on the Composition of Cement Pore Fluids", Proceedings of the British Ceramic Society, Chemistry and Chemically Related Properties of Cement, F.P. Glasser, ed., 35, September, 1984, pp. 419-429.

[45] Canham I., Page C.L. and Nixon P.J., "Aspects of the Pore Solution Chemistry of Blended Cements Related to the Control of Alkali Silica Reaction", Cement and Concrete Research, 17, 1987, pp. 839-844.

[46] Page C.L., Private Communication, Aston University, 1992.

[47] Neville A.M. and Brooks J.J., "Concrete Technology", Longman Scientific and Technical, Harlow, 1987, p. 106.

[48] Ramachandran V.S., "Applications of Differential Thermal Analysis in Cement Chemistry", Chemical Publishing Company Inc., New York, 1969, p. 95.

[49] Murat M., "Hydration Reaction and Hardening of Calcined Clays and Related Minerals II. Influence of Mineralogical Properties of the Raw-Kaolinite on the Reactivity of Metakaolinite", Cement and Concrete Research, 13, 1983, pp. 511-518.

[50] Murat M. and Cornel C., "Hydration Reaction and Hardening of Calcined Clays and Related Minerals III. Influence of Calcination Process of Kaolinite on Mechanical Strengths of Hardened Metakaolinite", Cement and Concrete Research, 13, 1983, pp. 631-637.

[51] Taylor H.F.W., "The Chemistry of Cement". Academic Press, London and New York, Vol.1, 1964, pp. 167-232.

[52] Justnes H., Meland I., Bjoergum O., Krane J. and Skjetne T., "Nuclear Magnetic Resonance - a Powerful Tool in Cement and Concrete Research". Advances in Cement Research, 3, No.11, 1990, pp. 105-110.

[53] MacTavish J.C., Miljkovic J.C. and Pintar M.M., "Hydration of White Cement by Spin Grouping NMR", Cement and Concrete Research, 15, 1985, pp. 367-377.

[54] Lasic D.D., Corbett J.M. Jin Jian, MacTavish and Pintar M.M., "NMR Spin Grouping in Hydrating Cement at 200 MHz", Cement and Concrete Research, 18, 1988, pp. 649-653.

[55] Müller D. and Gessner W, "Solid State Aluminium-27 Nuclear Magnetic Resonance Chemical Shift and Quadrupole Coupling Data for Condensed AlO_4 Tetrahedra", Journal of the Chemical Society, Dalton Transactions, 6, 1986, pp. 1277-1281.

[56] Hjorth J., Skibsted J. and Jakobsen H.J., "^{29}Si MAS NMR Studies of Portland Cement Components and Effects of Microsilica on the Hydration Reaction", Cement and Concrete Research, 18, 1988, pp. 789-798.

[57] Müller D., Rettel A. and Gessner W., "An Application of Solid State Magic Angle Spinning ^{27}Al NMR to the Study of Cement Hydration", Journal of Magnetic Resonance, 57, 1984, 152-156.

[58] Rocha J., Adams J.M. and Klinowski J., "The Rehydration of Metakaolinite to Kaolinite: Evidence from Solid State NMR and Cognate Techniques", Journal of the Chemical Society, Chemical Communications, 8, 1991, pp. 582-584.

[59] Lippmaa E.T., Magi M. Samoson A., Engelhardt G. and Grimmer A.R., "Structural Studies of Silicates by Solid-State High-Resolution ^{29}Si NMR", Journal of the American Chemical Society, 102, 1980, pp. 4889-4893.

[60] Justnes H., Meland I., Bjoergum O. and Krane J., "A ^{29}Si MAS NMR Study of the Pozzolanic Activity of Condensed Silica Fume and the Hydration of Di- and Tricalcium Silicates", Advances in Cement Research, 3, No.11, 1990, 111-116.

[61] Rodger S.A., Groves G.W., Clayden N.J. and Dobson C.M., "Hydration of Tricalcium Silicate Followed by ^{29}Si NMR with Cross-Polarisation", Journal of the American Ceramic Society, 71, No. 2, 1988, 91-96.

[62] Tong Y., Du H. and Fei L., "CP/MAS NMR Studies of the Initial Hydration Processes of Activated and Ordinary Beta-Dicalcium Silicates", Cement and Concrete Research, 20, 1990, 986-991.

[63] Pietersen H.S., Kentgens A.P.M., Nachtegaal G.H., Veeman W.S., and Bijen J.M.J.M., "The Reaction Mechanism of Blended Cements: A ^{29}Si NMR Study", Istanbul Conference A.C.I. SP 123-44, 1992, pp. 795-811.

[64] Lippmaa E.T., Mägi M., Tarmak M., Wieker W. and Grimmer, A.R., "A High Resolution 29Si NMR Study of the Hydration of Tricalciumsilicate", Cement and Concrete Research, 12, 1982, 597-602.

[65] Skibsted J., Hjorth J. and Jakobsen H.J., "Correlation Between ^{29}Si NMR Chemical Shifts and Mean Si-O Bond Lengths for Calcium Silicates", Chemical Physics Letters, 172, 279-283.

[66] Parry-Jones G., Al-Tayyib A.J. and Al-Mana A.I., "Evaluation of Degree of Hydration in Concrete Using ^{29}Si Magic Angle Spinning NMR in Solids", Cement and Concrete Research, 18, 1988, 229-234.

[67] Skibsted J. and Jakobsen H.J., "Direct Observation of Aluminium Guest Ions in the Silicate Phases of Cement Minerals by ^{27}Al NMR spectroscopy", Journal of the Chemical Society Faraday Transactions, 90(14), 1994, 2095-2098.

[68] Engelhardt G. and Michel D., "High Resolution Solid-State NMR of Silicates and Zeolites". John Wiley and Sons, Chichester, 1988.

[69] Mägi M., Lippmaa E.T., Samoson A., Engelhardt G. and Grimmer A.R., 88, 1518, 1984.

[70] Parry-Jones G., Al-Tayyib A.J., Al-Dulaijan S.U. and Al-Mana A.I., "^{29}Si NMR Hydration and Compressive Strength Study in Cement Pastes", Cement and Concrete Research, 19, 1989, pp. 228-234.

[71] Sorensen B., and Maahn E., "Penetration Rate of Chloride in Marine Structures", Nordic Concrete Research, 1, 1982, pp. 24.1-24.8.

[72] Kay E.A., Fookes P.G., and Pollock D.J., "Deterioration Related to Chloride Ingress", Concrete, 15, 11, 1989, pp. 22-28.

[73] Page C.L., Short N.R., and El Tarras A., "Diffusion of Chloride Ions in Hardened Cement Pastes", Cement and Concrete Research, 11, 1981, pp. 395-406.

[74] Byfors K., "Influence of Silica Fume and Fly Ash on Chloride Diffusion and pH Values in Cement Paste", Cement and Concrete Research, 17, 1987, pp. 115-130.

[75] Lambert P., Page C.L., and Short N.R., "Diffusion of Chloride Ions in Hardened Cement Pastes Containing Pure Cement Minerals", Proceedings of the British Ceramic Society, Chemistry and Chemically Related Properties of Cement, F.P. Glasser, ed., 35, September, 1984, pp. 267-276.

[76] Goto S., and Roy D.M., "Diffusion of Ions Through Hardened Cement Pastes". Cement and Concrete Research, 11, 1981, pp. 751-757.

[77] Lambert P., "The Corrosion and Passivation of Steel in Concrete". PhD. Thesis, Aston University, U.K., 1983.

[78] Crank J., "The Mathematics of Diffusion". Second Edition, Pub: Clarendon Press Oxford, 1975.

[79] Fick A., "Ueber Diffusion", Annaler der Physik. Lpz. 170, 1855, 59-86.

[80] Fourier J.B., "Theorie Analytique de la Chaleur œuvres de Fourier", 1822.

[81] Jost W., "Diffusion in Solids, Liquids and Gases", Academic Press, Revised Edition, 1960, p62.

[82] Sergi G., "Corrosion of Steel in Concrete: Cement Matrix Variables". PhD. Thesis, Aston University, U.K.,1986, p 54.

[83] Collepardi M., Marcialis A., and Turriziani R., "The Penetration of De-icing agents in Cement Pastes", Il Cemento, 3, 1972, pp. 143-149

[84] Cady P.D., "Corrosion of Reinforcing Steel in Concrete - A General Overview of the Problem", Chloride Corrosion of Steel in Concrete, ASTM STP 629, Tonini D.E. and Dean S.W., eds., ASTM, 1977, pp. 3-11.

[85] "Economics of Corrosion Control", Autumn Review Course Series 3, Number 2. Pub: Institute of Metallurgists, November 1974.

[86] Brown H.P., Engineering News, 65, 1911, p 684.

[87] Treadaway K.W.J., Brown B.L., and Cox R.N., "Durability of Galvanised Steel in Concrete", Corrosion of Reinforcing Steel in Concrete, ASTM STP 713, Tonini D.E., and Gadis J.M., eds., ASTM, 1980, pp. 102-131.

[88] Steel G.W., and Judy J.M., "Polymer Modified Concretes in Bridge Deck Overlay Systems", Chloride Corrosion of Steel in Concrete, ASTM, STP 629, Tonini D.E., and Dean S.W., eds., ASTM, 1977, pp. 110-115.

[89] Lundquist J.T. Jr., Rosenberg A.M., and Gaidis J.M., "Calcium Nitrate as an Inhibitor of Rebar Corrosion in Chloride Containing Concrete", Materials Performance, 18, March 1979, pp. 36-40.

[90] Flick L.D. and Lloyd J.P., "Corrosion of Steel in Internally Sealed Concrete Beams Under Load", Corrosion of Reinforcing Steel in Concrete, ASTM STP 713, Tonini D.E., and Gaidis J.M., eds., ASTM, 1980, pp. 93-101.

[91] Hausmann D.A., "Steel Corrosion in Concrete". Materials Protection, 6, November 1967, pp. 19-23.

[92] Tuutti K., "Corrosion of steel in concrete", Swedish Cement and Concrete Research Institute, Stockholm, Research Report F04, 1982, pp. 289-292.

[93] Page C.L., and Treadaway K.W.J., "Aspects of the Electrochemistry of Steel in Concrete", Nature, 297, No. 5862, 1982, pp. 109-115.

[94] Page C.L., "Mechanism of Corrosion Protection in Reinforced Concrete Marine Structures", Nature, 258, 1975, pp. 514-515.

[95] Sibbick R.G. and Page C.L., "Susceptibility of Various UK Aggregates to Alkali Aggregate Reaction", International Conference on Alkali Aggregate Reaction in Concrete, 1992, London, pp. 980-987.

[96] Mueller K.T., Sun B.Q., Chingas G.C., Zwanziger J.W., Terao T. and Pines A., "Dynamic-Angle Spinning of Quadrupolar Nuclei", Journal of Magnetic Resonance, 86, 1990, pp. 470-487.

[97] Pearson E.S. and Hartley H.O., "Biometrika Tables for Statisticians, Volume 1", Second Edition, Cambridge University Press, Cambridge.

[98] Sergi G., Yu S.W. and Page C.L., "Diffusion of Chloride and Hydroxyl Ions in Cementitious Materials Exposed to a Saline Environment", Magazine of Concrete Research, 44, No. 158, March 1992, pp. 63-69.

APPENDIX 1 WORKED EXAMPLE OF EVAPORABLE AND NON-EVAPORABLE WATER CONTENTS CALCULATION

The equations used for the determination of evaporable and non-evaporable water contents of cement pastes are given below [53].

$$\text{EVAPORABLE WATER (E.W.)(\%)} = \frac{M_O - M_{105}}{M_{950}} \{100\text{-LOI+AD}\}$$

$$\text{NON-EVAPORABLE WATER (N.E.W.)(\%)} = \frac{M_{105}\{100\text{-LOI+AD}\} - M_{950}\{100+\text{AD}\}}{M_{950}}$$

where;

M_O is the mass of hydrated cement paste sample (grammes)

M_{105} is the sample mass at 105°C (grammes)

M_{950} is the sample mass at 950°C (grammes)

LOI is the loss-on-ignition (% grammes/gramme of cement)

AD is the admixture total (% grammes/gramme of cement)

The following are worked calculations of evaporable and non-evaporable water from Table 1 Appendix 2.

DATA:

Mass of crucible	27.3770g
Mass of crucible and sample	35.1276g
Mass of crucible and sample at 105°C	33.6780g
Mass of crucible and sample at 950°C	32.7272g
Mass of sample (M_O)	7.7506g
Mass of sample at 105°C (M_{105})	6.3010g
Mass of sample at 950°C (M_{950})	5.3500g
LOI	0.8g/g

CALCULATIONS:

EVAPORABLE WATER (%) $= \frac{7.7506 - 6.3010}{5.3500} \times 99.2$

$= 26.879\%$

$= \underline{26.88\%}$

NON-EVAPORABLE WATER (%) $= \frac{(6.3010 \times 99.2) - (5.3500 \times 100)}{5.3500}$

$= 16.833\%$

$= \underline{16.83\%}$

TOTAL WATER CONTENT $= 26.879 + 16.833$

$= \underline{43.71\%}$

APPENDIX 2 EVAPORABLE AND NON-EVAPORABLE WATER CONTENTS

The following tables contain the experimentally determined evaporable and non-evaporable water contents of cement paste samples used in the unsteady state diffusion investigation (Chapter 5).

DEPTH (mm)	E.W. (%)	N.E.W. (%)	TOTAL WATER
3.5	26.88	16.83	43.71
10.5	25.21	17.34	42.55
17.5	23.01	17.76	40.77
24.5	22.87	17.40	40.27
31.5	22.43	17.13	39.56

TABLE A2.1
0% METAKAOLIN / WATER:CEMENT RATIO 0.4

DEPTH (mm)	E.W. (%)	N.E.W. (%)	TOTAL WATER
3.5	26.73	15.09	41.82
10.5	25.21	15.09	40.30
17.5	24.70	14.82	39.52
24.5	24.54	15.11	39.65
31.5	24.18	15.21	39.39
38.5	23.75	14.89	38.64

TABLE A2.2
10% METAKAOLIN / WATER:CEMENT RATIO 0.4

DEPTH (mm)	E.W. (%)	N.E.W. (%)	TOTAL WATER
3.5	27.49	14.38	41.87
10.5	26.13	14.12	40.25
17.5	25.69	14.18	39.87
24.5	25.44	14.44	39.88
31.5	25.11	14.30	39.41
38.5	25.05	14.32	39.37

TABLE A2.3
20% METAKAOLIN / WATER:CEMENT RATIO 0.4

DEPTH (mm)	E.W. (%)	N.E.W. (%)	TOTAL WATER
3.5	34.48	16.49	50.97
10.5	32.43	17.40	49.83
17.5	33.18	17.95	51.13
24.5	32.67	18.16	50.83
31.5	32.08	17.88	49.96
38.5	32.00	18.14	50.14

TABLE A2.4
0% METAKAOLIN / WATER:CEMENT RATIO 0.5

DEPTH (mm)	E.W. (%)	N.E.W. (%)	TOTAL WATER
3.5	35.14	15.67	50.81
10.5	32.83	16.12	48.95
17.5	31.93	16.26	48.19
24.5	31.35	16.07	47.42
31.5	30.88	15.96	46.84
38.5	30.43	16.24	46.67

TABLE A2.5
10% METAKAOLIN / WATER:CEMENT RATIO 0.5

DEPTH (mm)	E.W. (%)	N.E.W. (%)	TOTAL WATER
3.5	36.56	15.09	51.65
10.5	35.18	15.34	50.52
17.5	33.73	15.23	48.96
24.5	33.42	15.13	48.55
31.5	33.67	14.74	48.41
38.5	32.92	14.88	47.80

TABLE A2.6
20% METAKAOLIN / WATER:CEMENT RATIO 0.5

DEPTH (mm)	E.W. (%)	N.E.W. (%)	TOTAL WATER
3.5	43.03	20.02	63.05
10.5	43.96	18.43	62.39
17.5	42.57	18.17	60.74
24.5	41.79	17.63	59.42
31.5	42.34	17.92	60.26

TABLE A2.7
0% METAKAOLIN / WATER:CEMENT RATIO 0.6

DEPTH (mm)	E.W. (%)	N.E.W. (%)	TOTAL WATER
3.5	42.96	21.46	64.42
10.5	42.50	20.70	63.20
17.5	41.75	20.09	61.84
24.5	41.22	19.67	60.89
31.5	40.95	19.88	60.83

TABLE A2.8
10% METAKAOLIN / WATER:CEMENT RATIO 0.6

DEPTH (mm)	E.W. (%)	N.E.W. (%)	TOTAL WATER
3.5	41.76	20.09	61.85
10.5	41.48	19.47	60.95
17.5	41.53	19.44	60.97
24.5	40.69	19.31	60.00
31.5	40.83	19.56	60.39

TABLE A2.9
20% METAKAOLIN / WATER:CEMENT RATIO 0.6

APPENDIX 3 WORKED EXAMPLE OF TOTAL CHLORIDE ION CONCENTRATION CALCULATION

DATA:

Sample type	0% MK / W:C RATIO 0.5
Depth	10.5 mm
Absorbance	0.712
Sample mass ($M_{105sample}$)	0.8169 g
Solution volume	0.5 dm^{-3}

From the calibration curve, the chloride ion concentration = 0.514 mM

Hence, the total number of moles of Cl^- ions in the solution (i.e. the total number of moles of Cl^- ions in the paste sample) = 0.257 mM

The equivalent mass of sample dried at 950°C ($M_{950sample}$)

$$= \frac{M_{105sample} \times M_{950}}{M_{105}}$$

$$= \frac{0.8169 \times 3.1246}{3.6979}$$

$$= 0.69025 \text{ g}$$

Thus, the total chloride ion concentration = 0.275/0.69025

$$= \underline{0.372 \text{ mMg}^{-1}}$$

APPENDIX 4 TABULATED PORE SOLUTION INVESTIGATION RESULTS

The following tables contain the complete suite of results obtained during the pore solution investigation. Duplicate experiments are denoted by the letters (a) and (b).

%MK	AVE. $[OH^-]$ $moldm^{-3}$	AVE. $[Na^+]$ $moldm^{-3}$	AVE. $[K^+]$ $moldm^{-3}$	ION BALANCE	AVERAGE pH
0 (a)	0.321	0.077	0.282	+0.04	13.506
0 (b)	0.177	0.052	0.261	+0.13	13.248
10 (a)	0.343	0.046	0.286	-0.01	13.535
10 (b)	0.320	0.045	0.279	+0.004	13.507
20 (a)	0.312	0.041	0.278	+0.007	13.494
20 (b)	0.301	0.034	0.273	+0.006	13.479
ERROR	± 0.005	± 0.08	± 0.08	± 0.16	± 0.005

TABLE A4.1
PORE SOLUTION COMPOSITION OF 1 DAY OLD SAMPLES
BLENDED WITH MK 501 (0% CHLORIDE)

%MK	AVE. $[OH^-]$ $moldm^{-3}$	AVE. $[Na^+]$ $moldm^{-3}$	AVE. $[K^+]$ $moldm^{-3}$	ION BALANCE	AVERAGE pH
10 (a)	0.288	0.035	0.263	+0.01	13.459
10 (b)	0.292	0.036	0.263	+0.007	13.465
20 (a)	0.266	0.027	0.263	+0.02	13.425
20 (b)	0.285	0.027	0.277	+0.02	13.455
ERROR	± 0.005	± 0.08	± 0.08	± 0.16	± 0.005

TABLE A4.2
PORE SOLUTION COMPOSITION OF 1 DAY OLD SAMPLES
BLENDED WITH MK 505 (0% CHLORIDE)

%MK	AVE. $[OH^-]$ $moldm^{-3}$	AVE. $[Cl^-]$ $moldm^{-3}$	AVE.$[Na^+]$ $moldm^{-3}$	AVE. $[K^+]$ $moldm^{-3}$	ION BALANCE	AVERAGE pH
0(a)	0.366	0.05	0.137	0.282	+0.003	13.526
0(b)	0.210	0.05	0.105	0.241	+0.08	13.322
10(a)	0.365	0.04	0.110	0.264	-0.03	13.562
10(b)	0.335	0.04	0.123	0.255	+0.003	13.525
20(a)	0.337	0.03	0.108	0.274	+0.006	13.528
20(b)	0.317	0.04	0.099	0.274	+0.02	13.500
ERROR	± 0.005	± 0.05	± 0.08	± 0.08	± 0.21	± 0.005

TABLE A4.3
PORE SOLUTION COMPOSITION OF 1 DAY OLD SAMPLES
BLENDED WITH MK 501 (0.1% CHLORIDE)

%MK	AVE. $[OH^-]$ $moldm^{-3}$	AVE. $[Cl^-]$ $moldm^{-3}$	AVE.$[Na^+]$ $moldm^{-3}$	AVE. $[K^+]$ $moldm^{-3}$	ION BALANCE	AVERAGE pH
0(a)	0.330	0.30	0.272	0.294	-0.06	13.519
0(b)	0.207	0.27	0.213	0.244	+0.02	13.316
10(a)	0.380	0.20	0.262	0.279	-0.04	13.580
10(b)	0.339	0.25	0.257	0.271	-0.06	13.530
20(a)	0.397	0.13	0.287	0.252	+0.01	13.599
20(b)	0.365	0.17	0.284	0.243	-0.008	13.562
ERROR	± 0.005	± 0.05	± 0.08	± 0.08	± 0.21	± 0.005

TABLE A4.4
PORE SOLUTION COMPOSITION OF 1 DAY OLD SAMPLES
BLENDED WITH MK 501 (0.4% CHLORIDE)

%MK	AVE. $[OH^-]$ $moldm^{-3}$	AVE. $[Cl^-]$ $moldm^{-3}$	AVE.$[Na^+]$ $moldm^{-3}$	AVE. $[K^+]$ $moldm^{-3}$	ION BALANCE	AVERAGE pH
0(a)	0.320	0.70	0.650	0.331	-0.04	13.505
0(b)	0.175	0.79	0.593	0.312	-0.06	13.243
10(a)	0.399	0.53	0.608	0.286	-0.03	13.601
10(b)	0.334	0.68	0.627	0.294	-0.09	13.524
20(a)	0.450	0.44	0.618	0.265	-0.007	13.653
20(b)	0.365	0.56	0.631	0.271	-0.02	13.562
ERROR	± 0.005	± 0.05	± 0.08	± 0.08	± 0.21	± 0.005

TABLE A4.5
PORE SOLUTION COMPOSITION OF 1 DAY OLD SAMPLES
BLENDED WITH MK 501 (1.0% CHLORIDE)

%MK	AVE. $[OH^-]$ $moldm^{-3}$	AVE. $[Cl^-]$ $moldm^{-3}$	AVE.$[Na^+]$ $moldm^{-3}$	AVE. $[K^+]$ $moldm^{-3}$	ION BALANCE	AVERAGE pH
10(a)	0.297	0.66	0.678	0.271	-0.008	13.473
10(b)	0.298	0.66	0.695	0.286	+0.02	13.474
20(a)	0.365	0.48	0.588	0.254	-0.003	13.562
20(b)	0.376	0.50	0.603	0.241	-0.03	13.575
ERROR	± 0.005	± 0.05	± 0.08	± 0.08	± 0.21	± 0.005

TABLE A4.6
PORE SOLUTION COMPOSITION OF 1 DAY OLD SAMPLES
BLENDED WITH MK 505 (1.0% CHLORIDE)

%MK	AVE. $[OH^-]$ $moldm^{-3}$	AVE. $[Na^+]$ $moldm^{-3}$	AVE. $[K^+]$ $moldm^{-3}$	ION BALANCE	AVERAGE pH
0(a)	0.475	0.071	0.393	-0.01	13.676
0(b)	0.435	0.064	0.375	+0.004	13.638
10(a)	0.299	0.039	0.256	+0.004	13.475
10(b)	0.322	0.039	0.279	-0.004	13.507
20(a)	0.222	0.031	0.203	0.01	13.347
20(b)	0.239	0.033	0.211	+0.005	13.379
ERROR	± 0.005	± 0.08	± 0.08	± 0.21	± 0.005

TABLE A4.7
PORE SOLUTION COMPOSITION OF 7 DAY OLD SAMPLES
BLENDED WITH MK 501 (0% CHLORIDE)

%MK	AVE. $[OH^-]$ $moldm^{-3}$	AVE. $[Na^+]$ $moldm^{-3}$	AVE. $[K^+]$ $moldm^{-3}$	ION BALANCE	AVERAGE pH
10(a)	0.350	0.048	0.293	-0.009	13.544
10(b)	0.355	0.047	0.293	-0.01	13.550
20(a)	0.210	0.027	0.182	-0.001	13.322
20(b)	0.213	0.028	0.191	+0.006	13.328
ERROR	± 0.005	± 0.08	± 0.08	± 0.21	± 0.005

TABLE A4.8
PORE SOLUTION COMPOSITION OF 7 DAY OLD SAMPLES
BLENDED WITH MK 505 (0% CHLORIDE)

%MK	AVE. $[OH^-]$ $moldm^{-3}$	AVE. $[Cl^-]$ $moldm^{-3}$	AVE.$[Na^+]$ $moldm^{-3}$	AVE. $[K^+]$ $moldm^{-3}$	ION BALANCE	AVERAGE pH
0(a)	0.494	0.02	0.137	0.384	+0.007	13.694
0(b)	0.472	0.02	0.129	0.384	+0.02	13.674
10(a)	0.303	0.05	0.086	0.230	-0.04	13.481
10(b)	0.325	0.02	0.070	0.274	-0.001	13.512
20(a)	0.232	0.02	0.065	0.181	-0.02	13.365
20(b)	0.246	0.01	0.079	0.184	+0.007	13.391
ERROR	± 0.005	± 0.05	± 0.08	± 0.08	± 0.21	± 0.005

TABLE A4.9
PORE SOLUTION COMPOSITION OF 7 DAY OLD SAMPLES
BLENDED WITH MK 501 (0.1% CHLORIDE)

%MK	AVE. $[OH^-]$ $moldm^{-3}$	AVE. $[Cl^-]$ $moldm^{-3}$	AVE.$[Na^+]$ $moldm^{-3}$	AVE. $[K^+]$ $moldm^{-3}$	ION BALANCE	AVERAGE pH
0(a)	0.565	0.11	0.302	0.384	+0.01	13.752
0(b)	0.550	0.11	0.299	0.384	+0.02	13.740
10(a)	0.335	0.12	0.180	0.212	-0.06	13.525
10(b)	0.353	0.13	0.175	0.279	-0.03	13.548
20(a)	0.252	0.06	0.152	0.159	-0.001	13.401
20(b)	0.278	0.05	0.161	0.159	-0.008	13.444
ERROR	± 0.005	± 0.05	± 0.08	± 0.08	± 0.21	± 0.005

TABLE A4.10
PORE SOLUTION COMPOSITION OF 7 DAY OLD SAMPLES
BLENDED WITH MK 501 (0.4% CHLORIDE)

%MK	AVE. $[OH^-]$ $moldm^{-3}$	AVE. $[Cl^-]$ $moldm^{-3}$	AVE.$[Na^+]$ $moldm^{-3}$	AVE. $[K^+]$ $moldm^{-3}$	ION BALANCE	AVERAGE pH
0(a)	0.672	0.37	0.618	0.388	-0.04	13.828
0(b)	0.658	0.28	0.611	0.388	+0.06	13.818
10(a)	0.403	0.18	0.374	0.203	-0.006	13.605
10(b)	0.424	0.22	0.386	0.256	-0.002	13.628
20(a)	0.288	0.15	0.302	0.146	+0.01	13.459
20(b)	0.330	0.13	0.321	0.148	+0.009	13.518
ERROR	± 0.005	± 0.05	± 0.08	± 0.08	± 0.21	± 0.005

TABLE A4.11
PORE SOLUTION COMPOSITION OF 7 DAY OLD SAMPLES
BLENDED WITH MK 501 (1.0% CHLORIDE)

%MK	AVE. $[OH^-]$ $moldm^{-3}$	AVE. $[Cl^-]$ $moldm^{-3}$	AVE.$[Na^+]$ $moldm^{-3}$	AVE. $[K^+]$ $moldm^{-3}$	ION BALANCE	AVERAGE pH
10(a)	0.416	0.14	0.363	0.197	+0.004	13.619
10(b)	0.421	0.15	0.370	0.197	-0.004	13.624
20(a)	0.297	0.14	0.286	0.129	-0.02	13.473
20(b)	0.303	0.14	0.288	0.132	-0.02	13.481
ERROR	± 0.005	± 0.05	± 0.08	± 0.08	± 0.21	± 0.005

TABLE A4.12
PORE SOLUTION COMPOSITION OF 7 DAY OLD SAMPLES
BLENDED WITH MK 505 (1.0% CHLORIDE)

%MK	AVE. $[OH^-]$ $moldm^{-3}$	AVE. $[Na^+]$ $moldm^{-3}$	AVE. $[K^+]$ $moldm^{-3}$	ION BALANCE	AVERAGE pH
0(a)	0.501	0.081	0.443	+0.02	13.700
0(b)	0.502	0.084	0.443	+0.02	13.701
10(a)	0.263	0.050	0.217	+0.004	13.420
10(b)	0.261	0.039	0.218	-0.004	13.417
20(a)	0.163	0.029	0.131	-0.003	13.211
20(b)	0.164	0.025	0.142	+0.003	13.216
ERROR	± 0.005	± 0.08	± 0.08	± 0.21	± 0.005

TABLE A4.13
PORE SOLUTION COMPOSITION OF 36 DAY OLD SAMPLES
BLENDED WITH MK 501 (0% CHLORIDE)

%MK	AVE. $[OH^-]$ $moldm^{-3}$	AVE. $[Na^+]$ $moldm^{-3}$	AVE. $[K^+]$ $moldm^{-3}$	ION BALANCE	AVERAGE pH
10(a)	0.253	0.037	0.225	+0.009	13.403
10(b)	0.253	0.034	0.215	-0.004	13.403
20(a)	0.151	0.026	0.133	+0.008	13.179
20(b)	0.161	0.026	0.138	+0.003	13.207
ERROR	± 0.005	± 0.08	± 0.08	± 0.21	± 0.005

TABLE A4.14
PORE SOLUTION COMPOSITION OF 36 DAY OLD SAMPLES
BLENDED WITH MK 505 (0% CHLORIDE)

% MK	AVE. $[OH^-]$ $moldm^{-3}$	AVE. $[Cl^-]$ $moldm^{-3}$	AVE.$[Na^+]$ $moldm^{-3}$	AVE. $[K^+]$ $moldm^{-3}$	ION BALANCE	AVERAGE pH
0(a)	0.538	0.01	0.147	0.428	+0.03	13.731
0(b)	0.537	0.01	0.145	0.428	+0.03	13.730
10(a)	0.272	0.01	0.092	0.198	+0.008	13.435
10(b)	0.267	0.01	0.074	0.218	+0.01	13.427
20(a)	0.172	0.01	0.061	0.212	+0.09	13.236
20(b)	0.164	0.01	0.059	0.142	+0.03	13.243
ERROR	± 0.005	± 0.05	± 0.08	± 0.08	± 0.21	± 0.005

TABLE A4.15
PORE SOLUTION COMPOSITION OF 36 DAY OLD SAMPLES
BLENDED WITH MK 501 (0.1% CHLORIDE)

% MK	AVE. $[OH^-]$ $moldm^{-3}$	AVE. $[Cl^-]$ $moldm^{-3}$	AVE.$[Na^+]$ $moldm^{-3}$	AVE. $[K^+]$ $moldm^{-3}$	ION BALANCE	AVERAGE pH
0(a)	0.595	0.09	0.337	0.402	+0.05	13.775
0(b)	0.595	0.08	0.314	0.402	+0.04	13.775
10(a)	0.318	0.05	0.202	0.185	+0.02	13.503
10(b)	0.328	0.06	0.193	0.209	+0.01	13.516
20(a)	0.222	0.06	0.159	0.128	+0.005	13.346
20(b)	0.231	0.06	0.163	0.133	+0.005	13.364
ERROR	± 0.005	± 0.05	± 0.08	± 0.08	± 0.21	± 0.005

TABLE A4.16
PORE SOLUTION COMPOSITION OF 36 DAY OLD SAMPLES
BLENDED WITH MK 501 (0.4% CHLORIDE)

% MK	AVE. $[OH^-]$ $moldm^{-3}$	AVE. $[Cl^-]$ $moldm^{-3}$	AVE.$[Na^+]$ $moldm^{-3}$	AVE. $[K^+]$ $moldm^{-3}$	ION BALANCE	AVERAGE pH
0(a)	0.696	0.36	0.735	0.415	+0.09	13.843
0(b)	0.692	0.35	0.722	0.401	+0.08	13.840
10(a)	0.421	0.19	0.417	0.191	-0.003	13.624
10(b)	0.419	0.18	0.371	0.209	-0.02	13.622
20(a)	0.269	0.17	0.319	0.121	+0.001	13.430
20(b)	0.293	0.15	0.311	0.133	+0.001	13.466
ERROR	± 0.005	± 0.05	± 0.08	± 0.08	± 0.21	± 0.005

TABLE A4.17
PORE SOLUTION COMPOSITION OF 36 DAY OLD SAMPLES
BLENDED WITH MK 501 (1.0% CHLORIDE)

% MK	AVE. $[OH^-]$ $moldm^{-3}$	AVE. $[Cl^-]$ $moldm^{-3}$	AVE.$[Na^+]$ $moldm^{-3}$	AVE. $[K^+]$ $moldm^{-3}$	ION BALANCE	AVERAGE pH
10(a)	0.421	0.18	0.392	0.210	+0.001	13.624
10(b)	0.422	0.17	0.392	0.211	+0.01	13.625
20(a)	0.302	0.15	0.315	0.138	+0.001	13.480
20(b)	0.304	0.15	0.328	0.133	+0.007	13.483
ERROR	± 0.005	± 0.05	± 0.08	± 0.08	± 0.21	± 0.005

TABLE A4.18
PORE SOLUTION COMPOSITION OF 36 DAY OLD SAMPLES
BLENDED WITH MK 505 (1.0% CHLORIDE)

%MK	AVE. $[OH^-]$ $moldm^{-3}$	AVE. $[Na^+]$ $moldm^{-3}$	AVE. $[K^+]$ $moldm^{-3}$	ION BALANCE	AVERAGE pH
0(a)	0.490	0.060	0.407	-0.02	13.690
0(b)	0.517	0.069	0.443	-0.005	13.713
10(a)	0.272	0.037	0.221	-0.01	13.435
10(b)	0.275	0.041	0.221	-0.01	13.438
20(a)	0.149	0.026	0.106	-0.02	13.173
20(b)	0.140	0.029	0.109	-0.002	13.146
ERROR	± 0.005	± 0.08	± 0.08	± 0.21	± 0.005

TABLE A4.19

PORE SOLUTION COMPOSITION OF 100 DAY OLD SAMPLES BLENDED WITH MK 501 (0% CHLORIDE)

%MK	AVE. $[OH^-]$ $moldm^{-3}$	AVE. $[Na^+]$ $moldm^{-3}$	AVE. $[K^+]$ $moldm^{-3}$	ION BALANCE	AVERAGE pH
10(a)	0.262	0.035	0.236	-0.009	13.418
10(b)	0.251	0.030	0.236	+0.01	13.400
20(a)	0.151	0.021	0.138	+0.008	13.179
20(b)	0.152	0.022	0.140	+0.01	13.182
ERROR	± 0.005	± 0.08	± 0.08	± 0.21	± 0.005

TABLE A4.20

PORE SOLUTION COMPOSITION OF 100 DAY OLD SAMPLES BLENDED WITH MK 505 (0% CHLORIDE)

%MK	AVE. $[OH^-]$ $moldm^{-3}$	AVE. $[Cl^-]$ $moldm^{-3}$	AVE.$[Na^+]$ $moldm^{-3}$	AVE. $[K^+]$ $moldm^{-3}$	ION BALANCE	AVERAGE pH
0(a)	0.530	0.01	0.122	0.407	-0.01	13.724
0(b)	0.531	0.01	0.128	0.414	+0.001	13.713
10(a)	0.286	0.01	0.074	0.210	-0.01	13.456
10(b)	0.288	0.01	0.078	0.214	-0.006	13.459
20(a)	0.160	0.01	0.043	0.123	-0.004	13.204
20(b)	0.156	0.01	0.042	0.123	-0.001	13.193
ERROR	± 0.005	± 0.05	± 0.08	± 0.08	± 0.21	± 0.005

TABLE A4.21

PORE SOLUTION COMPOSITION OF 100 DAY OLD SAMPLES BLENDED WITH MK 501 (0.1% CHLORIDE)

%MK	AVE. $[OH^-]$ $moldm^{-3}$	AVE. $[Cl^-]$ $moldm^{-3}$	AVE.$[Na^+]$ $moldm^{-3}$	AVE. $[K^+]$ $moldm^{-3}$	ION BALANCE	AVERAGE pH
0(a)	0.607	0.08	0.294	0.386	-0.007	13.783
0(b)	0.617	0.08	0.290	0.407	0.000	13.790
10(a)	0.333	0.07	0.187	0.195	-0.02	13.522
10(b)	0.340	0.06	0.199	0.197	-0.004	13.531
20(a)	0.199	0.05	0.099	0.106	-0.04	13.299
20(b)	0.202	0.06	0.119	0.109	-0.03	13.305
ERROR	± 0.005	± 0.05	± 0.08	± 0.08	± 0.21	± 0.005

TABLE A4.22

PORE SOLUTION COMPOSITION OF 100 DAY OLD SAMPLES BLENDED WITH MK 501 (0.4% CHLORIDE)

%MK	AVE. $[OH^-]$ $moldm^{-3}$	AVE. $[Cl^-]$ $moldm^{-3}$	AVE.$[Na^+]$ $moldm^{-3}$	AVE. $[K^+]$ $moldm^{-3}$	ION BALANCE	AVERAGE pH
0(a)	0.704	0.27	0.644	0.407	+0.08	13.848
0(b)	0.699	0.30	0.614	0.407	+0.02	13.844
10(a)	0.437	0.19	0.408	0.206	-0.01	13.640
10(b)	0.439	0.19	0.413	0.214	-0.002	13.643
20(a)	0.272	0.16	0.277	0.125	-0.03	13.435
20(b)	0.284	0.15	0.289	0.127	-0.02	13.453

ERROR	± 0.005	± 0.05	± 0.08	± 0.08	± 0.21	± 0.005

TABLE A4.23

PORE SOLUTION COMPOSITION OF 100 DAY OLD SAMPLES BLENDED WITH MK 501 (1.0% CHLORIDE)

%MK	AVE. $[OH^-]$ $moldm^{-3}$	AVE. $[Cl^-]$ $moldm^{-3}$	AVE.$[Na^+]$ $moldm^{-3}$	AVE. $[K^+]$ $moldm^{-3}$	ION BALANCE	AVERAGE pH
10(a)	0.435	0.17	0.364	0.217	-0.02	13.638
10(b)	0.432	0.16	0.367	0.219	-0.006	13.635
20(a)	0.289	0.15	0.295	0.138	-0.006	13.461
20(b)	0.285	0.15	0.301	0.138	+0.004	13.455

ERROR	± 0.005	± 0.05	± 0.08	± 0.08	± 0.21	± 0.005

TABLE A4.24

PORE SOLUTION COMPOSITION OF 100 DAY OLD SAMPLES BLENDED WITH MK 505 (1.0% CHLORIDE)

%MK	% Cl^-	1 DAY $[Cl^-]/[OH^-]$	7 DAY $[Cl^-]/[OH^-]$	36 DAY $[Cl^-]/[OH^-]$	101 DAY $[Cl^-]/[OH^-]$
MK 501					
0	0.1	0.19	0.04	0.02	0.02
0	0.4	1.11	0.20	0.14	0.13
0	1.0	3.35	0.49	0.51	0.41
10	0.1	0.11	0.11	0.04	0.03
10	0.4	0.63	0.36	0.17	0.19
10	1.0	1.68	0.48	0.44	0.43
20	0.1	0.11	0.06	0.06	0.06
20	0.4	0.40	0.21	0.27	0.27
20	1.0	1.26	0.46	0.57	0.56
MK 505					
10	1.0	2.22	0.35	0.42	0.38
20	1.0	1.34	0.47	0.50	0.52

TABLE A4.25
$[Cl^-]/[OH^-]$ RATIOS FOR ALL CHLORIDE-CONTAINING SAMPLES

APPENDIX 5 DTA GLOSSARY [10,48,49,]

SYMBOL	CEMENT CONSTITUENT	APPROXIMATE TEMPERATURE IN °C
T	CSH GEL	120-130
E	ETTRINGITE	130-160
G	HYDRATED GEHLENITE	180-200
A1	TETRACALCIUM SULPHOALUMINATE HYDRATE ($C_3A.CS.12H.$)	200-230
A2	TETRACALCIUM ALUMINATE HYDRATE (C_4AH_{13})	260-300
F	FRIEDEL'S SALT	320
X	EXOTHERMIC TROUGH	-
C	CALCIUM HYDROXIDE	515-590
V	CALCIUM CARBONATE	750-800
D	DEVITRIFICATION OF GLASSSY PHASE	800-950

APPENDIX 6 WORKED EXAMPLE OF THE CALCULATION OF DIFFUSION COEFFICIENTS

The total chloride ion concentration, C_x, values (as presented in Table A6.1, for an unblended cement paste sample of water:cement ratio 0.5) have been 'corrected' for an average 'background reading'. The total chloride ion concentrations were measured according to the method and calculation described in Section 2.5 and Appendix 3 respectively. The same method and calculation were used to obtain the background reading for cement paste samples of the same age, water:solids ratio and percentage metakaolin replacement which had not been exposed to chloride ions. The total chloride ion concentration and background reading were calculated from an average of six experimentally determined values. The average background reading was then subtracted from each total chloride ion concentration in the calculation of the corrected chloride ion concentration values.

x (mm)	C_x (mMg^{-1})	erf(y)	$\Phi(z)$	z	y
1.75	0.866	0.131	0.5655	0.1650	0.117
3.5	0.696	0.302	0.6510	0.3880	0.274
7.0	0.510	0.488	0.7440	0.6557	0.464
10.5	0.290	0.709	0.8545	1.0559	0.747
14.0	0.207	0.792	0.8960	1.2591	0.890
17.5	0.080	0.920	0.9600	1.7507	1.238
21.0	0.038	0.962	0.9810	2.0749	1.467
24.5	0.015	0.985	0.9925	2.4324	1.720
28.0	0.003	0.997	0.9985	2.9677	2.099
35.0	0.002	0.998	0.9990	3.0902	2.185

TABLE A6.1
TOTAL CHLORIDE ION CONCENTRATION DATA, erf(y), $\Phi(z)$, z AND y VALUES FOR PLAIN OPC PASTE SAMPLES OF W:S RATIO 0.5

The error function is calculated thus:

$$\text{erf}(y) = 1 - \frac{C_x}{C_s}$$

where C_x is the total chloride ion concentration at depth x and C_s is the total chloride ion concentration of the surface layer (see section 5.4). The dimensions of the diffusion coefficient are independent of the units of concentration of the chloride ion so any consistent units may be used.

The error function is defined as:

$$\text{erf}(y) = \frac{2}{\Pi} \int_0^y \exp(-t^2)dt$$

and the cumulative distribution function (c.d.f.) of the standard normal distribution is defined as:

$$\Phi(z) = \frac{1}{\sqrt{2\Pi}} \int_{-\infty}^{z} \exp(-\frac{1}{2}t^2)dt$$

$\Phi(z) = 0.5$ and $\exp(-\frac{1}{2}t^2)$ is symmetric about $t = 0$ so if we let $z = \sqrt{2}y$ this gives:

$$\text{erf}(y) = 2[\Phi(z) - 0.5]$$

and so $$\Phi(z) = [1 + \text{erf}(y)] / 2$$

The inverse error function, y, can be obtained by using tables of the inverse standard normal c.d.f. [97]. The tabulated value of z corresponding to a given value of $\Phi(z)$ is divided by $\sqrt{2}$ to get the corresponding value of y.

Standard regression theory is then used to estimate the slope and confidence limits for the slope of the plot y against x. These are then transformed to the corresponding confidence limits for the diffusion coefficient, D. Since D is proportional to the

reciprocal square of the slope the limits for D will not be symmetric about the point estimate for D. This is done by the following method:

Calculate the sums of squares:

$$S_{xx} = \Sigma x^2 - \frac{\Sigma x^2}{n}$$

$$S_{yy} = \Sigma y^2 - \frac{\Sigma y^2}{n}$$

$$S_{xy} = \Sigma xy - \frac{(\Sigma x)(\Sigma y)}{n}$$

The intercept may be calculated thus:

$$a = [\ \Sigma y - \frac{S_{xy}}{S_{xx}} \Sigma x)] \ / \ n$$

The variance of the intercept, s_A^2, can be calculated by the relationship:

$$s_A^2 = s^2 \frac{\Sigma x^2}{nS_{xx}}$$

The 95% confidence limits for the intercept are:

$$a = \pm\ t_{.025}\ s_A$$

where $t_{.025}$ is the 2.5% point for t with n-2 degrees of freedom.

If zero lies within these confidence limits for the intercept this strongly suggests that the true value of the intercept term is really zero. This is the case with the chloride ion diffusion data. Theoretically and physically a zero intercept is reasonable since it represents the statement $C_S = C_S$. The slope, b, of y against x, should accordingly be estimated using a zero intercept model.

The slope, b, is calculated thus:

$$b = \frac{\Sigma xy}{\Sigma x^2}$$

The variance of the slope, s_B^2, can be calculated by the following:

$$s_B^2 = \frac{s^2}{\Sigma x^2}$$

where:

$$s^2 = \left[\frac{\Sigma y^2 - b\Sigma x y}{(n-1)}\right]$$

The 95% confidence limits for the slope are:

$$a = \pm t_{.025}\ s_B$$

where $t_{.025}$ is the 2.5% point for t with n-1 degrees of freedom.

Having calculated b we can evaluate $\hat{y}$ for each observed value of x and find the corresponding residuals $y - \hat{y}$

$$\{y = bx + e = \hat{y} + e \quad \text{where } e = y - \hat{y}\}$$

The confidence limits for the slope are calculated by assuming that the errors are independent and identically distributed at each observed point with a normal distribution of zero mean and a fixed variance (estimated by s^2). If these assumptions are reasonable the residuals should oscillate randomly about zero and should lie within a band of approximate width $\pm 2s$ on either side of zero.

For the data in Table A6.1 the points for the values of x = 28.0mm and x = 35.0mm give rise to comparatively large residuals. For the three reasons stated below it is preferable to omit these points in order to achieve a better description of diffusion.

As Φ approaches 1 small changes in Φ correspond with large changes in z hence any inaccuracies in C_x and erf(y) at high values of x (e.g. x = 28.0mm and x = 35.0mm) will be magnified by

the transformations involved in finding y. This should be borne in mind when deciding whether to drop observations corresponding to high values of x.

Sergi et al. [98] showed that both free and total chloride ion profiles in cement paste specimens exposed to unidirectional diffusion from a constant saline environment can be interpolated by Fick's Second Law. In the same paper it was confirmed that the relationship between the concentrations of free and bound chloride ions could be described by the Langmuir adsorption isotherm. The author suggests that the free chloride ion profile is adequately described by Fick's Second Law and that the total chloride ion profile is the sum of this and the bound chloride ion profile. Hence, at the diffusion front where the concentration of chloride ions is low (i.e. large values of x) the binding of the chloride ions is significant and a deviation from Fick's Second Law is expected.

It should also be noted that at low level of chloride ion the accuracy of the experimental determination of concentration is comparatively low.

APPENDIX 7 CORROSION INVESTIGATION RESULTS

A number of electrodes retained a proportion of swarf in the threaded holes used for the attachment of wires. Unfortunately the loss of this swarf during treatment with Clark's solution prevented the measurement of mass loss due to anodic corrosion. It is for this reason that some electrodes are without associated mass loss values.

CEMENT PASTE SAMPLE TYPE (% CHLORIDE)	CORRECTED MASS LOSS OF ELECTRODE (g)	EXPOSED ELECTRODE AREA (cm^2)
0	-	8.69
0	-	8.69
0	-	8.69
0	0.0068	8.69
0	0.0111	8.69
0	-	8.69
0	0.0010	8.69
0	0.0006	8.69
0.4	0.0036	8.69
0.4	0.0174	8.69
0.4	-	8.69
0.4	0.0011	8.69
0.4	0.0004	8.69
0.4	0.0018	8.69
0.4	0.0022	8.69
0.4	0.0033	8.69
1.0	0.0028	8.69
1.0	-	8.69
1.0	0.0003	8.69
1.0	0.0031	8.69
1.0	0.0055	8.69
1.0	0.0033	8.69
1.0	0.0011	8.69
1.0	-	8.69

TABLE A7.1
THE CORRECTED LOSSES IN MASS OF ELECTRODES EMBEDDED IN CEMENT PASTES CONTAINING 0% METAKAOLIN

CEMENT PASTE SAMPLE TYPE (% CHLORIDE)	CORRECTED MASS LOSS OF ELECTRODE (g)	EXPOSED ELECTRODE AREA (cm^2)
0	0.0016	9.25
0	0.0000	9.25
0	0.0029	8.69
0	0.0004	8.69
0	0.0010	8.88
0	-	8.88
0	0.0002	8.69
0	0.0040	8.69
0.4	0.0026	8.13
0.4	-	8.13
0.4	0.0003	8.69
0.4	-	8.69
0.4	0.0006	8.50
0.4	0.0030	8.50
0.4	0.0019	8.88
0.4	-	8.88
1.0	0.0021	8.13
1.0	0.0004	8.13
1.0	0.0057	8.50
1.0	0.0040	8.50
1.0	0.0040	8.69
1.0	0.0061	8.69
1.0	0.0037	8.50
1.0	0.0016	8.50

TABLE A7.2
THE CORRECTED LOSSES IN MASS OF ELECTRODES
EMBEDDED IN CEMENT PASTES CONTAINING 10% METAKAOLIN

CEMENT PASTE SAMPLE TYPE (% CHLORIDE)	CORRECTED MASS LOSS OF ELECTRODE (g)	EXPOSED ELECTRODE AREA (cm^2)
0	0.0008	9.44
0	0.0040	9.44
0	-	8.69
0	0.0013	8.69
0	0.0008	8.50
0	0.0012	8.50
0	-	8.69
0	0.0000	8.69
0.4	0.0011	9.25
0.4	0.0011	9.25
0.4	-	9.25
0.4	-	9.25
0.4	0.0003	8.69
0.4	0.0000	8.69
0.4	-	8.50
0.4	0.0013	8.50
1.0	-	8.88
1.0	0.0017	8.88
1.0	0.0010	8.50
1.0	0.0025	8.50
1.0	-	8.69
1.0	-	8.69
1.0	0.0012	8.69
1.0	0.0010	8.69

TABLE A7.3
THE CORRECTED LOSSES IN MASS OF ELECTRODES
EMBEDDED IN CEMENT PASTES CONTAINING 20% METAKAOLIN

EXPOSURE PERIOD (DAYS)	E_{CORR} (mV) (0% CHLORIDE)	E_{CORR} (mV) (0.4% CHLORIDE)	E_{CORR} (mV) (1.0% CHLORIDE)
24	-248	-251	-228
33	-235	-223	-235
40	-270	-254	-252
61	-270	-252	-227
68	-227	-252	-195
75	-225	-214	-166
164	-266	-195	-186
175	-255	-176	-186
185	-235	-178	-182
199	-225	-138	-157

TABLE A7.4
CORROSION POTENTIAL VALUES
(EXPRESSED IN mV RELATIVE TO S.C.E)
FOR MILD STEEL EMBEDDED IN PLAIN CEMENT PASTES
CONTAINING 0%, 0.4%, AND 1.0% CHLORIDE IONS

EXPOSURE PERIOD (DAYS)	I_{CORR} (0% CHLORIDE)	I_{CORR} (0.4% CHLORIDE)	I_{CORR} (1.0% CHLORIDE)
24	6.39	9.67	8.37
33	4.21	5.71	3.72
40	4.33	4.73	7.21
61	5.20	6.46	7.96
68	4.52	8.15	4.96
75	-	-	-
164	6.52	3.53	2.26
175	9.26	4.01	2.63
185	6.92	5.64	5.00
199	10.2	5.83	3.12

TABLE A7.5
CORROSION RATES (EXPRESSED IN $Acm^{-2} \times 10^{-8}$)
FOR MILD STEEL EMBEDDED IN PLAIN CEMENT PASTES
CONTAINING 0%, 0.4%, AND 1.0% CHLORIDE IONS

EXPOSURE PERIOD (DAYS)	E_{CORR} (mV) (0% CHLORIDE)	E_{CORR} (mV) (0.4% CHLORIDE)	E_{CORR} (mV) (1.0% CHLORIDE)
25	-273	-245	-259
34	-269	-248	-345
61	-208	-209	-265
70	-186	-195	-230
165	-125	-188	-148
182	-157	-246	-209
196	-134	-198	-183

TABLE A7.6
CORROSION POTENTIAL VALUES
(EXPRESSED IN mV RELATIVE TO S.C.E)
FOR MILD STEEL EMBEDDED IN CEMENT PASTES
CONTAINING 10% METAKAOLIN, 0%, 0.4%, AND 1.0% CHLORIDE IONS

EXPOSURE PERIOD (DAYS)	I_{CORR} (0% CHLORIDE)	I_{CORR} (0.4% CHLORIDE)	I_{CORR} (1.0% CHLORIDE)
25	6.27	7.92	7.86
34	5.16	5.58	9.66
61	2.64	6.20	10.72
70	1.56	4.41	5.99
165	1.98	5.21	7.18
182	1.78	6.94	2.59
196	1.57	3.82	9.19

TABLE A7.7
CORROSION RATES (EXPRESSED IN $Acm^{-2} \times 10^{-8}$)
FOR MILD STEEL EMBEDDED IN CEMENT PASTES
CONTAINING 10% METAKAOLIN, 0%, 0.4%, AND 1.0% CHLORIDE IONS

EXPOSURE PERIOD (DAYS)	E_{CORR} (mV) (0% CHLORIDE)	E_{CORR} (mV) (0.4% CHLORIDE)	E_{CORR} (mV) (1.0% CHLORIDE)
20	-254	-258	-309
41	-205	-214	-254
55	-194	-241	-287
61	-202	-200	-198
162	-92	-163	-140
173	-136	-175	-111
186	-144	-117	-136

TABLE A7.8
CORROSION POTENTIAL VALUES
(EXPRESSED IN mV RELATIVE TO S.C.E)
FOR MILD STEEL EMBEDDED IN CEMENT PASTES
CONTAINING 20% METAKAOLIN, 0%, 0.4%, AND 1.0% CHLORIDE IONS

EXPOSURE PERIOD (DAYS)	I_{CORR} (0% CHLORIDE)	I_{CORR} (0.4% CHLORIDE)	I_{CORR} (1.0% CHLORIDE)
20	4.83	-	10.94
41	4.37	4.53	-
55	5.88	-	6.55
61	4.71	7.12	7.32

TABLE A7.9
CORROSION RATES (EXPRESSED IN $Acm^{-2} \times 10^{-8}$)
FOR MILD STEEL EMBEDDED IN CEMENT PASTES
CONTAINING 20% METAKAOLIN, 0%, 0.4%, AND 1.0% CHLORIDE IONS

APPENDIX 8 PUBLICATIONS

This appendix contains the draft copy of a publication arising from the research described in this thesis. At the time of binding the paper had been accepted for publication in 'Cement and Concrete Research', Pergamon Press, USA.